The Evolution of Tidal Coastal Landscapes and the Controls on Pathways to Equilibrium

A thesis

submitted in fulfilment

of the requirements for the degree

of

Doctor of Philosophy in Earth Science

at

The University of Waikato

by

Amin Rahdarian

THE UNIVERSITY OF
WAIKATO
Te Whare Wānanga o Waikato

2024

Abstract

The evolution of tidal basins is fundamental to understanding the drivers of our vulnerable estuarine and lagoon environments, ultimately determining key ecological parameters such as intertidal area, inundation regime, connectivity and accommodation space. This thesis uses multiple methods including idealized modelling, field observation of an estuarine shoal covered with mangroves, and a calibrated and validated model with field data in order to explore how different components of tidal environments influence the short and long-term dynamics of tidal lagoons.

The idealised modelling specifically focused on the roles of initial bathymetry, bed sediment and mud concentration at open boundaries on shaping equilibrium profile development of tidal basins. The results of the model showed that geomorphological development (long-term evolution) is similar in sandy environments with different initial bathymetries and without a mud supply. This was concluded because the equilibrium profiles and tidal asymmetries evolved similarly at the end of simulations. However, residence time, development of channels and energy dissipation were observed to be different. In the case of available incoming mud from open boundaries, equilibrium bathymetry was dominated by the mud supply and sediments accreted all over the domain, forming a mudflat and a deeply incised ebb-dominated channel, with several minor side channels of which their size and number were dependent on mud concentration.

The response of tidal environments to sea-level rise has been previously studied often by neglecting the importance of initial configuration in the model. In such process-based modelling, different initial bathymetries are only considered to influence the time to reach a stable equilibrium condition but will always lead to identical equilibrium bathymetry. Here we demonstrated that initial profile not only affects some aspects of tidal basins such as channel formation, residence time and energy dissipation in equilibrium condition, but also impacts their geomorphological development under sea-level rise.

In the northern North Island of Aotearoa New Zealand, tidal environment evolution is mediated by mangroves. The governing dynamics on a recently evolving estuarine, mangrove-covered channel-shoal system in Whitianga Estuary, Aotearoa New Zealand. Observations of water level, flow velocity, suspended sediment concentration and bed sediment characteristics were used to

infer flow asymmetry and sediment transport pathways around the shoal. The impact of mangrove colonization on channel dynamics, sediment texture of upper layer and mud layer thickness was studied by a one-week field campaign. Due to changes in land use, the estuary was subjected to an increase in sediment supply, causing the tidal flats to elevate and provided suitable conditions for the expansion of mangroves in 1940s. By the use of historical images, the expansion of mangroves in Whitianga Estuary was captured and the results were combined with the measured data of water level, current and sediment dynamics in order to explore the short-term dynamics around the shoal and the role of vegetation as eco-engineers in inter-tidal environments. The shoal expanded laterally independent of mangrove colonization. However, observed mud layer thickness was larger around mangroves compared to un-vegetated parts of the shoal. The mangrove creek (which was a shoal channel before expansion of mangroves) was consistently ebb-dominated and the shoal channel located outside the forest on the edge of the shoal was flood-dominated. The results suggested that mangroves impose a control on their surrounding environment and can ultimately lead to a regime shift in channels and changes in sediment texture.

The understanding provided by the field observations was confirmed with a 2-D numerical model, developed in the Delft3D modelling system, which was calibrated and validated with the data collected from the field. This model was used to study the short-term influence of mangroves and tidal creeks on tidal circulation and large-scale tidal asymmetry. The results showed that the effect of vegetation on tidal asymmetry and flow routing was larger compared that of the tidal creeks. However, the small impact of the channels may be due to the small size of the creeks compared to the size of the forest. When vegetation was removed, tidal velocity asymmetry changed substantially whereas channel infilling caused a shift in tidal asymmetry inside the creeks and around the head of the creeks mostly (from being ebb-dominated to flood-dominated). Removing vegetation led to an increase in speed all over the forest except inside the creeks and elevated parts of the forest where velocity decreased. In a scenario in which channels were filled in, currents became weaker in the location of the creeks and velocity increased around the creeks and on the edge of the forest.

Furthermore, a scenario was designed in which morphology of the shoal in the 1940s prior to expansion of mangroves was simulated, aiming to quantify the hypothesis posed by field measurement with numerical models. The results of the model demonstrated that mangrove

colonization caused a regime shift in the channels, showing that as mangroves colonize inter-tidal areas, they play a critical role in shaping the geomorphology. In Whitianga Estuary, expansion of mangroves around changed a flood-dominated pre-existing shoal channel to an ebb-dominated mangrove creek, suggesting that mangroves are likely to be eco-engineers of the estuarine system.

The idealized modelling experiments helped identifying the parameters and elements that govern the long-term morphology and equilibrium of coastal tide-dominated environments and the way they respond to sea-level rise force. Results of this theoretical exploration showed that processes localised, and timescales for equilibrium development vary vastly across the landscape. Elucidating local changing to asymmetry became the focus of subsequent chapters, firstly with a field exploration, and then supported by numerical modelling. The fieldwork presented here elucidated the short-term hydrodynamics and suspended sediment dynamics in an estuarine shoal covered with mangroves. Moreover, observation of aerial images in a multi-decadal timescale combined with hydrodynamics inside a mangrove creek and a shoal channel highlighted the complex non-linear interactions of hydrodynamics and vegetation that lead to a regime shift of a channels in the mangrove forest in Whitianga Estuary, Aotearoa New Zealand. Finally, the results of the numerical model developed and validated by utilizing field data presented here provided insights into the detailed short-term hydrodynamics. Moreover, the scenarios designed by removing channels, vegetation and reconstructing the condition prior to mangrove expansion showed that the effect of vegetation extends beyond the footprint of the vegetation to the surrounding environment with implications for hydrodynamics, morphological evolution and channel dynamics.

Acknowledgements

I would like to thank my chief supervisor Karin R. Bryan for her supervision and patience during my PhD. I am grateful that I had the opportunity to work with you and appreciate your guidance and mentoring since I started this course. Thank you for your encouragement and inspiring me to work harder. I hope that I will have the opportunity to work with you again in future.

I would also like to thank my co-supervisor Mick van der Wegen for his support and guidance. I still haven't had the chance to meet you in person but over the years I learned a lot from your modelling tips, enjoyed our online discussions and appreciate your valuable inputs and helpful comments on my work.

I would like to thank Ben Stewart, Chris Morcom, Ted Conroy and Wagner Costa for their assistance in the one-week fieldwork in Whitianga Estuary in December 2020 which would have not been possible without their help and support.

This PhD study was funded by a University of Waikato Doctoral Scholarship. I am thankful that the University provided the funding so that I could undertake my PhD. I would also like to thank my office mates in Coastal Marine Group for the good memories that we shared together over the years.

Thank Christian Winter and other people in Coastal Sedimentology group at CAU Kiel who supported me to submit my thesis while I was working here.

Special thanks to my parents, brother and sister for their support, love and encouragement. I am grateful to have you in my life.

Table of Contents

List of Tables

List of Figures

Chapter 1: General introduction

Coastal zones with the elevation of less than 10 meters above mean sea level cover two percent of the land on Earth (McGranahan et al., 2007). However, 10 percent of the world's population lives in this zone. Human settlement and development in the coastal zone are often concentrated in low-lying tidal environments, because of popular recreational activities based around the coast, the ease of building on flat land, and access to food resources (McGranahan et al., 2007). Although these areas provide many resources, they are increasingly under the threat of natural hazards such as floods and storm surges associated with climate change and sea-level rise. The way in which low-lying land will respond to such pressures depends on eco-geomorphic processes, in particular the interplay between tidal channels, vegetation growth, tidal currents, sediment dynamics and the deposition or erosion of sediments (Blankespoor et al., 2017; Coco et al., 2013; Coco et al., 2014; Temmerman et al., 2007; Zhang et al., 2012). Therefore, improving our understanding and knowledge of the current and future eco-geomorphology of tidal environments is a key factor for sustainable coastal management of the coast.

Estuarine processes are defined as forces or energy sources causing a change in pre-existing topography. Estuarine Processes can vary in terms of the time-scale that the processes occur and the response time. Some processes like tidal, wave and sediment movement processes are usually classified in short-term (minutes to years) whereas some others like sea-level rise (or any climate change effect) are referred to as long-term process because they act in time-scales of a century and distances in the order of tens of kilometres (Morales, 2022). The concept of morphodynamics is based on the interplay of these forces/energy sources and the link between the processes and morphological changes (Cowell and Thom, 1995).

Tidal environments are one main component of coastal zones and are dynamic systems. Low lying tidal environments generally formed after the sea-level rose since the last glaciation around 20,000 years ago. Their gradual evolution started after sea level became stable, after which they infilled to approximate their current morphology with sediments (Hume and Swales, 2003). Tidal systems can be found in a variety of settings, including estuaries, tidal flats, lagoons, and coastal embayments (Boyd et al., 1992). Each tidal environment is at a different stage of evolution, depending on energy and the nature of the sedimentary setting. They can exist from centuries to

millennia if they stay in a condition of dynamic equilibrium or as long as the formation of new accommodation space exceeds the infilling rate (de Haas et al., 2018).

The goal of this thesis is to explore the dominant characteristics that contribute to the evolution of tidal environments, with a specific focus on Aotearoa New Zealand. The overarching aims are to investigate the initiation, short-term dynamics and evolution of tidal environments and how their morphological features and physical services are controlled by their anteceded conditions, channel dynamics, sediment supply and vegetation (mangroves). To address the knowledge gaps in understanding the dynamics of tidal environments, the overarching aim was addressed in three research topics, each including refined research questions and study approaches.

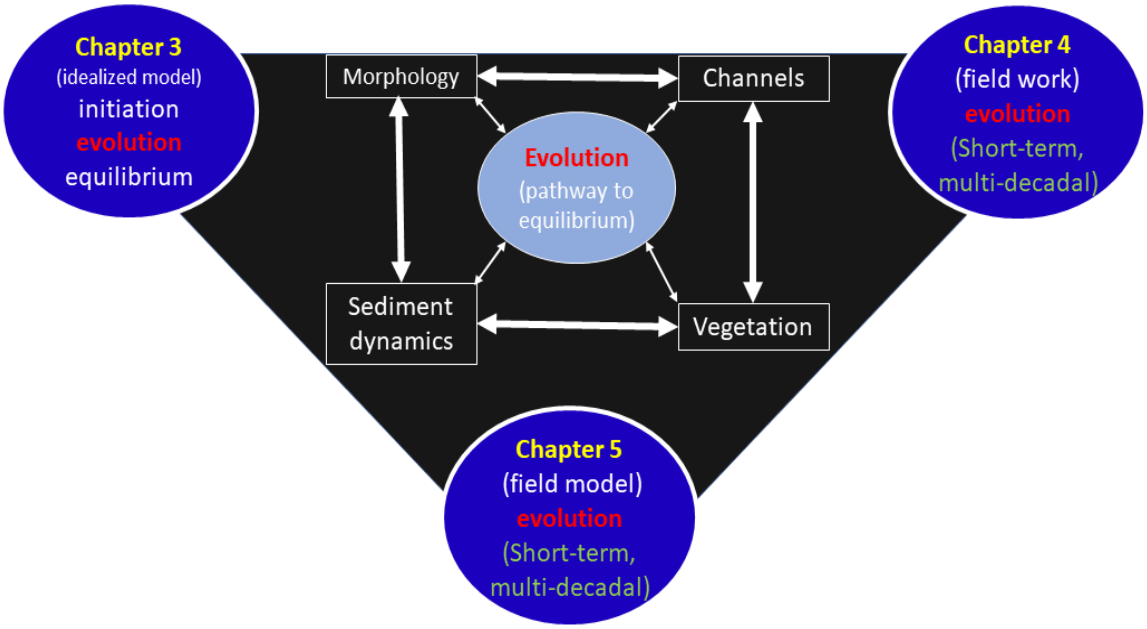

Figure 1. 1 shows the diagram demonstrating the connection between chapters and the overarching aim of the thesis.

1.1. Structure of thesis

Our estuaries are complex, often with constrictions and geometries that are shaped by the underlying geology. Sub-basins with a constricted geometry and deep entrance channels are associated with small bed shear stress values and high rates of flood-directed tidal velocity asymmetry in the sheltered basin centres, indicating a large potential for sediment deposition of

larger particles (de Ruiter et al., 2019). The goal of this thesis is to explore the dominant characteristics that connect the short-term dynamics and evolution of tidal environments, with a specific focus on the sediment properties (muddy versus sandy), sand supply in tidal basins, development of tidal channels and the effects of mangrove colonization on tidal environment evolution. These areas of focus were chosen because of their importance to our sub-tropical estuaries in New Zealand. The thesis starts with a theoretical exploration on generic geometries, but quickly moves to more relevant systems, using hydrodynamic modelling and field observations from Whitianga Estuary. The main overarching aim of this thesis is to utilize several methods including idealized numerical models, field observation, and a calibrated and validated model with field data in order to explore the elements that influence the short-term and long-term dynamics of coastal tide-dominated environments (such as tidal lagoons, tidal basins and estuaries). The role of initial profile (applicable for modelling experiments), sediment properties, channels and vegetation are the four specific components of tidal environments that are mainly studied in this thesis. I hypothesize that these four elements exert a substantial control on the initiation, short-term, long-term and pathway to equilibrium of tidal environments.

The third chapter (first paper) focuses mainly on initial profile, sediment properties and channels (3 out of 4 components), their impact on equilibrium (long-term dynamics) and the response of tidal basins to sea-level rise, although some of the factors that affect short-term dynamics (pathway to equilibrium) are also studied. Specifically, the effect of initial profile and different sediment properties (sandy bed and mixed mud and sandy bed) on the interplay of sediments, hydrodynamics and equilibrium morphology were studied that highlight the effect of these two elements on the evolution of tidal basins (long-term dynamics). Moreover, the role of channels on width-averaged flow asymmetry and residence time was also studied that revealed both short-term (pathway to equilibrium) and long-term (equilibrium) impact of this element on dynamics of tidal basins.

The fourth chapter's (second paper) focus is mainly on the impact of vegetation and channels (2 out of 4 components) on a tidal environment (the estuarine shoal covered with mangroves in Whitianga Estuary, Aotearoa New Zealand); the short-term interplay of hydrodynamics, sediments and vegetation are elucidated and the multi-decadal effect of vegetation dynamics on inducing a regime shift in channels is studied. The results of this chapter also provided a

background for the fifth chapter (third paper) and the data to validate and calibrate the numerical model of the mangrove forest.

The focus of the fifth chapter (third paper) is to use a hydrodynamic model calibrated and validated with field data in order to study the short-term impact of vegetation and channels (two out of four elements) on tidal circulation and flow routing in and around an estuarine shoal. In addition, the multi-decadal role of mangrove colonization on the dynamics of the channels (conversion of a shoal channel to a mangrove creek due to mangrove colonization and a regime shift in the channel) which was initially discussed in chapter 4 is studied by a numerical model.
A short description, the study approach and defined questions of each chapter as follows:

Chapter 2 Is a background Chapter, providing the context for the three research papers.

First research article (Chapter 3): On the influence of antecedent morphology on development of equilibrium bathymetry in estuaries past and future.

Objectives:

Tidal environments are not created equally and their characteristics vary from one to another. This will increase uncertainty in model results that are used to predict the equilibrium bathymetry and their resilience under SLR. Therefore, it is important to examine the key factors that can control their geomorphological development. This study aims to examine whether the results are independent from initial conditions or the equilibrium bathymetry is affected by antecedent morphology. By creating idealized tidal basins in the Delft3D model, the effect of different parameters on short-term dynamics and long-term evolution of tidal environments was studied in two cases of sandy and mixed muddy and sandy environments. In addition, the effect of initial bathymetry on resilience of tidal profiles under the effect of SLR was investigated. This article was published in *Journal of Geophysical Research – Earth Surface* in August 2022.

Research questions:

- What is the effect of initial bathymetry on evolution of tidal landforms?
- How can mud sediment supply control equilibrium condition in tidal environments?
- What is the effect of channels in equilibrium bathymetry of tidal environments?

- What is the response of tidal basins to SLR under different initial conditions?

Second research article (Chapter 4): Observations of Flow Pathways around a Recently-Colonised Estuarine Mangrove Shoal

Objectives:

This Chapter was designed to investigate the governing dynamics on a recently evolving estuarine, mangrove-covered channel-shoal system. Short-term influence of mangroves on their surrounding environment and how this control in a multi-decadal time-scale can lead to a regime shift in channels and changes in sediment texture was explored. Water levels, water velocity, suspended sediment concentration, sediment size, mud layer thickness and vegetation characteristics were measured during a field campaign to study flow routing, sediment dynamics and hydrodynamics around a shoal covered with mangroves and channels with different functions.

Questions:

- What are the governing dynamics and sediment pathways around an estuarine mangrove-covered shoal?
- Can colonization of mangroves control or change the dynamics of the channels?

Third research article (Chapter 5): The landscape-scale effects of vegetation and channels on tidal flooding and asymmetry around an estuarine shoal covered with mangroves

Objectives:

This Chapter was aimed at understanding the short-term morphodynamics in a mangrove forest and to simulate the pattern of water circulation in a mangrove forest by using field measurements to inform the creation of a model in Delft3D modelling system. In addition, based on historical images available from 1940, a scenario was designed to simulate the dynamics of the pre-existing shoal drainage channel that is converted to a mangrove creek after development of mangroves. This article is in preparation for submission to *Geomorphology* (Rahdarian et al., in prep).

Questions:

- What is the effect of vegetation on landscape-scale tidal asymmetry and tidal circulation?
- What is the role of channels in short-term landscape-scale dynamics and tidal asymmetry?
- What is the role of vegetation in multi-decadal changes geomorphology and channel regime-shifting?

Chapter 6 is a general discussion Chapter, bringing together the themes of the thesis and showing how they have collectively advanced understanding on the evolution of tidal basins.

Chapter 2: Background

In this Chapter, previous studies that are related to the topic of the thesis are reviewed. First a summary of previous numerical studies of tidal environments and equilibrium profiles will be presented. Following, a literature review about the initiation and evolution of tidal channels is presented. Next, studies with the focus on the response of tidal environments to sea-level rise will be reviewed. In the final section, a review of field observations and numerical modelling in mangrove forests is presented.

2.1. Tidal Environments

Tidal environments are an important component of coastal areas because they are located where significant land-ocean interactions take place. They are characterised by low bed slope regions (tidal flats) between the lowest and highest tidal level (Hibma et al., 2004), and shallow seaward regions where tidal currents dominate. Tidal environments are observed in a variety of systems ranging from sheltered to exposed coastal seas or the open ocean, and they can develop as back barrier basins, estuaries, deltas and coastal plains (Fagherazzi and Overeem, 2007).

The dimension and shape of tidal environments vary depending on tidal range, wave exposure, sediment supply characteristics and biological setting (Coco et al., 2013). Tidal flats in various climate zones can be divided into three parts based on exposure to air during tidal water level fluctuation: (1) the supratidal zone which is located above high water and inundated only during high spring tides and flooding events; (2) the intertidal zone which is located between high and low water; and (3) the sub-tidal zone that occurs below low water level and is rarely exposed to the air (Amos, 1995).

Tidal basins are among the most productive natural ecosystems in the world and play a crucial role in biogeochemical cycling. They provide ecosystem services, habitat for many species of living birds and a nursery for a variety of marine organisms (Zarzuelo et al., 2019). They also help protect the inland area from storm surges and sea-level-rise by providing a buffer zone between land and sea in coastal areas (Verschelling et al., 2018). Furthermore, tidal basins can supply nourishment to their fringing environment by exchanging water and materials between land and sea through channels. As sediments are deposited in these areas, they can also protect coastal areas against marine erosion (Bouma et al., 2016). The short-term dynamics and evolution of these

environments will ultimately determine their role in protecting coastal areas from the effects of future climate change.

Aotearoa New Zealand has a long coastline. Aotearoa New Zealand's coastal features span a wide range of environments, and tidal embayments and estuaries are common along its shorelines (Terry and Herdendorf, 1992). In Aotearoa New Zealand, about three hundred estuarine systems have been identified. These estuaries formed about 6,500 years ago when the sea began to flood river valleys (Green, 2006). They are highly valuable ecosystems because they are food harvesting areas and a natural habitat, and a key factor to maintain the biodiversity and the water quality of the sea; they also act as a nursey grounds for marine species. Mangroves and salt marshes are two halophytic vegetation types that are often found in such ecosystems in Aotearoa New Zealand. These environments are under increasing threat due to changes in land use and catchment activities (Jones, 2008). Major changes in land management occurred in Aotearoa New Zealand after settlement of Europeans. In the last 150 years, sedimentation in estuaries increased up to 10 times compared to the time prior to the arrival of people (where it was less than 1 mm per year), due to the impact of forest removal and urban development (Hume and Swales, 2003).

Early work on understanding the evolution of tidal environments was generally undertaken using 1-D cross-shore mathematical models to study the relationships between hydrodynamics, sediment transport and equilibrium shape with the focus on mudflats. Key findings were that increasing tidal range makes the mudflat steeper and higher sediment supply leads to a smaller mudflat slope; tides and waves lead to convex-up and concave-up profiles, respectively. In general, any change in sediment properties in favour of deposition will lead to a flatter profile (Roberts et al., 2000). Pritchard et al. (2002) used a mathematical model (1D cross-shore) to describe the morphological evolution of intertidal mudflats. The flat was linear below MSL and convex up above MSL. They stated that the cross-shore width of the flat increases with sediment supply and it is independent from tidal range. The characteristics of the convex-up profile in this study was similar to the one that was theoretically described by Friedrichs and Aubrey (1988) and empirically by Kirby (2000). The main effect of mud on large-scale morphology is that it deposits in areas where sand would not deposit and decreases the tidal prism and as a result, the estuary becomes more confined and the width becomes smaller. In addition, mud increases the elevation of the shoals and can transform shoal surface from intertidal to supratidal (Braat et al., 2019).

Two distinct timescales have been identified for long-term morphodynamic evolution of tidal embayments. The first one which took place after the first decades has been related to pattern formation. The second timescale has been related to continuous deepening of the profile and minor adaptation during 1600 years. This finding was stated in van der Wegen and Roelvink (2008) that used both 1D and 2D process-based models. They also showed that equilibrium in the model was not reached. However, within a millennium, the development of longitudinal profile is determined by the interaction between the profile itself and tides. Later, long-term behaviour of intertidal flats that are controlled by cross-shore currents was studied by developing a 1D cross-shore model by Maan et al. (2015). They highlighted that static equilibrium in inter-tidal environments cannot exist. Deposition and erosion in the bed is minimized after a few decades when the initial imbalance is removed, but after that the flat either builds up or retreats. Hibma et al. (2004) simulated evolution of shoals after 300 morphological years in an idealized domain using Delft3D modelling system. Morphodynamic equilibrium was reached at the end of their simulation and the wavelength of the equilibrium was independent of the initial perturbation. A static equilibrium with a zero tidally averaged sediment transport could not be found in the results. Starting from different initial perturbations, the equilibrium bathymetries were not identical, but the pattern characteristics were the same.

2.2. Tidal Channels

Tidal channels (also known as networks, courses or creeks) are widespread and abundant in intertidal environments and tidal basins, salt marshes and mangrove forests. Three major components are usually found in intertidal environments: (1) un-vegetated tidal flats; (2) vegetated areas (covered with mangroves or salt marshes); and (3) tidal channels. Channels are one of the most important features of such environments because they control hydrodynamics and sedimentary characteristics of the tidal basin and fringing open water and the connection between them (D'Alpaos et al., 2005; Fagherazzi and Overeem, 2007; Hughes, 2012).

Channels are major flow pathways for water, sediments, pollution and other material between inner and outer part of tidal basins (Kearney and Fagherazzi, 2016). As a consequence, they affect short-term (tidal range, tidal flow velocity, sediment exchange) and long-term (tidal basin equilibrium) circulation and evolution of the tidal landforms (Stefanon et al., 2010).

Numerical experiments with the Delft3D modelling system at laboratory scale and natural estuary scale have shown that the initiation and morphodynamic evolution of tidal networks is affected by initial bathymetry, friction parametrization, sediment transport and bed slope (Zhou et al., 2014). In another work, channel patterns were studied by idealized simulations of short tidal basins in Delft3D model in Marciano et al. (2005). Their theoretical analysis showed that the branching channel pattern in a tidal basin is controlled by bottom slope and water depth, the tidal flow and sediment properties. They also stated that numerical model simulates channel patterns if the initial hypsometry is not far from equilibrium. Besides, it was shown that width and spacing of the channels decrease as the slope and water depth decreases. In addition, this low slope (which is approximately half the typical forest slope) causes a considerable asymmetry within the forest. Inspired by salt marshes in China, Schwarz et al. (2014) modelled mudflats covered with salt marshes to study in the impact of vegetation on tidal channel initiation and inheritance. They found that the interplay between vegetation and mudflat heterogeneity influences the initial channel development. They also showed that channels are mainly formed by the interaction of vegetation and flow. Presence of existing mudflat channels caused the plant-flow interaction influence to be smaller on the landscape.

Many studies have focused on describing (1) the initiation and evolution process of tidal systems (2) channel dynamics in vegetated and un-vegetated environments and (3) the impact of vegetation on hydrodynamics and sedimentation using idealized modelling. Initially, idealized modelling of tidal environments based on shallow water equations – mostly neglecting the Coriolis force, density differences, wind and waves - were used to study channel formation and tidal creek head-ward incision (Rinaldo et al., 1999a; Rinaldo et al., 1999b; Hibma et al., 2004; D'Alpaos et al., 2005; van der Vegt et al., 2007). Tidal channels were mostly attributed to tidal erosion but in some cases depositional processes were mentioned as the cause of channel formation (Hood, 2010). Later, researchers used numerical models with schematized domains in order to simulate the evolution processes and equilibrium of tidal basins. Their results showed that the morphological evolution of tidal systems is dependent on tidal range and depth of the initially un-channelized basin; tidal basins with a deep inlet or low tidal range could remain un-channelled over long timescales (van Maanen et al., 2013a; Lauzon et al., 2018; Mariotti and Canestrelli, 2017). Channel networks form due to interaction between hydrodynamics, sediment transport and evolving topography. Channel network formation is faster when tidal range

increases and when initial basin is deeper. Both tidal range and initial bathymetry affected the final basin hypsometry. Morphology evolves to reduce morphodynamic activity (van Maanen et al., 2013a). van Maanen et al. (2011) presented a model based on the ELCOM hydrodynamic model to simulate long-term morphological evolution of tidal channel networks in schematized domains. Their results showed that if significant bathymetric changes do not occur, hydrodynamic conditions evolve towards more homogeneous states as a response to morphodynamic evolution. Also, tidal asymmetry and large-scale tidal flow are modified by tidal channel formation that occurs during morphological evolution.

The equilibrium state of idealised tidal networks (in which morphology and hydrodynamics are stable) is often reached within 500 morphological years. The central part of tidal network reaches equilibrium first and some regions at the extremities may not reach dynamic equilibrium (within the time frames test), which is believed to be due to initial state (Xu et al., 2017).

There are some general theories about tidal channel initiation which are based on both erosion and deposition processes (Perillo and Iribarne, 2003). While development of tidal channels is usually described by erosional processes, Hood (2006) presented a conceptual model using GIS statistical analysis tools to show depositional processes as the main driver of channel initiation and growth in Skagit marshes, USA. The processes of channel initiation in depositional model are different. In a rapidly prograding system, blind tidal channel formation is depositional and they are inherited from the antecedent distributary network. Belliard et al. (2015) used an eco-morphodynamic model to study the formation and evolution of tidal networks. The model system consists of the WWTM and STABEM models, and an ecological module was used to incorporate vegetation into simulations. One result of the study was that both erosional and depositional processes were identified as drivers for channel initiation and development. However, channel initiation stems from erosional processes, while channel elaboration results from depositional processes. In addition, sediment supply accelerated the development of tidal networks. The formation of tidal channels is mainly initiated when water drainage over the tidal flat during flood and ebb tides is not efficient.

Convex-up profiles with sharp transition between lower and higher inter-tidal zone have been shown to favours creek formation. Where creeks are present, bed shear stress redistribution develops a profile that would not exist in the absence of the creeks (Hanssen et al., 2022). Channel

length, width and depth can be influenced by the morphology (elevation and slope of tidal basin) and hydrodynamics (tidal range and wave exposure) (Fan, 2012; Vandenbruwaene et al., 2012). The length of channels in equilibrium is proportional to the critical flow speed for channel erosion. Moreover, analytical models have been used to show that channel convergence causes bed concavity which shorten equilibrium channels (Seminara et al., 2010).

The role of the channels in water drainage and large-scale tidal circulation may vary based of the scale and size of the channels compared to the area of the tidal flats. Sullivan et al. (2019) used delft3D model to investigate the effect of channels on drainage density and hydrodynamics of a channel-marsh system in Grove creek, USA. Their results showed that by removing the first and second order creeks (smaller and minor channels), the drainage density decreased but the over-marsh circulation was not significantly affected. However, when third and fourth order creeks were removed, not only drainage density was reduced by 80%, tidal asymmetry was also affected and the system converted to flood dominated from being ebb dominated.

2.3. Sea-level rise (SLR)

Rising sea level as a consequence of climate change threatens low-lying areas and tidal environments. There are different future global mean sea-level rise values reported by the year 2100 based on the 1995-2014 average sea-level, ranging from 55 cm for SSP1-1.9 scenario to 1.02 for SSP5-8.5 scenario (Khojasteh et al., 2022). However, in some cases researchers anticipate higher values of sea-level rise up to 2 meters by the of the century (Bamber et al., 2019; Khojasteh et al., 2023). Hence, recently there has been a broad interest in predicting how estuarine processes and properties will be affected by sea-level rise in future. These studies are mostly carried out by the use of numerical models. There are two main approaches used for studying the fate of estuaries and tidal basins under sea-level rise effects: 1- static modelling where the projected sea-level rise is forced to the model water level open boundaries at the beginning of the simulation and 2- dynamic modelling where the sea-level rise is added gradually to the mean sea-level, which also investigates how different estuarine properties such as tidal regime and bathymetry change in time (Palmer et al., 2019).

Recent studies have shown that the fate of wetlands depends on the SLR rate. However, in most case studies suggest that tidal flats will be drowned with current most likely SLR scenarios. The response of the tidal inlet depends on three factors: the sediment demand of the system,

availability of sediments, and sediment import and distribution (Van Goor et al., 2003). For example, ASMITA was used to calculate the probability of tidal flat survival in idealized environments similar to the ones observed in Dutch Wadden Sea, results showed that former tidal inlets were drowned under 80 cm to 1m of SLR per century (Van Goor et al., 2003). However, later the response of a large tidal basin in Dutch Wadden Sea area to relative SLR was modelled using the Delft3D modelling system under relative SLR over a 110-year time period and in contrast to the results of Van Goor et al. (2003), the tidal flat could only keep up their elevation under low SLR rates (Dissanayake et al., 2012). Their results indicated that the flood dominance of the system will increase, resulting in erosion of the ebb-tidal delta and accretion of the basin. Under SLR conditions, tidal flats were drowned but in the scenario that SLR was excluded, tidal flats continued to develop (Dissanayake et al., 2012). In another study, the response of estuarine geomorphology to climate change effects was explored by running the ROMS numerical model in Sacramento/San Joaquin Delta, California. Scenarios of present-day conditions, SLR and changes in freshwater flow and sediment supply were carried out. The elevation did not keep up with SLR in any of the simulations (Ganju and Schoellhamer, 2010). They also noted that minor changes in freshwater flow affected the results the least and decreasing the sediment supply reduced the net deposition in the estuary. Similarly, van der Wegen (2013) used a Delft3d process-based model to simulate the impact of SLR on tidal basins. Starting from a flat bathymetry, morphodynamic development was fast and after a century, a channel-shoal pattern emerged. Although the basin shifted from exporting sediment to importing and sediments moved landward, the landward sediment transport was limited and SLR eventually drowned the basin. In addition, a higher tidal amplitude led to a more pronounced channel-shoal pattern and faster development.

Tidal currents, sediment supply and vegetation are identified as main drivers for morphodynamic evolution and adaptation of tidal environments to SLR conditions. The modelled response of an idealized tidal embayment to SLR using the hydrodynamics model ELCOM revealed that SLR causes headward erosion of the tidal channels. In addition, both a larger tidal range and SLR lead to a decrease in the presence of channels. SLR can cause an exporting-sediment basin to convert to importing sediment. Moreover, a loss of intertidal area was observed to increase flood dominance and sediment import and an increase in the surface area can increase the ebb dominance and sediment export (van Maanen et al., 2013b). Starting from unchanneled tidal basin, mangroves have a strong control on tidal channel development. Although headward

incision of channels is reduced by vegetation, mangroves lead to higher channel density by enhancing branching of tidal channels due to extra flow resistance and additional drag produced by mangroves. Channel networks expand landward during SLR (van Maanen et al., 2015). 2D idealized model setups inspired by Western Scheldt Estuary in Delft3D modelling system revealed that the bed is most dynamic near the channel-shoal interface. When the model in equilibrium was forced by SLR, the sandy shoal accreted and by adding mud to the system, the shoal was more resilient to SLR (Elmilady et al., 2020). Later, Elmilady et al. (2022) applied Delft3D numerical model in 2D mode to run an idealized tidal basin from initial condition with mild slope and random meandering to equilibrium condition and study the response of the system to SLR. Large-scale channel-shoal patterns were formed due to positive feedback between morphology and hydrodynamics, although the morphological activity was observed to slow down over time. A better morphodynamic adaptation was the result of larger sediment supply. Shoals accreted under SLR conditions after flood dominance increased and sediments were imported into the system. Field measurements of water level, tidal inundation and velocity in Minnamurra River estuary, Australia, combined with the depth-averaged hydrodynamic model Telemac2D and an empirical wetland elevation model (WEM) showed that tidal range inside the estuary increased under SLR, with a non-linear relationship to SLR rate, which was related to eco-geomorphologic feedbacks (Kumbier et al., 2022b).

2.4. Mangroves

Mangroves are one type of halophytic vegetation that cover wide intertidal areas of the world, although these trees and shrubs are restricted to tropical and subtropical regions (Woodroffe et al., 2016). Mangrove forests occupy nearly 138,000 km^2 of coastlines and sheltered saline environments where sediments build mudflats in the mouth of rivers, tide-dominated or wave-dominated regions (Swales et al., 2015a). Mangroves are a group plants categorized in 70 species within 19 families. They are typically taller than 0.5 m, residing in low-energy inter-tidal environments. *A. alba* Bl., *A. integra* N. C. Duke, *A. marina* (Forsk.) Vierh., *A. officinalis* L. and *A. rumphiana* Hallier f. are five mangrove species that are commonly found in Australasia. *Avicennia marina sub australasica* is the indigenous Aotearoa New Zealand flora that have inhabited Aotearoa New Zealand coastlines for approximately 19 million years (Duke, 1991; Morrisey et al., 2007).

Mangrove forests provide valuable services in coastal regions. They enhance the resilience of coastal communities: for example, they can create habitats for a variety of organisms from the sea; they are nursery areas for fishes and juvenile crabs; they enhance the mechanism of land-building by sediment trapping and protect coastlines from erosion; they can act as a natural buffer during tropical cyclones and extreme weather conditions by mitigating waves and attenuating storm surges; and, they are also economically important as a supply of timber and fuel wood. Anthropogenic activities such as clear cutting, changes in erosion and deposition rates and effects of climate change can change the distribution of mangroves with time (Swales et al., 2019).

Mangrove forests consist of two major components: (1) the forest (2) and the creek. The forest area is usually bigger than the creek area and can be considered as terrestrial during low tide and an aquatic environment during high tide; however, the creek area mostly remains wet even at low tide (Mazda et al., 2005; Wolanski et al., 1980).

Vertical and horizontal movements of water in mangrove forests are influenced by the trees and mangrove root systems. Mangrove roots are very dense in the forest area; this leads to increased friction and flow resistance and makes the water flow with lower velocities in the forest, and sediments to be trapped within root systems, resulting in lower sediment transport capacity and a more stabilized substrate.

In the past decades, researchers have classified mangrove forests. One classification by Cintron and Novelli in 1984 grouped mangroves into three types of forests based on their topographic features were defined: (1) fringing forest type (2) riverine forest and (3) basin mangrove forest type (Mazda and Wolanski, 2009).

Fringing mangrove forests: This type of mangrove forest mostly occurs in sheltered coastlines where the shore is exposed to both tides and waves. Fringing mangroves occur in low gradient landforms and their bottom slope characteristics continue gradually to open sea water. Significant tidal creeks do not occur in fringing mangrove forests, and because of dense vegetation, trees and roots dissipate waves (Mazda and Wolanski, 2009).

Riverine mangrove forests: Riverine mangrove forests are on floodplains alongside banks of rivers, and are composed of tidal creeks and mangrove swamps. Riverine forests are inundated during the highest tides and are exposed during the lowest tides; waves are hardly found in these

swamps since they are dissipated along tidal creeks. During flood tide, tidal flow first inundates the channels and when it overtops the creek bank, water flows in the swamp. During ebb tide, water in the swamp is conveyed to the creeks by a flow that is perpendicular to the creeks (subjected to high vegetation friction) and then flushes out of the system (Kobashi and Mazda, 2005; Mazda and Ikeda, 2006).

Basin mangrove forests: This type of mangrove forest, which grows in a pond-like topography, is defined as partially impounded depression. Basin mangroves are inundated by spring high tides during wet seasons, but during dry seasons, they are inundated only during a few of the highest tides. The pressure gradient difference between the basin and open water drains the water through the groundwater system and makes the water level decrease slowly in the basin (Mazda et al., 1990).

In each type of landform, mangrove growth initiated in specific hydrodynamic and topography conditions; their evolution processes and time scales may be different as they are highly dependent on water circulation, sediment supply and material exchange between mangrove forest and the fringing environment. In addition, response of mangroves to climate change is highly dependent on how they to adjust their bottom level during accelerated sea-level-rise, and this may lead to different resilience of mangroves in each type of landform.

Although numerical models are being used to simulate morphodynamics of tidal environments, there are many parameterizations within the model that are poorly tested. Field measurements are necessary in order to properly improve our understanding of the complicated interaction of water, sediments and vegetation. Furthermore, results of numerical models without validation by observational data are not reliable. There are few studies that focus on in-situ measurements of sediment trapping, flow velocities, water inflow and outflow regimes in tidal basins and vegetated environments. One of the first efforts was to measure fine sediment load carried by tidal water from coastal waters and trapped by vegetation within mangroves in Cairns, Australia (Furukawa et al., 1997). Subsequently, water level, current velocity and flow pattern measurements within mangrove forests and in the bank of creeks were carried out by many other researchers (Aucan and Ridd, 2000; Kobashi and Mazda, 2005; Horstman et al., 2013; Horstman et al., 2015; Montgomery et al., 2018; Montgomery et al., 2019).

Depending on the topography, different flow routing and tidal asymmetry have been observed in mangroves. In a mangrove forest in Trang province, Thailand, flow velocities decreased when bed levels increased and where mangroves were denser. The creek-flow stage was not observed in low lying mangroves and tidal flows were sheet flows. Whereas within the higher elevated mangroves, a distinct creek flow was observed at water levels below the vegetation before the sheet flow started (Horstman et al., 2013). Furthermore, Horstman et al. (2015) studied flow dynamics by using field data and results of Delft3D model in Trang River mangrove forest, Thailand, and showed that in the high-elevation mangrove forest, tidal exchange was dominated by creek flow. The results of the model showed that tidal dynamics are dependent on topographic characteristics of the elevation of the mangroves. Water level and velocity data were measured in a mangrove forest located in Whitianga Estuary, Aotearoa New Zealand. The flow in the creek and the forest was consistently ebb dominant and flood dominant, respectively. At flooding tide, they observed the maximum tidal flow speed at overbank water levels but at ebbing tide, it occurred at water levels below the creek bank. They also observed that the flow speed asymmetry declined landward inside the creek (Horstman et al., 2021). Although mangrove creeks in most case are highly ebb-dominated, there are some contrasting cases that the creek is slightly ebb dominated which is not in accordance with what is observed in other similar mangrove forests. This behaviour that was observed in mangrove-creek systems of a mangrove forest in Cocoa creek in spite of a very large forest area compared to the creek volume, is mainly because of the very low slope of the forest (Aucan and Ridd, 2000). Later, Bryce et al. (2003) studied observations of tidal height, currents and suspended sediment concentrations from 1992 to 1996 in Cocoa Creek, Australia to investigate the relationship between hydrodynamics, sediment transport and geomorphology. Tidal asymmetry of Cocoa Creek was observed to be both ebb and flood dominated, controlled by the interaction between tidal forcing and intertidal storage effects. During creek flow stage, flood dominance was observed whereas the flow was ebb-dominated at overbank tides. The results of observations of tidal flow in a riverine-type mangrove forest in Aira-River mangroves, Japan demonstrated that inside the forest near the bank of the creek, a velocity component parallel to a tidal creek reduces in the direction perpendicular to the creek which supports the horizontal circulation of water within the forest (Mazda et al., 2005). Schettini et al. (2020) showed field data of tidal circulation and sediment dynamics in Furo Grande channel and around Amazon Mangrove coast which was measured during dry season. Currents on the flats were ebb dominated and inside the creek, the flow was flood-dominated consistently. The flood

dominance inside the channel was attributed to the geometry of the system. Currents on the flat were slower in the channel and favoured in deposition. The current speed in the channel was reported to be ~1 m/s and suspended sediment concentration ranged between 50 to 350 mg/l.

Developed models of mangrove forests, validated and calibrated with in-situ observations, enable understanding of its dynamics in larger spatial and temporal scales since long-term field data collection is time consuming and costly. Numerical modelling within mangrove forests was first used to simulate flow in mangroves creeks. One of the first studies in mangroves was about field data and proposed a mathematical model to simulate the hydrodynamics in Hinchinbrook mangrove forest, Australia. Currents in mangroves were less than 10 cm/s and velocities in the creek were up to 200 cm/s. Although the sediment load was high and siltation was observed around the sheltered coastline, siltation did not occur inside the creek. The model could successfully simulate the hydrodynamics, showing self-scouring of creek due to the surrounding mangroves (Wolanski et al., 1980). In addition, it was stated that the vegetation density impacts the physical characteristics of the creek. Wolanski (1992) described hydrodynamics of a mangrove forest around the Coral creek, Australia by the use of numerical models. The model was verified against two observation points in the creek. In addition, the groundwater flow, trapping and buoyancy in the forest, and the mixing mechanism were discussed. Following, Currents and sediment transport in mangroves of Middle creek, Australia were explored by using field data and a numerical model was used to study the interaction of tidal currents. Tidal speed never exceeded 20 cm/s in mangroves. The Manning coefficient in mangroves was reported to be up to four times higher in mangroves compared to the tidal creek. Moreover, high suspended sediment concentrations (up to 15 mg/l) were reported inside the tidal creek and sediment rate of 0.1 cm/year inside mangroves was observed (Furukawa et al., 1997). Since then, process-based models have been used to simulate water circulation, sediment dynamics of mangrove forests and effect of vegetation on flow routing (e.g. (Mazda et al., 1995; Horstman et al., 2015)).

Mangroves in Aotearoa New Zealand occur in a lot of estuaries along the coastlines of North Island. The New Zealand mangrove, Manawa, is classified as a sub-species within Avicenna marina (Morrisey et al., 2010). Mangrove forests in Aotearoa New Zealand mostly expand in sheltered environments such as estuaries and tidal basins (Morrisey et al., 2010; Horstman et al., 2018). These forests which are dominated by *Avicenna var. australasica* cover about 260 km^2 of land in inter-tidal zones (Spalding, 2010) from 34°27' to 38°05' in North Island (Horstman et al., 2018).

Mangrove cover in Aotearoa New Zealand has changed considerably since early 20th century. At first, urban development followed by settlement of Europeans led to loss of mangroves. Since 1930s, removal of forests and changes in land use led to an abrupt sediment supply. Estuarine infilling with eroded sediments from the land provided a suitable condition for rapid expansion of mangroves when tidal environments elevated and flats shifted from being sand dominated to mud dominated (Swales et al., 2021).

The effect of sea-leve rise on mangroves is dependent on several factors such as SLR rate, sediment supply, hydrodynamic, wave conditions and topography (Woodroffe, 1990). Therefore, this affect is expected not to be in the same pattern for all mangrove forests (Soares, 2009). However, Xie et al. (2022) coupled 1-D Delft3D hydrodynamic model with vegetation dynamic model to run idealized cases and study the effects of tidal range, wind waves, sediment supply and vegetation dynamics under the effect of SLR; and they stated that mangroves in micro-tidal areas are more vulnerable; macro-tidal conditions with large sediment supply promoted accretion which helps reduce vulnerability of mangrove under slow SLR rates. As long as sea level rise is not accelerating too quickly, high mangroves are capable of adjusting the sea-bed elevation with sea level by trapping sediments (van Maanen et al., 2015). However, their sediment accretion rate may not be high enough to adjust their elevation to revised predictions of accelerated sea level and so they are highly vulnerable to the climate change impacts (Swales et al., 2015a). Thus, managing mangroves requires enhancing our knowledge of their complex short-term dynamics and interactions with their fringing environments, which underpin their resilience to the effects of sea-level-rise.

Chapter 3: On the influence of antecedent morphology on development of equilibrium bathymetry in estuaries past and future

Amin Rahdarian[1,2], Karin R. Bryan[1], Mick van der Wegen[3,4]

[1] School of Science, Faculty of Science and Engineering, University of Waikato, Hamilton, New Zealand.

[2] Institute of Geosciences, Christian-Albrechts-Universität Zu Kiel, CAU, Kiel, Germany

[3] IHE-Delft Institute for Water Education, Delft, Netherlands.

[4] Deltares, Delft Netherlands.

Contribution of Authors:

Chapter 3 presents "On the influence of antecedent morphology on development of equilibrium bathymetry in estuaries past and future", published in *Journal of Geophysical Research – Earth Surface* in August 2022. Numerical model setups were designed by Amin Rahdarian with the direction and advice from Karin R. Bryan and Mick van der Wegen. Amin Rahdarian wrote the initial draft and it was edited based on co-author's comments and feedbacks.

Abstract

Although analytical and numerical models have been widely used to explore evolution and equilibrium morphology in tidal environments, less attention has been paid to examining the impact of initial bathymetry on the model outcomes. Here we use two-dimensional idealised models with contrasting initial bathymetries to study how the interactions between antecedent morphology and tidal exchange processes determine the establishment of an estuarine equilibrium bathymetry, and how these interactions mediate the morphodynamic response to rising sea levels. In all model runs with sandy beds, inter-tidal zones reach the equilibrium condition first and equilibrium profiles are similar for points close to mean seal level. However, key aspects like channel formation, residence time and energy dissipation do not evolve to the same state and are inherited from the initial bathymetry. This implies that responses to SLR are different as well. Conversely, in cases with mud and sand input at the boundaries, equilibrium occurs more quickly and the equilibrium bathymetry and channel formation are dominated by the boundary mud concentration. General implications of the study are that predictions of coastal response to changes such as SLR depend on initial bathymetric conditions.

3.1. Introduction

Situated at the interface between the land and ocean environments, tidal embayments and estuaries are the primary zone where mixing and processing of land-origin fresh water, nutrients and sediments occur. These areas belong to the most productive natural ecosystems in the world, playing a critical role in bio-geomorphological cycling (Hibma et al., 2003; Zarzuelo et al., 2019). Tidal creeks and channels are key landforms with embayments and estuaries that connect the ocean and inter-tidal zones.

Despite their importance, we are still exploring the underlying processes that lead to the development of the characteristic morphology of the inter-tidal, including channels and shoals. Idealised morphodynamic modelling of tidal environments based on the shallow water equations shows that tide-induced erosional processes play an important role in channel formation and tidal creek head-ward incision (Rinaldo et al., 1999a; Rinaldo et al., 1999b; Hibma et al., 2004; D'Alpaos et al., 2005; van der Vegt et al., 2007). Rare cases also show the importance of depositional processes (Hood, 2010). Schematised domains have shown that the formation process can take time, and deeper tidal basins or smaller tidal ranges can remain un-channelised over surprisingly long timescales (van Maanen et al., 2013a; Mariotti and Canestrelli, 2017; Lauzon et al., 2018; Zhang et al., 2018), whereas larger morphodynamic development occurs in shallower basins under larger tidal ranges (van Maanen et al., 2013a). These cases show that, in principle, morphological development depends on the magnitude and distribution of spatial energy gradients in the domain.

The pathway to establishing an equilibrium geomorphology of tidal environments is often studied with simplified models, informed by field observations (Klein, 1985; Amos, 1995). In fact, much of our understanding of equilibrium conditions has developed using profile models, which are computationally cheap. Such models suggest that in an accreting tidal flat, the profile tends to evolve toward a prograding convex-up shape, arising from fine sediment input, whereas erosion-dominated equilibrium profiles arise on receding coasts accompanied by concave-up beds (Kirby, 2000). Similar results have been found in more recent studies, where steeper mudflats are related to larger tidal ranges and lower sediment supplies and wave-dominated forces lead to concave-up profiles (Roberts et al., 2000; Friedrichs, 2011). In addition, observations of tidal flat profiles confirm that as the tidal range increases, the shape of the tidal flats favoured to be more convex-

up (Dieckmann et al., 1987; Bearman et al., 2010). However, some beach or estuarine tidal flat exhibited a mixed shape between concave-up and convex-up profiles (Dai et al., 2007; Dai et al., 2018). van der Wegen et al. (2017) suggests that energy dissipation levels decrease and become more uniformly distributed over the basin, as the morphology evolves. The adaptation timescale of entire basins, ~ centuries, (van der Wegen and Roelvink, 2008) is much longer than smaller-scale features such as mudflats, ~decades (van der Wegen et al., 2017).

The effect of initial conditions on equilibrium is still not clearly established, with results of process-based models showing contrasting outcomes for different spatial scales. In an example from a tidal embayment, results of long-term process-based model that simulates the Dutch Wadden Sea morphological evolution show that initial bathymetry can affect mega-scale simulated equilibrium conditions (Dastgheib et al., 2008). Another early study using the Delft3D process-based model to predict the initial formation and evolution of channel-shoal patterns showed that different initial perturbations resulted in same pattern characteristics, but not identical equilibrium conditions (Hibma et al., 2004). Conversely, in a work that mainly focused on whether inter-tidal flats reach equilibrium or not, an idealised 1-D cross-shore model was developed with initially linear profiles to show that final profile shapes were not dependent on initial shape and slope (Maan et al., 2015). Similarly, long-term and short-term morphodynamic simulation of tidal flats using a dynamic equilibrium theory showed that the initial profile will only change the time to reach stable conditions and does not affect general evolution process and equilibrium profile (Hu et al., 2015).

Modelling exercises exploring development pathways to morphological equilibrium provide an interesting perspective on real life systems. Generally, two major morphological timescales are distinguished for tidal coast evolution. One timescale, with the duration of decades, is related to the evolution of channel-shoal systems. The second timescale is related to the bed profile development of the entire tidal basin system with a typical duration of centuries to millennia (van der Wegen and Roelvink, 2008). Under constant forcing conditions, smaller-scale systems like mudflats and beaches may reach equilibrium within years, whereas larger systems like estuaries and tidal basins will take decades to centuries or even millennia. However, forcing conditions are rarely constant. Daily- to seasonally-varying forcing conditions on mudflats such as wind waves, sediment supply and storms have short morphodynamic adaptation timescales leading to morphodynamic variations superimposed on equilibrium conditions (van der Wegen et al., 2019).

In contrast, changing forcing conditions may also intervene with the adaptation timescale of the whole system so that equilibrium conditions are never reached. Such an example is the impact of SLR on larger tidal basins. Varying forcing conditions and the long adaptation timescale of larger systems suggest that many estuarine systems are not in equilibrium and that, despite best intentions, the initial bathymetry applied in many modelling studies exploring SLR impact is not necessarily an equilibrium condition. This raises questions on the impact of the initial bathymetry on the eventual model outcomes.

In face of rising sea levels, there is increasing pressure to provide predictions of morphological change to underpin the development of coastal adaptation strategies. One of the difficulties in moving to more complex models and systems (more realistic cases) is that outcomes from models of simple systems (e.g., linear systems which include limited processes and forcing) may not depend on initial conditions, while initial conditions can dominate in models with strong non-linearities (Taylor Perron and Fagherazzi, 2012). Therefore, in such cases, environments subjected to similar processes and conditions may have different equilibrium characteristics or reach their equilibrium states over different timescales. Compounding this issue is the challenge of selecting a suitable antecedent morphology. We do not know the initial conditions of the systems we aim to model because they formed before modern day observation networks existed. Major geological development of estuarine systems occurred early in the middle Holocene when the rapid SLR caused flooding continental shelfs, and the influence of river sediment supplies allowed coastlines to prograde. Yet, establishing this condition may be critical to reproducing the modern-day morphology of estuarine systems.

This study aims to explore how differences in initial bathymetry affect the morphodynamic development of tidal embayments. The feedback between initial profiles and the hydrodynamics, mediated by the bed-sediment composition, ultimately impacts the equilibrium morphology that evolves as well as its response to SLR. Our specific hypothesis is to isolate the attributes of the evolving inter-tidal flat that retain a strong memory of the initial morphology, and those which evolve more quickly to a more generic condition. We explore these questions using simulations of multiple tidal coasts starting from different initial conditions using Delft3D process-based models. We will show that different stages of morphological evolution are associated with substantially different hydrodynamic regimes, which in turn, can change the way in which the tide shapes these coastal ecosystems.

3.2. Methods

We use Delft3D modelling software to implement two-dimensional idealised models using different profiles for initial conditions for our simulations. Delft3D is a software suite developed by Deltares that allows for a multi-disciplinary modelling approach. In this study, we use a subset of modules to simulate flow, sediment transport and bed level change. Delft3D-FLOW is a process based hydrodynamic simulation program that calculates non-steady flow by solving the shallow water equations (Lesser et al., 2004). To investigate how the initial bathymetry affects process-based modelling results, we explore conditions leading to equilibrium profile development for each case. Once equilibrium conditions are established, SLR scenarios are applied to equilibrium profiles to investigate the influence of initial bathymetry on the response of tidal coasts to SLR forcing.

Three different cases representing idealised bed level configurations were implemented in the Delft3D modelling system: 1- irregular bathymetry (with no specific pattern); 2-concave-up bathymetry; and, 3-convex-up bathymetry, starting from approximately 25 meters below mean sea level at the offshore boundary to 5 meters above mean sea level at the land boundary (Figure 3.1). Simulations were performed on a schematic rectangular basin with a length of 15 km and a width of 5 km. The grid cell size was 100×100 m, while the time step was 1 minute. The seaward (western) boundary was forced by a 3-meter M2 and 0.5 meter S2 tide chosen to provide a spring-neap cycle, and a wide inter-tidal domain relative to the grid resolution. Since the alongshore does not vary substantially in cross-shore direction, a no-flux condition was applied to northern and southern cross-shore boundary conditions to limit the model to cross-shore tidal propagation.

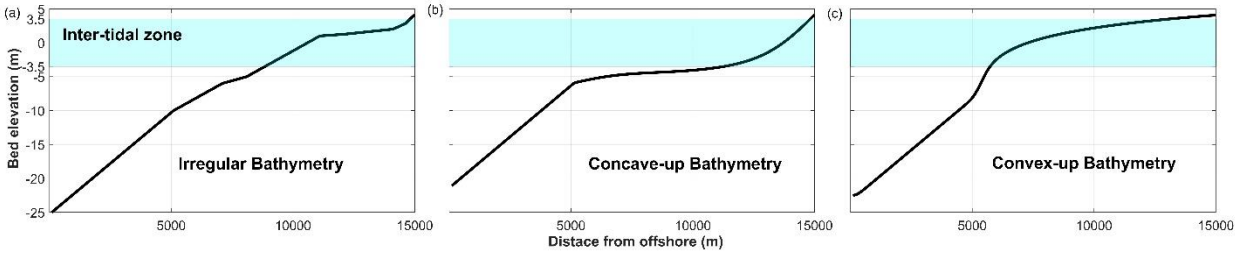

Figure 3. 1 Three different initial profiles named as (a) irregular bathymetry (b) concave-up bathymetry and (c) convex-up bathymetry

Sediment transport and morphodynamics are predicted within the Delft3D sediment module that supports both bedload and suspended load transport. Two types of sediment configuration were applied in our models: 1- sandy sediment and 2- mixed mud and sand sediment. The median sand diameter was 200 μm with a specified density of 2650 kg/m^3 and 1650 kg/m^3 dry bed density. The initial sand layer thickness was set to 20 meters. The initial mud layer thickness in the mixed mud and sand case was zero meters. For mud, a critical bed shear stress for erosion of 0.3 N/m^3 with erosion parameter 5×10^{-5} kg/m^2/s was chosen (Best et al., 2018). The mud influx concentration was set to 0.025 kg/m^3. Model parameters are summarised in Table 1. In contrast to sand influx which depends on local flow velocities, mud influx is thus treated as supply limited. An equilibrium sediment concentration was set at the inflow boundaries. This implies that the inflow sand concentration is calculated internally within the model using an equilibrium sediment concentration profile (depending on local, tide-varying flow velocities). The inflow concentration is compensated for higher sediment concentrations during outflow by the Thatcher-Harleman time lag that is set as 120 minutes (Thatcher and Harleman, 1972). Thus, this lag represents the time that sediment concentrations decay from the outflow concentration to the equilibrium concentration. This accounts for the fact that sediments need time to settle in the water column, also at the turning of the tide.

Table 3. 1 Summary of model parameters.

Parameter	Value	Parameter	Value
Grid Size	100 × 100 meter	Mud layer thickness	0 meter
Simulation time	30 years	Dry bed density (mud)	500 kg/m^3
Time step	1 minute	$T_{critical}$ for erosion	0.3 N/m^3
Reference density for hindered settling	1600 kg/m^3	Erosion parameter	5×10^{-5} kg/m^2/s
Sand layer thickness	20 meter	Mud layer thickness	0 meter
Median sand diameter	200 μm	Tracer concentration	1 kg/m^3
Specific density (sand)	2650 kg/m^3	Morphological scale factor	100
Dry bed density (sand)	1600 kg/m^3	Fresh settling velocity	0.5 mm/s
Sand concentration at open boundary	0 kg/m^3	Saline settling velocity	0.5 mm/s

Delft3D enhances process-based morphodynamic modelling by activating a morphological acceleration factor (Roelvink, 2006). We choose a morphological factor of 100 within the 30-year period model run to study the bed evolution over a 3000-year time scale. Preliminary tests indicate that the 3000-year time scale is long enough for our environments to reach the stage that

morphology only slightly changes (<1% changes) and we consider this condition as the "equilibrium condition" in our models.

In order to study the hydrodynamic characteristics of each morphological development stage in higher temporal resolution (file size restrictions precluded saving every time step in the long runs), we created a short (2-month) hydrodynamic simulation every 500 years of the morphological run. The purpose of these higher resolution runs is to study the influence of each morphological stage on processes controlling the physical drivers shaping coastal ecosystems, such as mixing and transport of, e.g., sediments, nutrients and pollutants. The hydrodynamic implications of the morphological changes are assessed using changes to tidal prism, tidal asymmetry, residence time and energy dissipation as metrics of change. These aspects are chosen because they relate how the hydrodynamics might contribute to the ecosystem in terms of providing a mechanism to flush nutrients, sediments and contaminants, and the likelihood of retention and /or burial within the system.

Tidal asymmetries for each model run are computed by dividing peak velocity during flood tide by peak velocity during ebb tide for a spring tide in each temporal stage. Tidal asymmetry shows the net direction of sediment transport within the model (Friedrichs and Aubrey, 1988; Hunt et al., 2016). For each simulation, tidal asymmetry is assessed by computing the ratio between peak flood and ebb velocities for a spring tide at each time step. Then, tidal asymmetry index is computed by averaging this velocity ratio over the computational grid. An index refers to flood dominance if larger than one, and ebb dominance if smaller.

A tracer was released in these short runs, with uniform initial concentration of 1 kg/m^3, to calculate the residence time associated with each morphological stage. Residence time indicates how efficiently water circulates in the flat, and how much time is available for sediment dynamics. For every 500th morphological year, a tracer with 1 kg/m^3 was released in each domain and an exponential model was fitted to the tracer concentration decay curve (over the two-month high-resolution model time frame). The residence time index (RT_{index}) is:

$$C = C_0 \ e^{-kt} \quad (1)$$

$$RT_{index} = \frac{1}{k} * \ 10^{-3} \quad (2)$$

where C is concentration of the tracer at the time t, C_0 is the initial concentration, and k is the decay rate constant.

The energy dissipated by transport of sediment and shear stress is defined in a two-dimensional hydrodynamic modelling as (Rodríguez-Iturbe et al., 1992; van der Wegen et al., 2008):

$$p_{cell} = [\ g \frac{n^2}{\sqrt[3]{h}}\ \ \rho_w\ \ (\bar{u}^2 + \bar{v}^2)^{1.5}\ \ + (\rho_s - \rho_w)\ g(S_x^2 + S_y^2)^{\ 0.5}\ ] \quad (3)$$

where p_{cell} is the energy dissipated per grid cell per second (kg m^2 / s^3), $\bar{u}$ and $\bar{v}$ are depth-averaged velocities in the x and y directions respectively (m/s), S_x , S_y are sediment transport components (m^3/m/s), ρ_w and ρ_s are the density of water and sediment (kg/m^3), n is Manning's coefficient (s/m$^{1/3}$) and g is gravitational acceleration (m/s^2). The first term on the right-hand side stands for energy dissipation due to friction and the second term represents the dissipation by sediment transport.

In order to study the influence of initial bathymetry on response to SLR, we also designed scenarios in which the sandy bed models were forced by SLR associated with three different Representative Concentration Pathways (RCPs) for 200 years after reaching the equilibrium condition. SLR scenarios are explored using the RCP 8.0, RCP 6.0 and RCP 2.6 predictions. Therefore, after the 30-year model run, SLR was exponentially imposed to seaward boundary and the model was run for another 2 years with a morphological factor of 100.

3.3. Results

3.3.1. Bed Level Development

All initial bathymetries appeared far from equilibrium because significant morphological change initiated immediately (Figure 3.2). Development of the sandy tidal flats and mixed mud and sand environments was very different under equal hydrodynamic forcing. In sandy systems, bed development occurred mostly in the first 500 morphological years and modified slowly for the rest of the simulation period. Channels and patterns formed during the evolution process on each of the three profiles are different, but width-averaged transects of the bathymetry show that the morphological development leads to similar equilibrium profiles within inter-tidal zone (Figure 3.2). In all irregular, convex-up and concave-up profiles, the bed experiences both deposition and

erosion and the lower part of inter-tidal zone is the area where the most changes occur. The inter-tidal zone in all sandy cases evolves toward a similar slope, while the foreshore differs in each case, with a more prograding shore when initially more sediment was available. In the irregular bathymetry case, the lower intertidal area erodes, while sediment deposits in the upper intertidal zone (Figure 3.2a-1). The convex-up profile erodes in all parts of intertidal zone (Figure 3.2c-1). The concave-up profile mostly accretes throughout the intertidal, except at the upper extreme, where it hardly changes (Figure 3.2b-1).

In mixed mud-sand environments, rapid changes happen within the first 100 morphological years, reaching equilibrium in a shorter time period compared to sandy systems. Bed level changes after 500 years of simulation are negligible compared to initial development. In irregular and convex-up bathymetries, initially sediments erode in inter-tidal area and the bed accretes in sub-tidal area. However, after 200 years of simulation, incoming mud sediment from boundaries deposit in the inter-tidal area (Figure 3.2d-1 & 3.2f-1). In the concave-up bathymetry, sediments deposit everywhere in the domain from the time that development starts (Figure 3.2e-1). In all cases, mud influx causes sediment accretion in the flats and gradually a deeply incised main ebb-tidal channel is formed in order to circulate the tidal water in the domain. Note that minor differences in channel morphology are likely due to the grid configuration (as shown in Coco et al. (2013)). Most of the areas surrounding the channels accrete until they reach the high tide elevation and become morphologically inactive. After reaching equilibrium conditions, all three bed profiles developed into a similar pattern consisting of a main channel with minor side channels for better water discharge during the ebb tide, surrounded by an accreted area at the high tide elevation that is dry in some parts even during spring tide. The shape, length, and depth of the main channel and also the number of side channels are different in each profile (Figure 3.2) and width-averaged transect of bathymetry shows that incoming mud is the main factor that controls morphology and causes the profile to accrete to the point of drying completely.

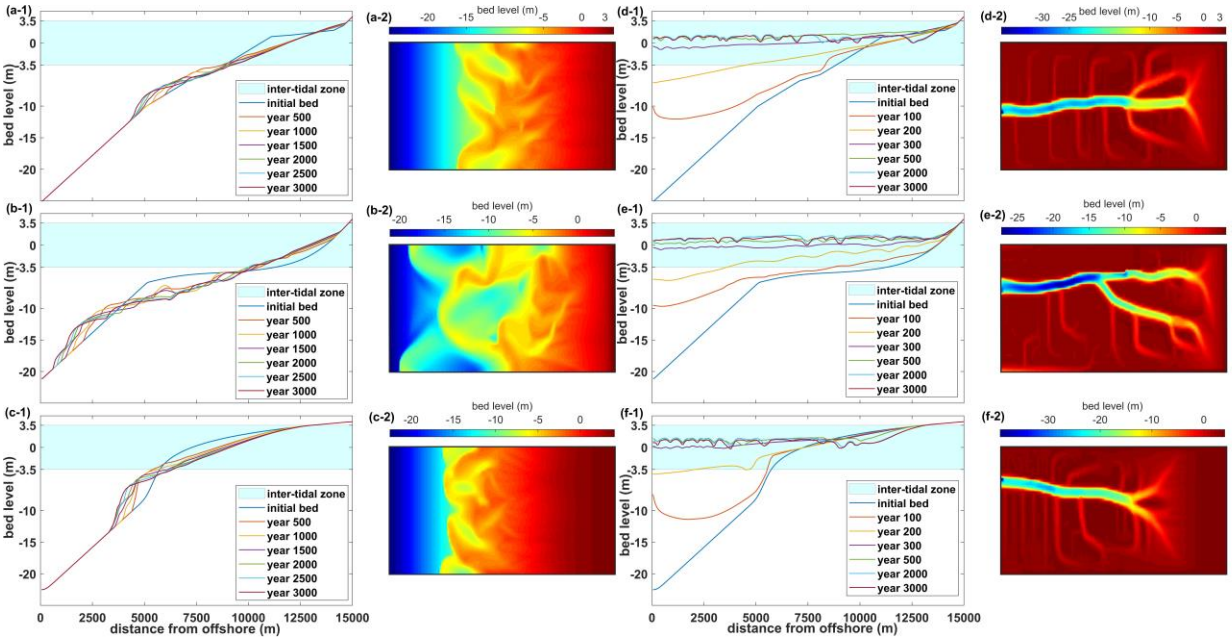

Figure 3. 2 The width-averaged profile evolution, for the model run with an irregular initial profile and sand sediment. (a-1); a concave-up initial profile and sand sediment (b-1); a convex-up equilibrium bathymetry with sand sediment (c-1); an irregular profile evolution with mud and sand sediment (d-1); a concave-up profile evolution with mud and sand sediment (e-1); and a convex-up equilibrium bathymetry with mud and sand sediment (f-1). Panels (a-2, b-2, c-2, d-2, e-2 and f-2) show the bed level after 3000 years for each scenario.

In summary, results of both sandy systems and mixed mud-sand environments show that all three profiles function similarly through reaching equilibrium conditions and forming final bed shapes, but the detail of the patterns and the shape of profiles were not the same. In addition, the initial profile has a larger impact on the final geometry of the sandy cases than for the muddy cases. This is likely because sand supply by the boundary is absent and sand redistribution and initial sand availability in the system are more important for the final state, while the muddy system imports more sediment that is distributed more evenly over the domain and thus becomes less impacted by the initial sediment availability.

3.3.2. Tidal characteristics during evolution in sandy environments

In order to study the hydrodynamic conditions that led to the observed morphological evolution, width-averaged stage velocity curves were created in multiple cross sections. Figure 3.3 shows bed profiles (dark black line) and stage-velocity curves at intervals of every 500 morphological years for each bathymetry starting from initial bed to equilibrium condition in the sandy environment. Changes in hydrodynamic condition are mainly related to the first 500

morphological years and after that time some minor modifications occur until the equilibrium condition is reached.

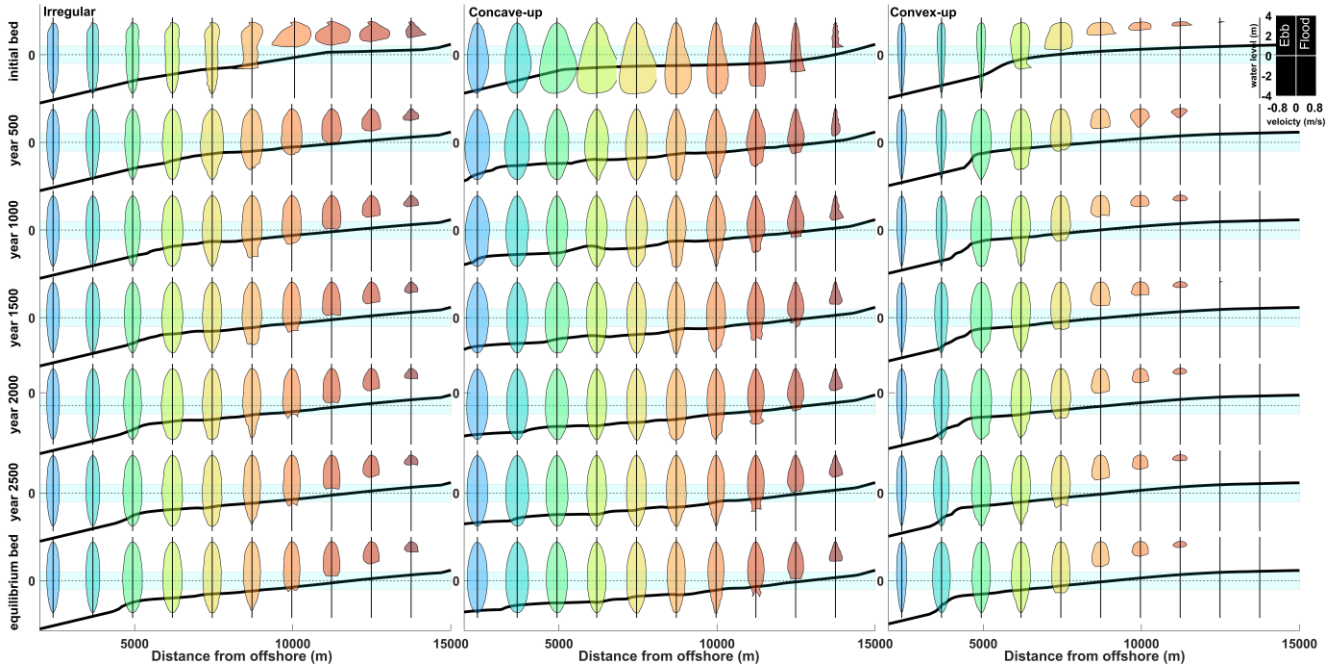

Figure 3. 3 Width-averaged profiles and stage-velocity curves during bed development plotted at intervals of every 500 morphological years for irregular (left panels), concave-up (middle panels) and convex-up profiles (right panel) with sandy sediment. Note the profile elevations are plotted on a different scale than the water elevations in the stage plots. Conversely, all stage plots and all profile plots are to the same scale respectively. The light blue shading is the tidal range. Stage-velocity curves are plotted in different colours for enhanced visualisation. The panel on the top right corner shows the reference axes.

In the irregular bathymetry case (Figure 3.3, left panels), initially no significant asymmetries can be observed in the deeper zone, but the upper sub-tidal area and upper inter-tidal area are mainly flood-dominated and the middle part of inter-tidal zone is ebb-dominated. The concave-up profile is generally flood-dominated in the beginning, except in the sub-tidal area. In the convex-up bathymetry case, the flat has no asymmetry in the sub-tidal zone, but cross-sections within inter-tidal area show ebb-dominant asymmetries. Asymmetric tides occur when the tidal wave interacts with the bathymetry and domain geometry and in our model residual sediment transport is directly influenced by convexity and concavity, with flood-dominant conditions bringing in new sediment to fill depressions and vice versa. Equilibrium conditions develop in sandy tidal environments to allow water to circulate more efficiently in the domain by removing asymmetries in lower and middle part of tidal zone. The stage-velocity curves eventually show equal water velocity during ebb and flood. Each initial basin configuration functions differently

before evolution, but after reaching equilibrium condition, similar patterns can be observed, especially comparing conditions at equal depths in the three cases.

3.3.3. Hydrodynamic response

3.3.3.1. Tidal prism

The tidal prism is defined as the amount of water that leaves the flat from flood to ebb tide during each tidal cycle. Deeper and wider inter-tidal flats have larger tidal prisms allowing a larger accommodation volume for sediment deposition (Swales et al., 2016). In sandy environments, the tidal prism changes are small, and these changes occur mostly in the first 500 years due to morphological development, with only slight subsequent changes due to localised bed modifications (Figure 3.4-a). The tidal prism in each case becomes more similar over the three profiles, but never the same even after equilibrium is essentially reached. The tidal prism continuously decreases in the concave-up sandy bathymetry because the initial flood-dominated current results in residual sediment transport from the seaward boundary and, as a consequence, sediment accretion makes the inter-tidal area contract. Conversely, in the convex-up bathymetry, the inter-tidal area erodes due to higher flow velocities during ebb, so a wider inter-tidal area results in higher tidal prism. In the irregular profile, some sediment eroded from the lower inter-tidal area by ebb-dominated flow is deposited in the upper inter-tidal area, but the rest migrates seaward to accumulate in the uppermost sub-tidal zone so, as a result, the inter-tidal area expands, and tidal prism increases over time.

The patterns are quite different in the mixed mud-sand environments, where the large mud influx and sediment accretion causes the tidal prism to drop abruptly in all three profiles, changing very little after 500 morphological years. In summary, sandy tidal flat bed development does not result in the same tidal prism; conversely, mixed mud-sand environments all end up with relatively similar tidal prisms (Figure 3.4-a).

3.3.3.2. Tidal asymmetry

None of the profiles is close to equilibrium condition initially and, as the bed develops, tidal asymmetry values start changing toward equilibrium conditions. As shown earlier, the irregular and concave-up bathymetry start out as flood-dominant, while the convex-up bathymetry initially

exhibits ebb-dominance. In sand environments, as the system approaches an equilibrium, the initial tidal asymmetry cancels out as the index tends to one (Figure 3.4b). Conversely, in mixed mud-sand environments, the asymmetry index decreases continuously over time and ebb-dominance is observed after reaching equilibrium. In this condition, tidal asymmetry is mainly controlled by the ebb-tidal channel that develops due to mud accretion and head-ward incision through time. An averaged tidal asymmetry index approaching 1 is not a good indicator for equilibrium conditions when mud is the main agent of morphological change.

3.3.3.3. Residence time

In all model runs, residence time decreases as the bed evolves (Figure 3.4-c). Before development starts, residence time in concave-up bathymetry is the greatest, followed by the irregular and then convex-up profiles. The difference is related to both different sized inter-tidal zones and tidal asymmetries. In the convex-up profile, ebb-dominant asymmetries result in bigger velocities during ebb and more effective flushing of the tracer from the system than in the case of the other two profiles (Figure 3.4-c). In sandy environments, bed level changes and formation of channels and bed patterns during evolution result in better circulation of water up to a 30% decrease in residence time. In mixed mud-sand flats, mud accretion and development of the deep ebb-dominated channel causes the residence time to decrease up to 70% of the initial value in the first 500 morphological years and the 3 initial bathymetries do not have significant differences in residence time (Figure 3.4-c).

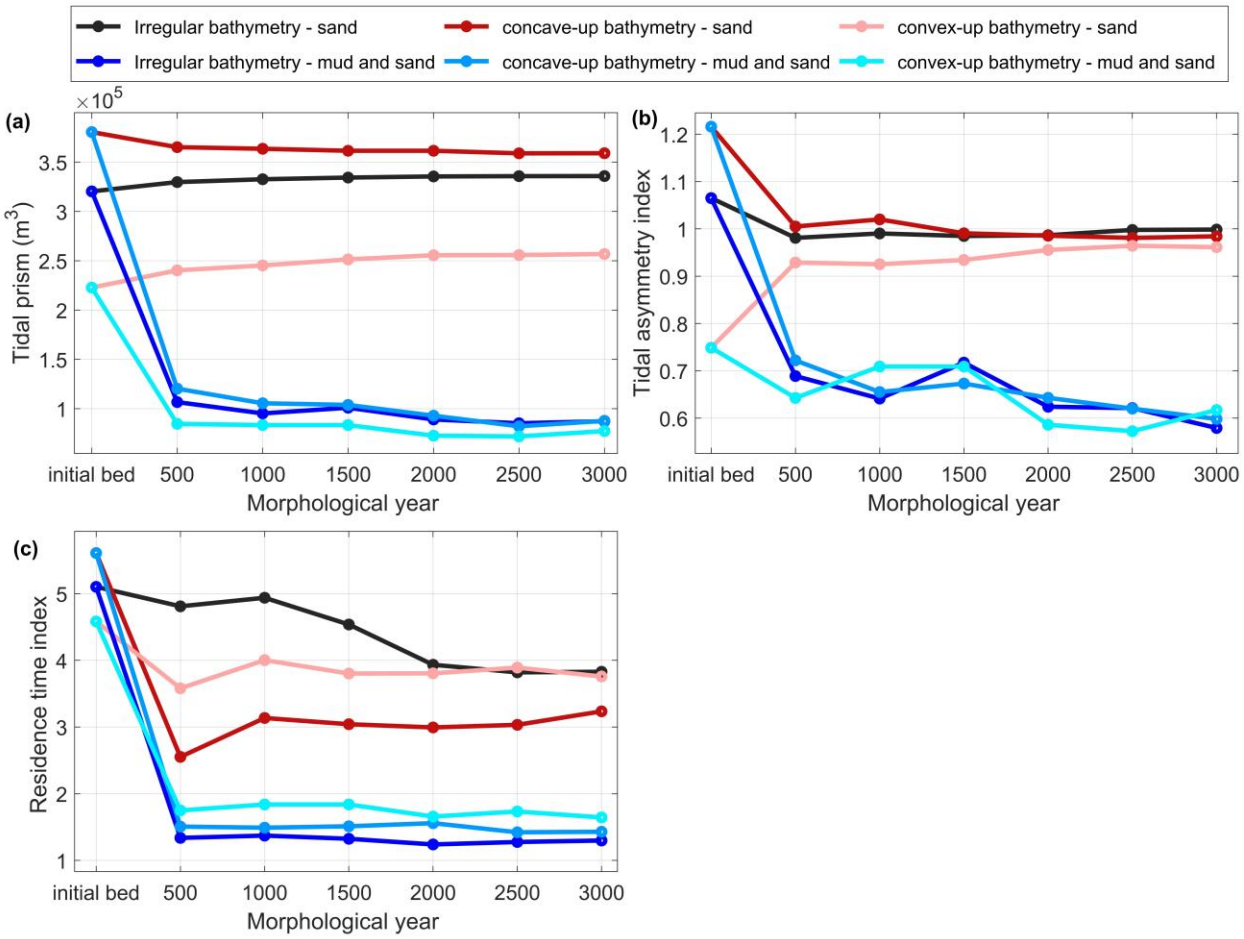

Figure 3. 4 Tidal prism changes in every 500 morphological years in Irregular, concave-up and convex-up bathymetry with sand sediment and in mixed mud and sandy flats. (b) Tidal asymmetry index (Vmax flood / V max ebb) changes during bed evolution in Irregular, concave-up and convex-up bathymetry with sand sediment and in mixed mud and sandy flats for every 500 morphological years. (c) Calculated residence time index during bed evolution in Irregular, concave-up and convex-up bathymetry with sand sediment and in mixed mud and sandy flats for every 500 morphological years.

3.3.3.4. Energy dissipation

Every 500 years, energy dissipation is computed locally on the computational grid and then averaged spatially (Figure 3.5) for both sandy and mixed mud and sand environments. Initially energy dissipation in concave-up profile is higher than in the irregular and convex-up profiles due to a bigger tidal area. Within sandy flats, energy dissipation increases for the convex-up profile from year 1000 to 2000, associated with erosional processes that lead to wider inter-tidal area and higher velocities. However, generally the residual sediment transport and bed shear stress

decrease during the evolution process as equilibrium is approached and this causes an associated decrease in energy dissipation over time.

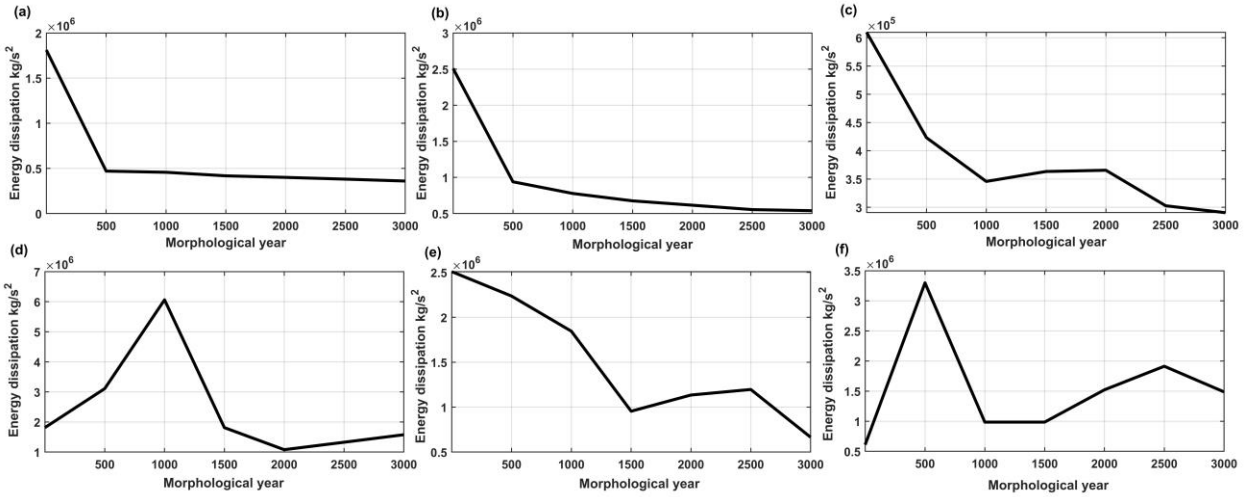

Figure 3. 5 Integrated energy dissipation over one tidal cycle calculated every 500 morphological years in (a) irregular bathymetry with sand sediment (b) concave-up bathymetry with sand sediment (c) convex-up bathymetry with sand sediment (d) irregular bathymetry with mixed mud and sand sediment (e) concave-up bathymetry with mixed mud and sand sediment (f) convex-up bathymetry with mixed mud and sand sediment.

In each case, energy dissipation reduces over time, however the way in which it reduces is different. In mixed mud and sand environments, energy dissipation first increases in the irregular and convex-up profiles because of the formation of an ebb-dominated channel and high velocities. In the concave-up profile, mud accretion decreases energy dissipation. For all three bed profiles, energy dissipation is higher after reaching equilibrium in mixed mud and sand environments relative to sandy tidal flats (Figure 3.5).

3.3.4. Role of channels

3.3.4.1. Sandy environments

As the sandy tidal flats evolve, the morphology becomes substantially channelised, the impact of which is not apparent in basin-wide averaged metrics discussed up to now. Figure 3.6b shows channels that are created in an inter-tidal cross section at 10km from the offshore boundary from the irregular bathymetry (Figure 3.6a) after having reached equilibrium. To study the role of channels, we extracted flow at four points inside and outside of channels with different elevations (points in Figure 3.6b). Stage-velocity curves confirm that peak water velocities are higher and more ebb-dominant in the deeper parts compared to the points outside the channel (Figure 3.6c).

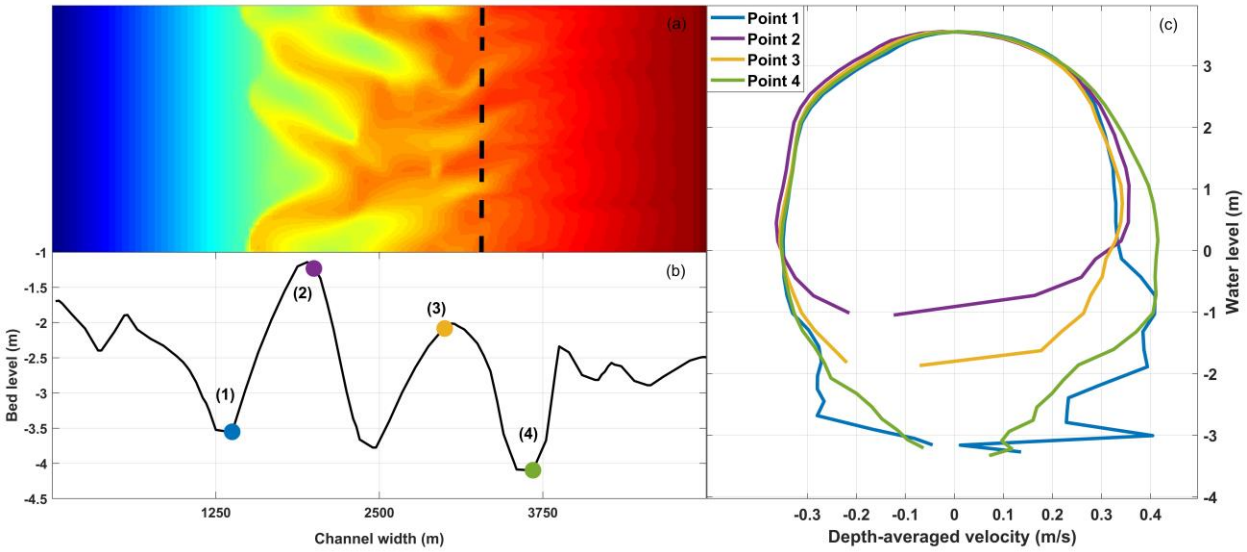

Figure 3. 6 Shows (a) the location of selected cross section (b) location of the point in the cross section and (c) stage-velocity curves for selected points in a tidal cycle.

In addition, we created a scenario where we removed the alongshore variability caused by channels and shoals by alongshore averaging of the equilibrium profile. Results show that channels improve water circulation and reduce residence time (Figure 3.7a) but do not affect the basin-wide averaged tidal asymmetries (Figure 3.7b). Although asymmetries can be observed locally in some cross sections (Figure 3.3 – equilibrium bed panel), the tidal flat is generally in the same equilibrium either with or without channels (Figure 3.7b).

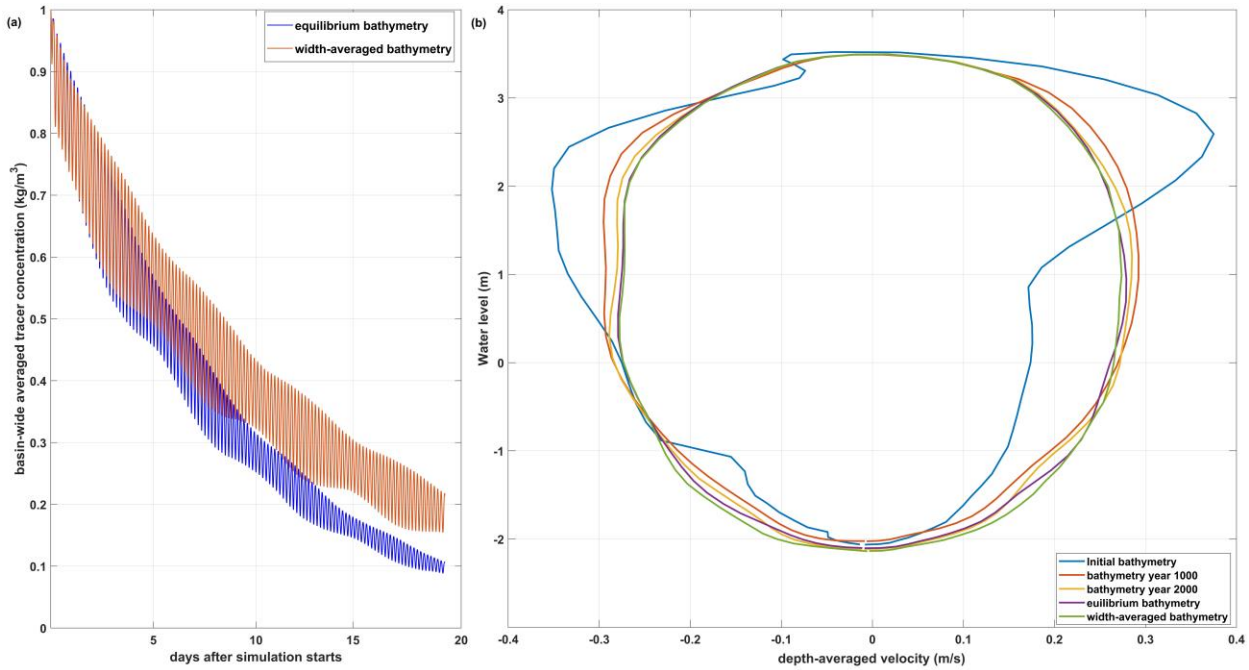

Figure 3. 7 Shows (a) tracer concentration decay for a 20-day simulation in equilibrium condition and for width-averaged bathymetry (b) stage-velocity curve for one tidal cycle in initial condition, bathymetry after 1000 years, bathymetry after 2000 morphological years, equilibrium bathymetry and bathymetry for a width-averaged bathymetry (which channels are removed).

3.3.4.2. Channel development in muddy environments

Figure 3.8 shows the relationship between the development of channels with width-averaged stage-velocity curves for three cross sections in the mixed mud-sand irregular bathymetry. Before morphological changes start, cross sections (a) and (b), located in sub-tidal area, are wet during both low tide and high tide and no significant tidal asymmetries can be observed, while cross section (c) is only wet during high tide. Mud accumulates more quickly in cross section (c) and after a short time of bed development, a main creek is formed while deposition of sediments increases the elevation of other points in the cross section. After reaching the equilibrium state, the width-averaged stage-velocity curve becomes smaller (currents are reduced), except in the main ebb-tidal channel, which is the main conduit for water circulation, other points are only wet during high tide. In cross section (b) and (a), development starts with several narrow and shallow channels that are more effective at flushing while the elevation of the bed increases due to mud accretion. Throughout the evolution process, the number of shallow channels decreases as they join together to form deeper channels allowing water to flow with higher velocities. After reaching

equilibrium, ebb-dominance is observed in the main creek, with flood-dominance in cross sections closer to land and within side channels.

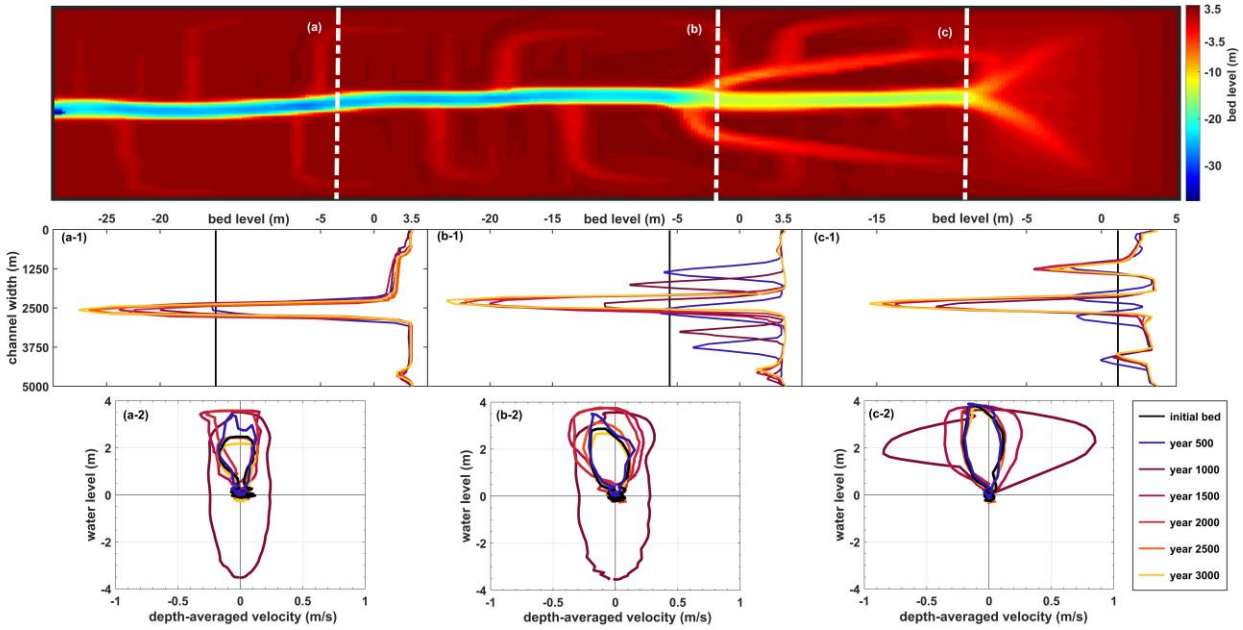

Figure 3. 8 The top panel shows the location of three selected cross sections within irregular bathymetry with 0.025 g/l mud concentration imposed at the boundary in equilibrium condition. (a-1) shows the channel development in cross section a (b-1) in cross section b and (c-1) in cross section c. The bottom panel illustrates stage-velocity curves during bed development (a-2) in cross section a (b-2) in cross section b and (c-2) in cross section c.

Clearly, the evolution of the mud-sand profiles is heavily influenced by the new mud entering the domain from the seaward boundary and accumulating in the domain. To investigate the effect of mud concentration on the profile equilibrium shape another series of simulations was undertaken with five different input mud concentrations at the open boundaries ranging from 0.005 to 0.18 g/l. In all model runs (and similar to previous mud-sand runs), the flat is infilled by mud sediment deposition and water circulates by a main channel with some minor side channels. Sediments stored in the bed increase by expanding seaward into the sub-tidal area. By increasing mud concentration, the slope of equilibrium profile and the width of the main channel decreases and the size and number of side channel increases to drain water efficiently (Figure 3.9f). This pattern continues until accumulation of sediment is high enough to completely fill the flat and the domain functions as an exposed mudflat incised by channels (Figure 3.9e).

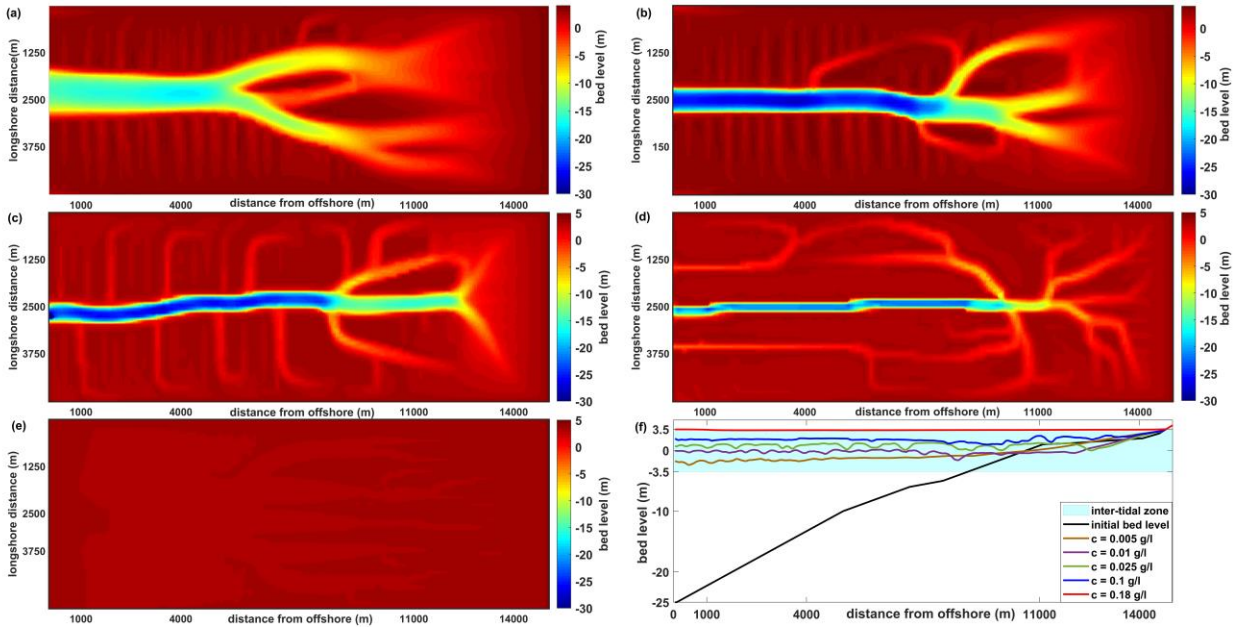

Figure 3. 9 Equilibrium bathymetry of irregular bathymetry for mixed mud and sand sediment with (a) c=0.005 g/l (b) c=0.01 g/l (c) c=0.025 (d) c= 0.1 g/l (e) c = 0.18 g/l mud concentration and (f) shows the initial and equilibrium transects of bathymetry for different mud concentrations.

3.3.5. Sandy environment under SLR

In order to explore if different profiles react differently to SLR forcing, sandy equilibrium profiles were exposed to different SLR scenarios based on available Representative Concentration Pathways (RCP) predictions. To this end, we extended simulations for another 200 morphological years and RCP 8.5, RCP 6.0 and RCP 2.6 predictions were simulated by imposing exponential SLR, reaching 2 m, 1.5 m and 1.2 m at the end of the simulation period, to the offshore boundary. In irregular and concave-up bathymetry, as sea-level rises, sediments accrete in sub-tidal area but the supra-tidal area degrades because of erosional processes. By increasing SLR with different RCP scenarios, the final slope of the profile decreases (Figure 3.10). For all RCP scenarios, irregular and concave-up bathymetries are not able to keep pace with mean sea-level increases, so the inter-tidal area disappears as the tidal flat drowns (Figure 3.10a & 3.10b). This is mainly because of SLR acceleration, limited sediment supply and the lag between forcing and morphological response of the bed. The sediment supply from the offshore remains limited so that SLR leads to a sediment redistribution in areas where shear stresses are highest (i.e., the shallow, inter-tidal regions).

Conversely, the results show that with the convex-up bathymetry, in supra-tidal and upper inter-tidal areas sediments deposit and bed elevation increases over time (Figure 3.10c).

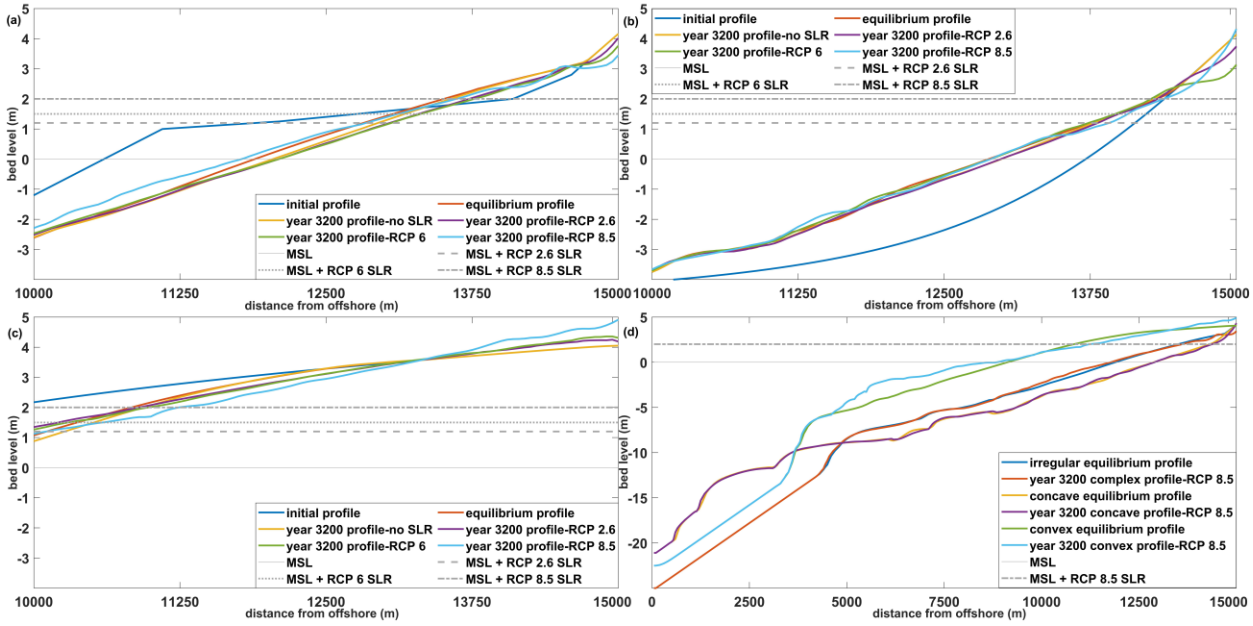

Figure 3. 10 Shows initial bathymetry transects, the equilibrium profile and the equilibrium profile evolved with various SLR projections for the irregular (a), concave-up (b) and convex-up (c) bathymetries. Panel (d) shows three bathymetries in equilibrium condition and under RCP 8.5 projection

3.4. Discussion

Our model results show that a morphodynamic equilibrium state is not only dependent on forcing and sediment budget but also on the initial bathymetry. Dynamic equilibrium and equilibrium conditions have been studied in the past using analytical and numerical models as basis for understanding how tidal environments function and how they might function in the future. Equilibrium profiles are generally dependent on the tidal forcing and sediment fluxes and, in some cases, the shape of developed tidal flats can be dependent of length of the basin (Schuttelaars and De Swart, 2000; Seminara and Tubino, 2001). Similar to recent numerical and analytical models showing a convex-up equilibrium bed profile of tide-dominated environments (Kirby, 2000; Roberts et al., 2000; Friedrichs, 2011; Maan et al., 2015), our model results show similar patterns. Irregular and concave-up profiles ended up with a constant slope in the inter-tidal area and convex-up curves in the sub-tidal area and the convex-up profile lost the degree of convexity.

Nevertheless, an overall convex-up profile shape can be observed in all the equilibrium profiles, consistent with past work.

However, our results show that although the response to different initial bathymetries is similar, some key aspects like channel formation, residence time and energy dissipation do not evolve to the same state. There are many one-dimensional models that necessarily ignore the dominant role of the channels in pattern evolution (Roberts et al., 2000; Pritchard and Hogg, 2003). Such aspects are highly relevant to determining how the equilibrium tidal flat functions in shaping a coastal ecosystem. Although not affecting the overall ebb-flood asymmetry of the system, channels change the flushing and tidal prism characteristics, which determine how sediment is distributed and accumulated. In addition to the role of channels, the geomorphic processes by which the morphology reached equilibrium were different. On average, the convex-up bathymetry eroded, but the concave-up bathymetry deposited sediments. Most of the erosion occurs during the ebb tide whereas deposition occurs during the flood tide when sediments are brought from the offshore area. Furthermore, the short-term dynamics and the timescale over which they reach equilibrium are different for each case. Figure 3.11 shows width-averaged initial profiles of irregular, concave-up and convex-up bathymetry, aligned by cross-shore location of the zero-elevation point. Initially, all three profiles are far from the equilibrium condition but at the end of the simulation some equilibrium similarities can be observed, confined to the inter-tidal zone (specifically the middle inter-tidal). Due to low velocities and bed shear stress in upper inter-tidal zone, morphology has not changed substantially compared to initial values.

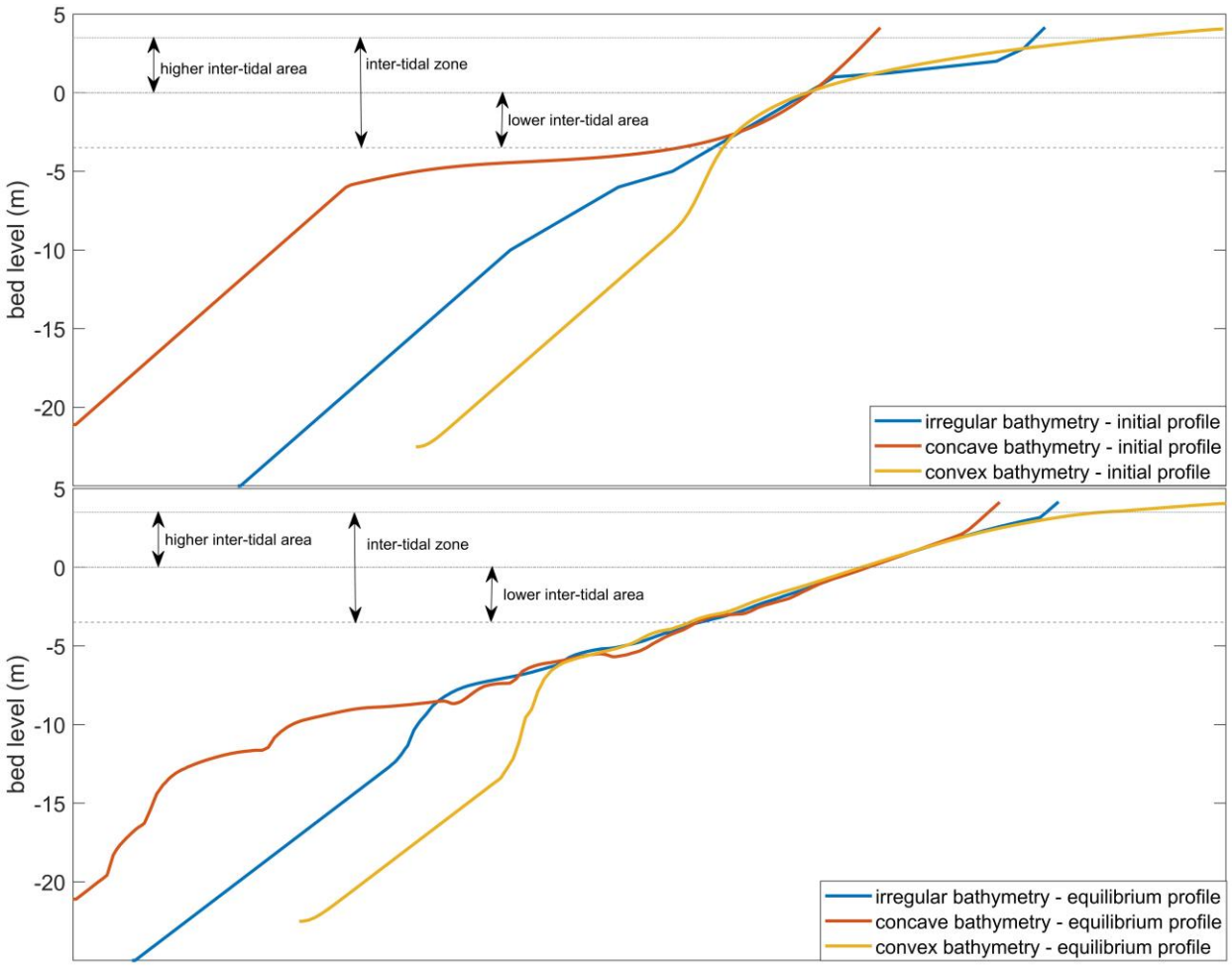

Figure 3. 11 Top panel shows width-averaged initial profiles of irregular, concave-up and convex-up bathymetry aligned by the cross-shore location of the zero-elevation point. Bottom panel shows width-averaged equilibrium profiles of irregular, concave-up and convex-up bathymetry aligned on top of each other based on the point with zero elevation.

Development of morphology in the mixed sand and mud environment was somewhat different from the sandy case. The main channel develops due to depositional processes of incoming mud from the boundaries; but minor and side channels that initiate after the main channel is created are incised because the water drainage over the tidal flat during flood and ebb tides is not efficient. Perillo and Iribarne (2003) show that tidal channels can develop either due to erosional processes, where they are carved into the underlying sediments, or depositional processes, where sediment deposition in surrounding areas causes water to concentrate in channels. Our results show that erosion and deposition develop the morphology in tandem. Water begins to converge

in lower friction areas where flow is slightly more efficient, and with time, channels are scoured as the efficiency differences between channels and flat increase.

In our results from the sandy cases, equilibrium is shown to be initiated at a “critical active point”. Past results have shown equilibrium to develop from the influence of bed shear stress and asymmetry on sediment transport, but our runs show that the patterns are highly localised. The tidal asymmetry influences the residual sediment transport so that sediments will be removed in case of surplus and will be deposited in the areas that sediment is needed. Figure 3.12 shows width-averaged profile evolution (panel a), bed level change (panel b) and bed shear stress (panel c) for the model run with an irregular initial profile (other profiles show similar patterns). The part that is in the offshore area of the domain is a morphologically passive zone, where no bed level changes happen because the bed shear stress is at a minimum here. Morphological changes start from a critical active point in the profile; a point that is ebb-dominated and has the highest value of velocity and bed shear stress in the domain (at around 8500 m in the domain), and gradually radiate seaward and landward (the green line shows progression of the zone with highest bed level change in the domain). Bed shear stresses higher that critical bed shear stress for erosion cause sediments to erode at the critical point and deposit in neighbouring cells; in turn, neighbouring cells become the cells with the highest bed shear stress values, and this loop continues until almost all the points with high velocities are removed. This process leads to redistribution of bed shear stress and decreasing energy dissipation in the domain (showing in Figure 3.5). As the model gets closer to equilibrium condition, this process slows down because points are either located in a morphologically passive zone or mean bed shear stress values are lower that critical values. Eventually this process leads to the equilibrium state reported in the literature, where the residual sediment transport and energy dissipation is minimised (Van Goor et al., 2003; Hibma et al., 2004), also considered for mudflats (Roberts et al., 2000; Pritchard and Hogg, 2003).

Our model result shows that the trajectory to the equilibrium state depends on the supply rather than on the tidal asymmetry/bed shear stress alone. Similar to previous work in sandy flats, the tidal asymmetry index approaches unity—which is a more symmetric condition and thus residual sediment transport decreases over time. Conversely, on muddy flats, the equilibrium condition is approached quickly and is associated with continued accretion of mud all over the domain and creation of a main ebb-dominated channel with growing side channels. The whole system remains

ebb-dominated even in its equilibrium state. Gao and Collins (1994) associate the short period to reach equilibrium condition with the role of high sediment concentration at inflow boundaries. Conversely, the limited sediment supply in sandy environments means that the equilibrium condition develops more slowly (the domain runs out of available sand to shape the regions at the fringes of the morphologically-active zone) and the shape of profile is inherited from initial conditions. The main drivers of the rate to equilibrium are the tidal prism, duration of ebb and flood, freshwater discharge, and sediment supply. Without sediment supply there is a two-way interaction between bed shape and tidal prism and asymmetries. In the case where we have sediment supply, equilibrium condition is highly controlled by the mud concentration and develops five times faster than in sandy environments.

In the sand only environments, most of the morphological pattern development is sub-tidal and patterns are not maximised in the zone that reaches equilibrium, whereas in muddier environments, patterns occur predominantly in the exposed regions. The natural sandy-subtidal patterns are oriented differently, probably due to the propagation direction of the tide in these regions. In natural environments, low-energy inter-tidal regions with mud generally tend to become vegetated due to the combination of stable substrate and the availability of nutrients stored in muddy sediments.

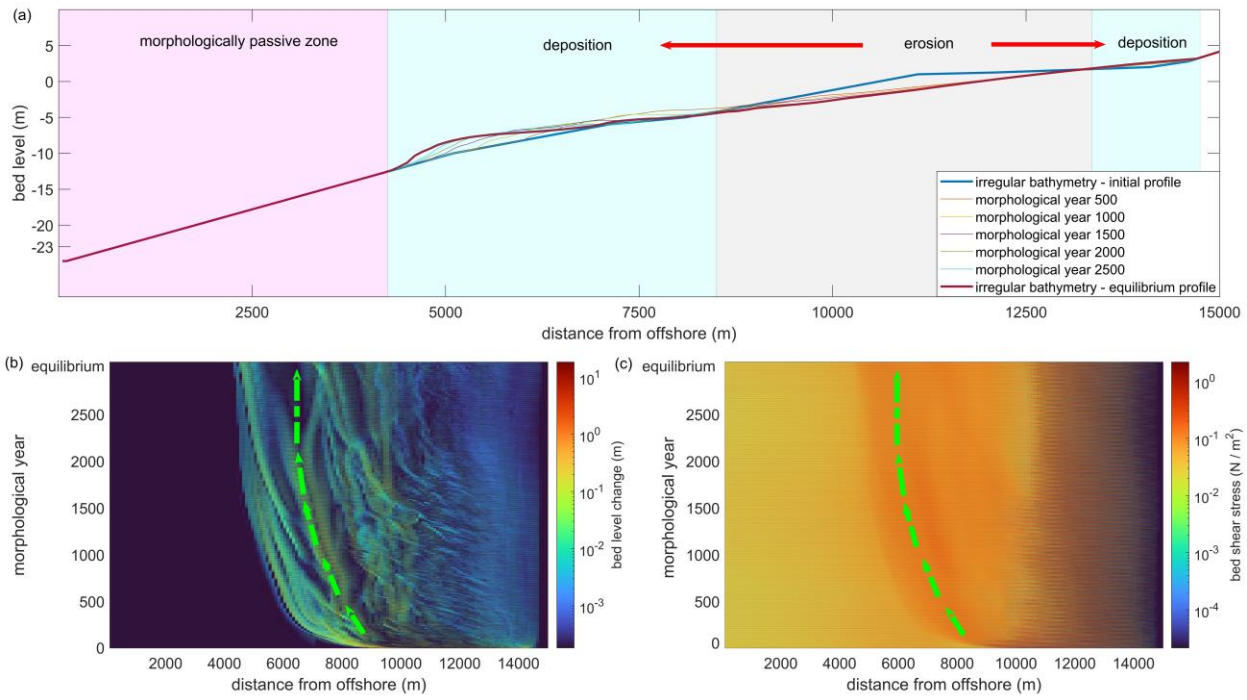

Figure 3. 12 (a) The width-averaged profile evolution, for the model run with an irregular initial profile and sand sediment. (b) Bed level change per year for the model run with an irregular initial profile and sand sediment. (c) Bed shear stress for the model run with an irregular initial profile and sand sediment. The green line shows progression of the zone with highest bed level change in the domain (shown on panel a).

The difference in the way our sandy profiles reach equilibrium becomes significant when the effects of SLR are explored, where the profile is moved from equilibrium by an external force. There are many recent studies on resilience of tidal coastal environments under the effects of SLR, most showing accretion. For example, Dronkers (2005) show that SLR leads to larger water depth and increasing flood dominance, generating a landward residual sediment transport and sediment accretion so that the bed adjusts to a new shallower equilibrium condition. With this conclusion and without considering the effect of bed profile, we should expect infilling. However, Friedrichs et al. (1990) show that the response of the bed to SLR depends on the local geometry so that some bathymetries fill in faster during SLR and some other will flush more efficiently. Our results support this work; the initial bed condition is critical in predicting the resilience of tidal flats to SLR effects. Note that we neglect local and seasonal events that alter the equilibrium condition, which would alter the response in an unknown way.

In reality, the response to SLR will be highly dependent on sediment supply. We did not attempt the SLR simulations for the mixed sand and mud configurations because our results show such sensitivity to loading at the boundary that SLR is probably not the dominant driver of climate

change response. Sensitivity to loading has been shown in many previous studies. For example, Ganju and Schoellhamer (2010) and Elmilady et al. (2019) studied morphological changes of Suisun Bay and San Pablo Bay, respectively, under several SLR scenarios and none of the cases had deposition rates that were high enough to keep pace with SLR and most of inter-tidal areas struggled to adjust their elevation to SLR rate. Similarly, Van Goor et al. (2003) used a model named ASMITA in order to predict the response of tidal environments to SLR and they concluded that survival of these inter-tidal areas depends on if sediment import matches SLR rate. There are interesting subtle changes in the distribution of sediments (encapsulated by our three equilibrium profiles which are similar but differ in detail), that occur as the coastline responds to SLR. The irregular and concave-up bathymetries both degraded with SLR, whereas sediments accreted in shallow regions in the convex-up profile.

3.5. Conclusion

We ran process-based simulations with the Delft3D morphodynamic model to investigate the role of initial bathymetry in shaping the pathway to equilibrium of tidal environments. Idealised models were created with the intention of simulating development of fringing tidal flats and growing bed features that occur along coasts in both sandy and mixed mud/sand tidal environments. Pathways to equilibrium were different for the three-case study initial geometries, differences which would be highly relevant to establishing ecological conditions, and which in turn, affected the way that they reacted to SLR. When sandy tidal flats are forced by SLR after reaching the equilibrium state, irregular and concave-up initial profiles degraded within upper inter-tidal and shallow areas, but convex-up profile accreted. These upper inter-tidal regions are particularly important to coastal ecosystems, because they are areas where vegetation grows. Tidal asymmetry, residence time and residual sediment transport in equilibrium states were observed to be more dependent on sediment type and forcing and functioned similarly in the three case study profiles. In contrast, aspects like equilibrium profile shape, tidal prism, energy dissipation and resilience under SLR (for the sandy case) were dependent on initial profile shape. Given that the conditions under which tidal coasts are evolving change constantly, the way in which a profile responds to equilibrium is critical to determining how resilient that coastline and it is associated ecosystems are to future conditions.

Chapter 4: Observations of Flow Pathways around a Recently-Colonised Estuarine Mangrove Shoal

Amin Rahdarian[1,2], Karin R. Bryan[1], Mick van der Wegen[3,4]

[1] School of Science, Faculty of Science and Engineering, University of Waikato, Hamilton, New Zealand.

[2] Institute of Geosciences, Christian-Albrechts-Universität Zu Kiel, CAU, Kiel, Germany

[3] IHE-Delft Institute for Water Education, Delft, Netherlands.

[4] Deltares, Delft Netherlands.

Contribution of Authors:

Chapter 4 presents "Observations of Flow Pathways around a Recently-Colonised Estuarine Mangrove Shoal", to be submitted to *Marine Geology*. Field measurement in Whitianga Estuary was planned by Amin Rahdarian with the advice from Karin R. Bryan and Mick van der Wegen. Karin R. Bryan, Ben Stewart, Chris Morcom, Ted Conroy and Wagner Costa assisted in the field for measurements and sampling. I wrote the initial draft and it was edited based on my co-author's feedbacks.

Abstract

Large sediment loading to the coast can accelerate estuarine infilling, which promotes the establishment of salt marshes or mangroves. Bio-geomorphic feedback ensues where channels and shoals gradually evolve in tandem as the vegetation gains a foothold. The aim of this work is to explore the governing dynamics on a recently evolving estuarine, mangrove-covered channel-shoal system in Whitianga Estuary, Aotearoa New Zealand. Observations of water level, flow velocity, suspended sediment concentration and bed sediment characteristics were used to infer flow asymmetry and sediment transport pathways around the shoal. Historical images were combined with the measurements to qualitatively link the observed, short-term processes to the influence of expanding vegetation on multi-decadal evolution. Comparisons of flow asymmetry in two contrasting drainage channels (in close proximity) on the shoal show that rapid colonisation by mangroves can quickly change the flow asymmetry from flood to ebb dominant. Although mangroves opportunistically colonise the higher ground at the centre of the shoal, they become eco-engineers creating their own environment as evidenced by the abrupt change in sediment textural environment, even outside the immediate area of new vegetation. Although many studies have focused on spatial flow patterns associated with mangrove vegetation, our observations show evidence of the speed at which colonisation fuels geomorphological change.

4.1. Introduction

Intertidal flats are morphological features of many estuaries worldwide. They help protect the hinterland against erosion and flooding by attenuating waves, provide valuable ecosystem services and comprise unique habitats (Bouma et al., 2016). Estuarine intertidal areas are often morphologically complex, characterised by locally-elevated regions, tidal levees, and intersecting features like drainage channels, chutes and off-cuts (Elmilady et al., 2020; Friedrichs, 2011; Hanssen et al., 2022; van Dijk et al., 2014). This morphology plays an important role in the way that tidal water is exchanged between the estuary and fringing vegetated ecosystems, ultimately regulating supply and release of matter like sediments, nutrients, and contaminants. The formation of intertidal shoals is associated with morphodynamic instability where a positive feedback between hydrodynamics and morphology leads to development of estuarine shoals (Elmilady et al., 2020). The shape of the shoal evolves with the interplay between tidal currents and river discharge (van der Wal et al., 2002; Wu et al., 2020), mediated by wind waves (Elmilady et al., 2022; Zheng et al., 2021), sediment supply and transport dynamics (McLachlan et al., 2020; Rahdarian et al., 2022). In addition, vegetation attenuates waves and redirects flow and associated morphological processes (Swales et al., 2019; Woodroffe, 1992; Young and Harvey, 1996). The estuaries' larger scale morphology determines the location of intertidal shoals to a large extent (Dam et al., 2016; van der Wegen and Roelvink, 2012).

Mangroves are as strikingly dominant influence on estuarine intertidal morphology in many parts of the world. Mangroves are halophytic and are common in tropical and subtropical regions of the world (Woodroffe et al., 2016). Due to anthropogenic activities and climate change effects, mangroves have been under threat with a global area reduction rate of 1 to 2% per year (Duke et al., 2007). Contrastingly, mangroves are expanding in New Zealand due to deforestation leading to an increase in fine sediment supply from the catchments infilling the estuaries (Horstman et al., 2018). Mangroves cause complex changes to the frictional drag experienced by estuarine tidal currents (Horstman et al., 2021). Higher stages of the tide are associated with flooding sheet flow, where large areas of the forest are inundated, whereas ebb flow concentrates in drainage channels at low tide (Horstman et al., 2013). In areas of rapid expansion, coastal communities are extremely concerned that the dominant control on flows of colonising mangroves would likely exacerbate infilling rates (Stokes et al., 2023).

Simplified modelling and observations from relatively uniform settings have provided the foundation for understanding dynamics around mangrove-covered areas. Initially, studies were focused on predicting the hydrodynamics within mangrove forests (Kobashi and Mazda, 2005; Wolanski, 1992; Wolanski et al., 1980). Subsequent studies related flow patterns and drag variations to sediment dynamics and sediment trapping inside the mangrove forest (Furukawa et al., 1997; Horstman et al., 2021; Horstman et al., 2013; Knight et al., 2008; Krauss et al., 2003; McLachlan et al., 2020; Schettini et al., 2020). Tidal dynamics are extremely sensitive to spatial friction differences throughout the forest (Horstman et al., 2021). Simplified models have been used to highlight the role of storage space, tidal flat slope and the degree of channelization, in addition to the drag imposed by the vegetation itself (Montgomery et al., 2022; Montgomery et al., 2019). Although many studies have shown the dominant role that mangroves play in sediment accumulation in intertidal areas, recent models have shown that mangroves can reduce sedimentation by diverting sediment-rich flows away from intertidal regions (Xie et al., 2023).

Many of these recent studies have focused on areas where a lack of direct river sediment supply simplified the dynamics. Rivers supply sediments of substantially different character, often in episodic flood events, which are accompanied by substantial reworking of the morphology. When a river debouches into a mangrove dominated tidal fringe, modelling studies show that the dynamics may be complex, as stratified river and estuarine flows mix while fanning out across the high friction vegetated intertidal area (Vundavilli et al., 2021). Field studies confirming these interactions are even more rare.

The overarching aim of this work is to explore the governing dynamics on a recently evolving estuarine mangrove-covered channel-shoal system. The objectives are to (1) determine the detailed tidal hydrodynamics and sediment pathways occurring in the channel, mangrove forest and on the shoal, (2) use this understanding to infer the morphodynamic evolution of the shoal over the decadal timescales during which mangroves have been expanding around the shoal. We use detailed high spatial and temporal resolution measurements of flow, suspended sediment concentration (SSC), sediment flux, and bed sediment characteristics on a small mixed sand and muddy shoal in Whitianga Estuary, Aotearoa New Zealand (Figure 1a). The shoal is located on the inner bend of a tidal river channel, and the contrasting character of two much smaller channels (the shoal channel and mangrove creek) that drain the ebbing water off the shoal. These detailed processes will be qualitatively linked to multi-decadal eco-geomorphological evolution processes by comparison to historical aerial and satellite imagery.

4.2. Materials and methods

4.2.1. Study site

Whitianga Estuary is located on the northeast coast of Aotearoa New Zealand (Figure 1a) and, with an area of 12.9 km^2, it is the biggest estuary in the Coromandel Peninsula (Woods, 2012). The Estuary contains large areas of mangroves, salt marshes and some unvegetated tidal flats. Mangrove expansion has occurred in Whitianga Estuary, but not to the extent observed in other estuaries in the Coromandel (Woods, 2012). Mangroves have likely existed in the Estuary for thousands of years and were documented in the trip of Captain Cook's ship Endeavour in 1796 when he describes Whitianga as a low flat environment covered with mangroves (Horstman et al., 2018). Currently, approximately 5.2 km^2 of the area is covered by mangroves and salt marshes (Reeve, 2008). Our study site is located in the central part of the Estuary (Figure 1a) (36°53'13.08"S, 175°41'40.80"E), and includes the tidal river (the Waiwawa River), a tidal shoal and the mangrove forest (Figure 1a). The study area also includes a mangrove drainage creek within the forest (Figure 1b & 1c) and a shoal channel (Figure 1d). Multiple smaller creeks with different widths and directions within the forest make up a complex morphology.

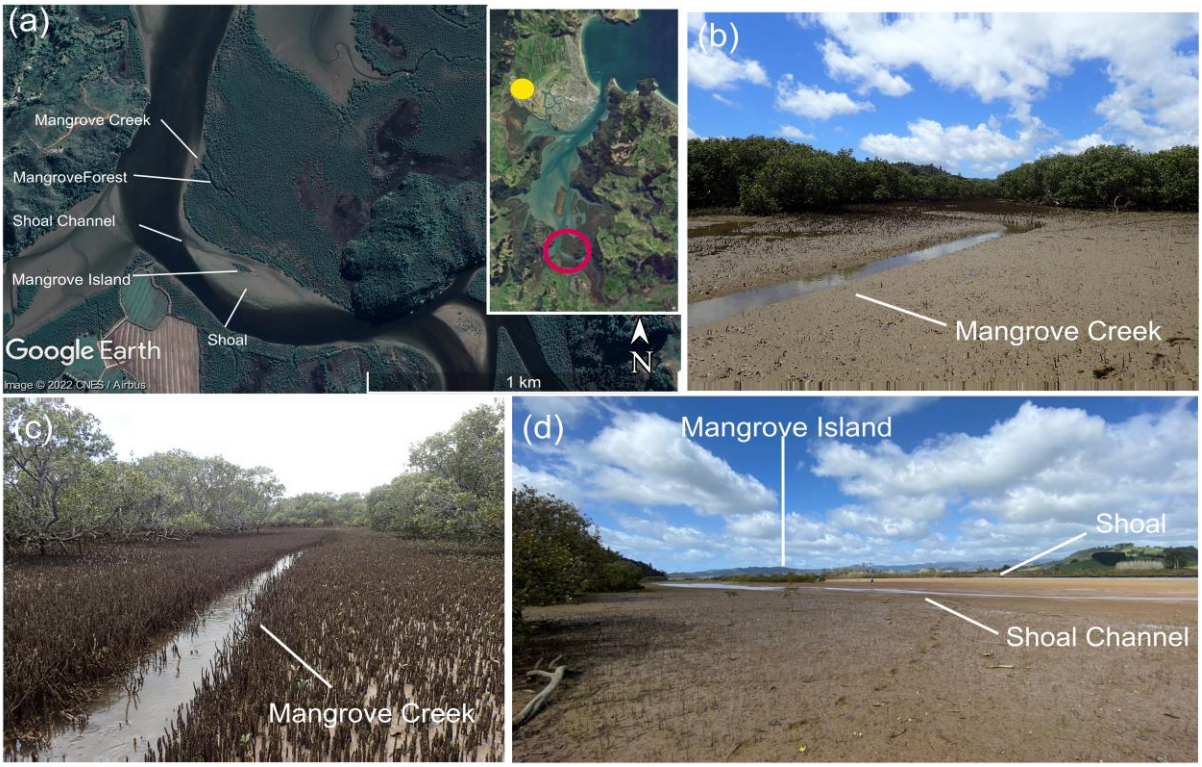

Figure 4. 1 (a) Map showing the location of the site in Whitianga Estuary with red circle on the aerial image provided by Google Earth plus the location of Whitianga weather station that is shown with the yellow circle. (b) Photo taken at the entrance of the mangrove creek. (c) Photo taken inside the forest. (d) Photo of the fringe on the left side, a shoal channel in the middle and the mangrove island at the centre of the image.

4.2.2. Decadal evolution

Since the 1940s, mangrove forests in Aotearoa New Zealand have been progressively expanding (Swales et al., 2015b). This was mainly a consequence of deforestation, which caused infilling of estuaries with fine sediments eroded from the catchments and expanded inter-tidal flats (Horstman et al., 2018; Swales et al., 2021; Thrush et al., 2004). Similar to other estuaries in Aotearoa New Zealand, Whitianga Estuary experienced an increased sediment supply after deforestation of river catchments since mid-19th century which occurred after the settlement of Europeans. This extensive land erosion led to vertical accretion of tidal flats which consequently favoured expansion of mangroves (Horstman et al., 2018; Jones, 2008; Swales et al., 2007). In 1944, mangroves were only present in the north-eastern part of the study site, and the modern-day mangrove creek was a braided shoal channel that developed along the inner bend of the shoal (Figure 2). Establishment of new mangroves on the river side of the shoal channel (which has now changed into the modern-day mangrove creek) started between 1944 and 1966. In 1970, the

newly grown part of the forest became increasingly dense. Between 1970 and 1984, major changes were the establishment of mangroves between the old and the new mangrove area, accompanied by shrinkage of the channel and conversion of the shoal channel into a mangrove creek. During this transition, the shoal channel changed from being wide and braided into its current form of a strongly sinuous, narrow channel. The initiation of the new shoal channel (which remains today) started in the 1980s with formation of a short channel that was deeper and wider at the entrance, which eventually led to a fully incised channel along the inner bend of the shoal. Generally, vegetation has expanded toward the river (Figure 2). However, mangroves have not prograded noticeably since the 1970s except the emergence of the new 'mangrove island' on the shoal that started growing in early 2000. The mangrove island expansion rate has been considerably lower than historic expansion rates in the area. This may be due to catchment sediment supply reduction or because the Estuary is running out of accommodation space.

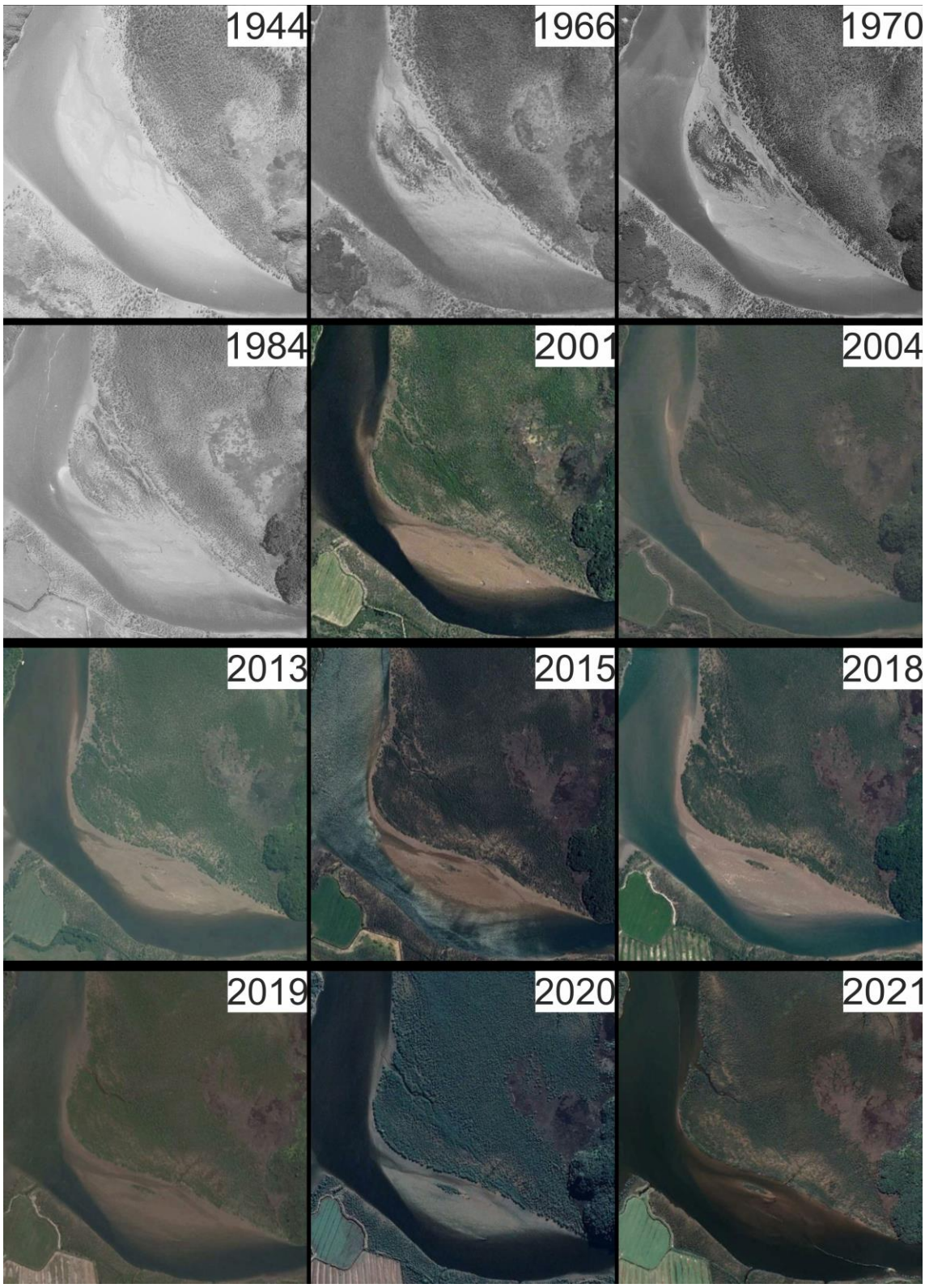

Figure 4. 2 Historical images of the study site between 1944 and 2021 provided by RetroLens (https://retrolens.co.nz/) and Google Earth.

4.2.3. Data collection

Data were collected between 14th and 18th of December 2020 during spring tides with the aim of providing a comprehensive spatial map of current and sediment fluxes over the shoal and new growth areas. Given the complexity of the site, and the limitation on instrument availability, a deployment plan was developed around maintaining a subset of sites stationary and moving another subset of instruments to different locations between tides. This set of spring tides was chosen (1) because there was minimal variation over the week (2 to 10 cm difference between the high tides) (2) because the water level was high enough so that the forest (and instruments) was inundated to a depth whereby the instruments could return clear readings. Vegetation and sediment properties were also sampled over the region. The bathymetry of the forest was derived from LiDAR, surveyed in 2008 by the Waikato Regional Council and Land Information New Zealand (LINZ, 2008). Following Montgomery et al. (2022), within the forest the lowest value of the data elevation point cloud within every 10 m × 10 m area was considered as the topography in order to prevent incorrect bed level measurements caused by the detection of trees. Bed level of the stations located inside the river (not measured by LiDAR) was derived from observations of water depth collected in the river and assuming that the high tide water elevation was the same in the river and on the nearby shoal.

4.2.3.1. Hydrodynamic data

Hydrodynamic data were collected by a set of nine instruments consisting of five Nortek Aquadopps (2 MHz), two Nortek Vectors and two Sontek Tritons (Figure 3). Four of the Aquadopps were deployed in the river (stations R1, R2), entrance of tidal creek (C1) and the entrance shoal channel (B1) for the whole period of field work. The other instruments were deployed at a station for two tidal cycles (one day and one night) and were moved to other locations in the morning for the following two tidal cycles. This approach enabled us to collect data over a total of 17 stations during a 5-day data collection each for two tidal cycles. We named stations that were located around the creek inside the forest as C1 to C5, and those that were around the inter-tidal flat and the shoal as B1 to B11.

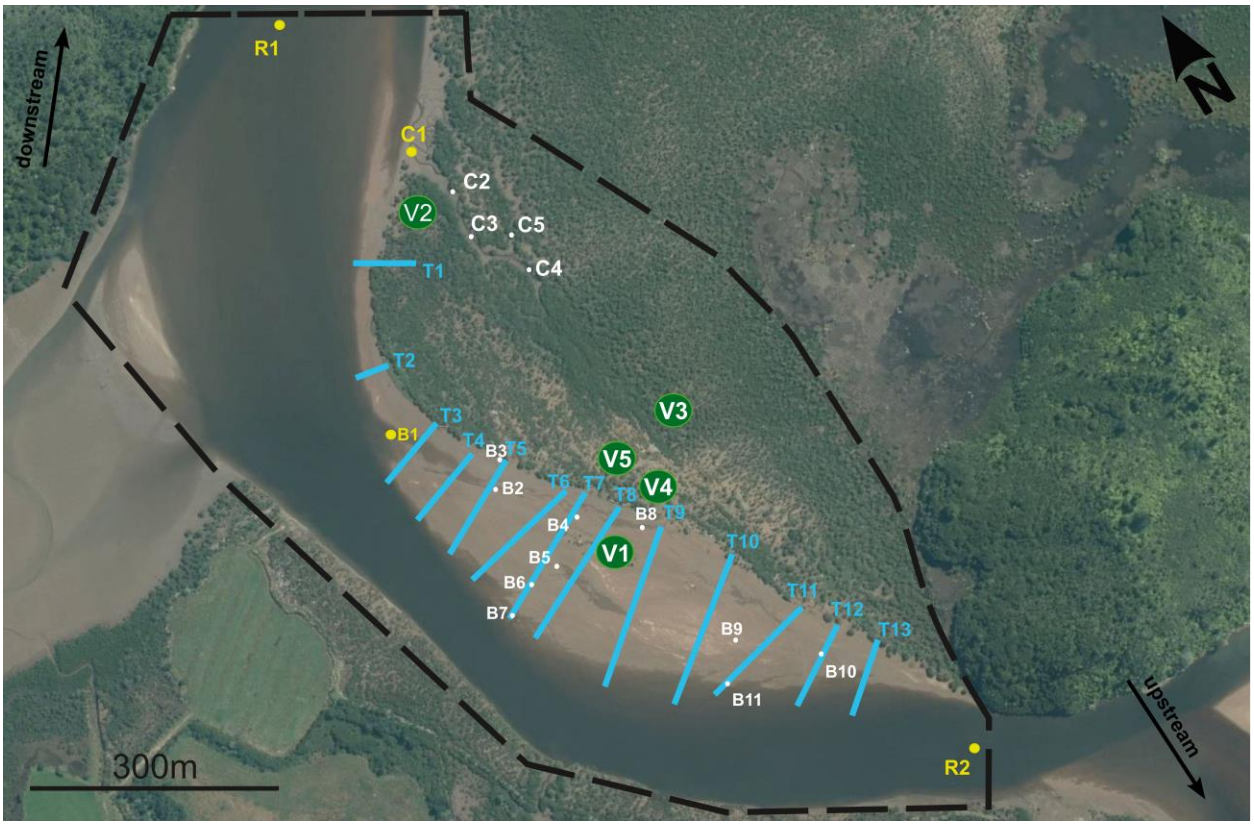

Figure 4. 3 Map showing the location of the river stations (R1-R2), channel stations (C1-C5), shoal stations (B1-B11), vegetation stations (V1-V5) and the T1-T13 transects where sediment samples were collected. Static stations and mobile stations are marked with yellow and white colour, respectively.

Optical backscatter sensors (OBS) were attached to the frames in order to collect information on suspended sediment concentration SSC. Details of station names, deployment locations, and sampling protocols are shown in Table 1 (at stations C5, B3 and B5 there were no OBS sensors connected to instruments). OBS sensors were calibrated separately for each station. The responses of the OBS were converted to SSC by calibrating water samples that were made in the lab with bed sediments collected at each station in the field. This method has been used successfully in previous studies to calibrate the OBS sensors (MacDonald, 2009; Lovett, 2017). First a bucket with a stirring rod was filled with water and the OBS sensor placed in the bucket; sediments were gradually added to the bucket in known amounts. In order to stay in voltage range that was recorded by the OBS in the field, a second OBS sensor was deployed in the bucket, which logged to an external consul. For each deployment site, five water samples with different SCC ranging from the minimum to the highest value of optical backscatter recorded by the OBS sensors in counts (in the field) were extracted in the lab. After that, each water sample was

filtered, dried and weighed in order to determine the SSC of the water samples. The relation between OBS voltage reading and SSC was obtained using a linear regression (the r^2 ranged between 87% and 91%).

Cumulative suspended sediment flux and pathways were calculated using velocity and suspended sediment concentration calculated as $S_{(t_f)} = \sum_{t=0}^{t_f} u_{(t_i)} SSC_{(t_i)}\, dt$ similar to the method in McLachlan et al. (2020) (Initial location X_0 was set at low tide, and was the station location).

Table 4. 1 Details of instrument deployments, locations of sites shown in Figure 2. The Nortek Vectors (NV) were burst sampled, whereas the Nortek Aquadopps (NA) and Sontek Tritons (ST) sampled continuously.

Station	Instrument	Start time	End time	Instrument height above bed	Sampling interval
R1	NA	14th 09:00:00	17th 05:00:00	0.15 (m)	30 (s)
R2	NA	14th 09:00:00	17th 05:00:00	0.15 (m)	30 (s)
C1	NA	14th 09:00:00	18th 09:00:00	0.15 (m)	5 (s)
C2	NV	14th 09:00:00	15th 16:00:00	0.20 (m)	450 burst sampling every 900 (s)
C3	NV	14th 09:00:00	15th 16:00:00	0.20 (m)	450 burst sampling every 900 (s)
C4	NA	14th 09:00:00	15th 16:00:00	0.15 (m)	5 (s)
C5	ST	14th 09:00:00	15th 16:00:00	0.18 (m)	60 (s)
B1	NA	14th 09:00:00	18th 09:00:00	0.15 (m)	5 (s)
B2	NV	15th 16:00:00	16th 14:00:00	0.18 (m)	450 burst sampling every 900 (s)
B3	ST	15th 16:00:00	16th 14:00:00	0.18 (m)	60 (s)
B4	NV	15th 16:00:00	16th 14:00:00	0.20 (m)	450 burst sampling every 900 (s)
B5	NV	16th 14:00:00	17th 17:00:00	0.18 (m)	450 burst sampling every 900 (s)
B6	NV	16th 14:00:00	17th 17:00:00	0.17 (m)	450 burst sampling every 900 (s)
B7	NA	16th 14:00:00	17th 17:00:00	0.10 (m)	5 (s)
B8	NA	15th 16:00:00	16th 14:00:00	0.13 (m)	5 (s)
B9	NV	17th 17:00:00	18th 09:00:00	0.16 (m)	450 burst sampling every 900 (s)
B10	NV	17th 17:00:00	18th 09:00:00	0.17 (m)	450 burst sampling every 900 (s)
B11	NA	17th 17:00:00	18th 09:00:00	0.09 (m)	5 (s)

4.2.3.2. CTD data

At station R1, an RBRconcerto was deployed at the bottom of the river attached to the same frame as the Nortek Aquadopp in order to measure water temperature, salinity and depth during the deployment period. Vertical variations in the water column (used to trace river and ocean water), were collected by a profiling conductivity, temperature and depth sensor (an RBRmaestro) once over the week at R1 and R2 at each of the four tidal stages: 1-low tide 2-incoming tide after low tide 3- high tide 4-outgoing tide after high tide (so 8 surveys in total). In each of these surveys, between 4–5 profiles were collected across the width of the river. Profiles were collected from a single canoe, so a 15-minute delay in time occurred to allow travel between the two stations R1 and R2.

4.2.3.3. Vegetation Survey

The mangrove forest is predominantly composed of *Avicennia marina*, the only species of mangrove that occurs in Aotearoa New Zealand. Mangrove vegetation was characterised at 5 sites shown in Figure 3. Sites were selected based on the age of the vegetation by observing historical aerial images in order to encompass a range of vegetation densities and ages. The vegetation survey consisted of 3 parts (following methods in Horstman et al. (2021) and Montgomery et al. (2018)): trees taller than one meter; trees shorter than one meter; and, pneumatophores. Five selected stations were located on the mangrove island (V1), in the muddy part of the forest close to the mangrove creek (V2), in the older part of mangrove forest (V3), in the denser area on the shoal (V4) and in the less dense area close to the outer fringe (V5). At each site, the number of trees were counted in a 5 m × 5 m quadrat (large quadrat), then height of the trees, stem density and the diameter at 30 cm above the bed were measured for five randomly selected trees greater than and less than 1 m. On the 4 corners and at the centre of the large quadrant, the number of all, and the height and width (bottom, mid, top) of 5 randomly selected pneumatophores were measured in 0.5 m × 0.5 m quadrats using callipers.

4.2.3.4. Sediment samples and mud-layer-thickness measurements

In addition to at the stations where the instruments were deployed, sediment samples were collected (from the top 1 cm layer) with a surface scrape along thirteen transects starting from

inside the forest to the river. The depth of the recent mud layer was also measured using an Edelman auger along the transects. Dried sediment samples were analysed for sediment particle size and organic content. Particle size distribution was measured by the Mastersizer 3000 particle size analyser and sediments were categorized using the median diameter on Wentworth sediment classification (Wentworth, 1922). Organic matter was measured using the loss-on-ignition method. Samples were first placed in the oven for at least 2 hours at 101 °C and weighed. After initial drying, samples were transferred to the furnace at 550 °C for 4 hours, then cooled to room temperature and weighed again (Dean, 1974). Organic matter loss-on-ignition percentage was calculated based on equation given below:

$$LOI = \frac{af - ds}{af} \times 100$$

Where LOI is the carbon matter percentage based on loss-on-ignition method, and af is the weight of the sample after taking out of the furnace and ds is the dried sample weight.

4.2.3.5. Data processing

Low quality hydrodynamic data were removed when the signal-to-noise was below 50 counts for Nortek Aquadopps and Vector current meters, and below 70 counts for Sontek current meters (Horstman et al., 2021). Data collected when the instrument was out of the water, and when cells within the profile were out of the water, were removed. Velocity was recorded in relative x-y-z direction and in situ external compass bearings on each instrument were used to rotate the velocity data to true north and east. Velocity data were depth-averaged and magnitude was calculated as $\sqrt{u^2 + v^2}$ (which *u* and *v* are eastward and northward velocities, respectively) and a positive/negative sign was assigned to the velocity magnitude based on the flooding/ebbing tide. The flood and ebb tide were specified as follows: a positive velocity in x or eastward direction (a negative velocity in x or westward direction) for stations located within mangrove forest, and a negative velocity in y or southward direction (a positive velocity in y or northward direction) for stations located in the river was considered to be flooding (ebbing) tide. Sampling protocols are listed in Table 1 and were chosen to maximise resolution within the restrictions of battery life. This study is focused on tidal flows rather than waves (which were not present) and turbulence, and so Nortek Aquadopp and Sontek data were low-pass filtered, and the Nortek Vector data were burst-averaged.

Water level was derived from pressure variations measured by each sensor, assuming hydrostatic pressure. The bed elevation of the stations on intertidal zone was converted to depth relative to MSL by using the river stations to determine local MSL and assuming that the water surface gradient was zero at high tide. Local atmospheric pressure was removed using atmospheric observations from the NIWA database (https://cliflo.niwa.co.nz/) (Horstman et al., 2021). The pressure sensors were also affected by variations in temperature within the instrument housings. Because most of the stations are located in inter-tidal zone and the instruments were out of water and exposed to air during low tides, a relationship between temperature logged inside the housing and pressure could be derived using a polynomial fit and used to correct timeseries for this temperature effect (Figure 4).

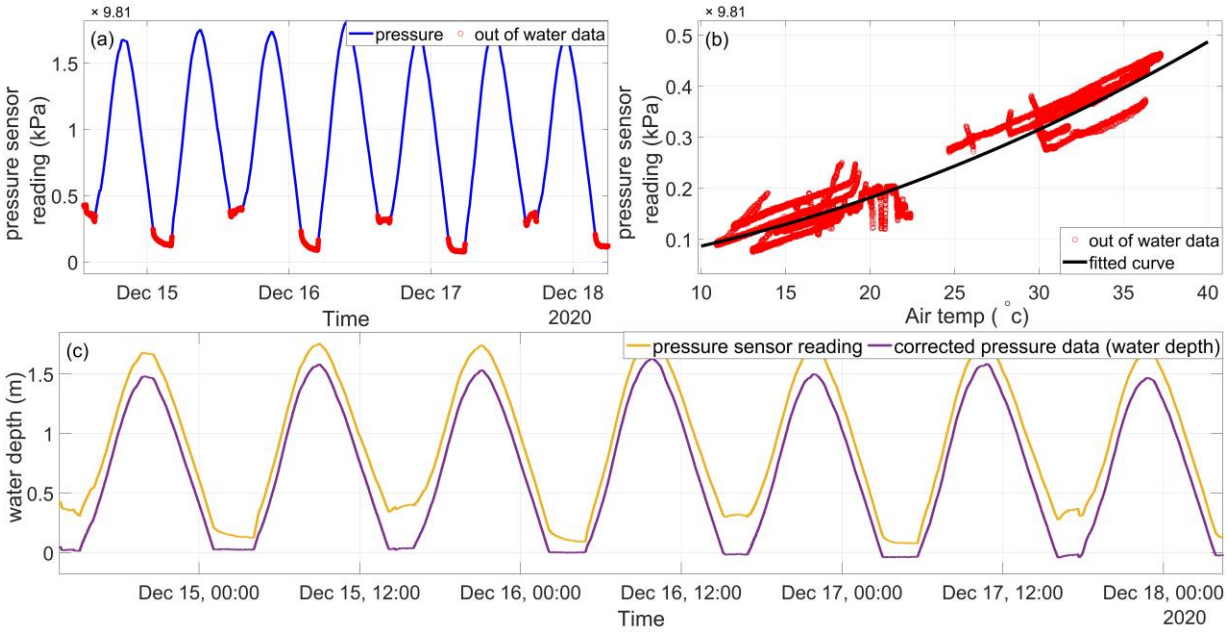

Figure 4. 4 (a) Water depth timeseries prior to correction for the Aquadopp that was deployed in station B1. Out of water data marked in red. (b) Polynomial fit of water level data to temperature when exposed. (c) Comparison between water level prior to and after temperature and atmospheric pressure corrections were applied.

4.3. Results

4.3.1. Water level and flow velocity

The largest tidal constituent at the entrance to Whitianga Estuary is the semi-diurnal M_2 and the two other dominant constituents are S_2 and N_2 (constituents were extracted from the NIWA tidal

model output https://tides.niwa.co.nz/, using the Utide Matlab software). The tidal range during the experiments was nearing spring (Figure 5). Given that average elevation of the forest was approximately 0.5 meters relative to MSL, the inundation depth within the forest was ~0.5 meters. The currents in the river channel were mostly tidal (with very little asymmetry, Figure 5-a2) and the amplitude of spring tides was approximately 1.9 m. At the river stations, tidal current reached 0.6 m/s during flood and 0.45 m/s at ebb tide (higher velocities at station R2 relative to R1 were observed during flood tide, which may be due to across-river variations). Station C1 was located at the entrance of the mangrove creek draining the forest and currents were concentrated over a short duration during ebb tide, with similar peak velocities to the ones observed in the river channel, up to 0.4 m/s during ebb tide. At the stations located around the shoal (B1-B11), in general, higher velocities were observed at the stations that were located in the shoal channel (0.4 m/s at B1) and close to the edge of the shoal (0.6 m/s at B7), compared to an average of ~0.25 over the centre of the shoal. Currents attenuated over a short distance within the mangrove creek, from 0.12m/s (flood) and 0.55m/s (ebb) to 0.1 m/s (flood) and 0.15 m/s (ebb), which is a ~0.72% reduction (at ebb) over 95 metres.

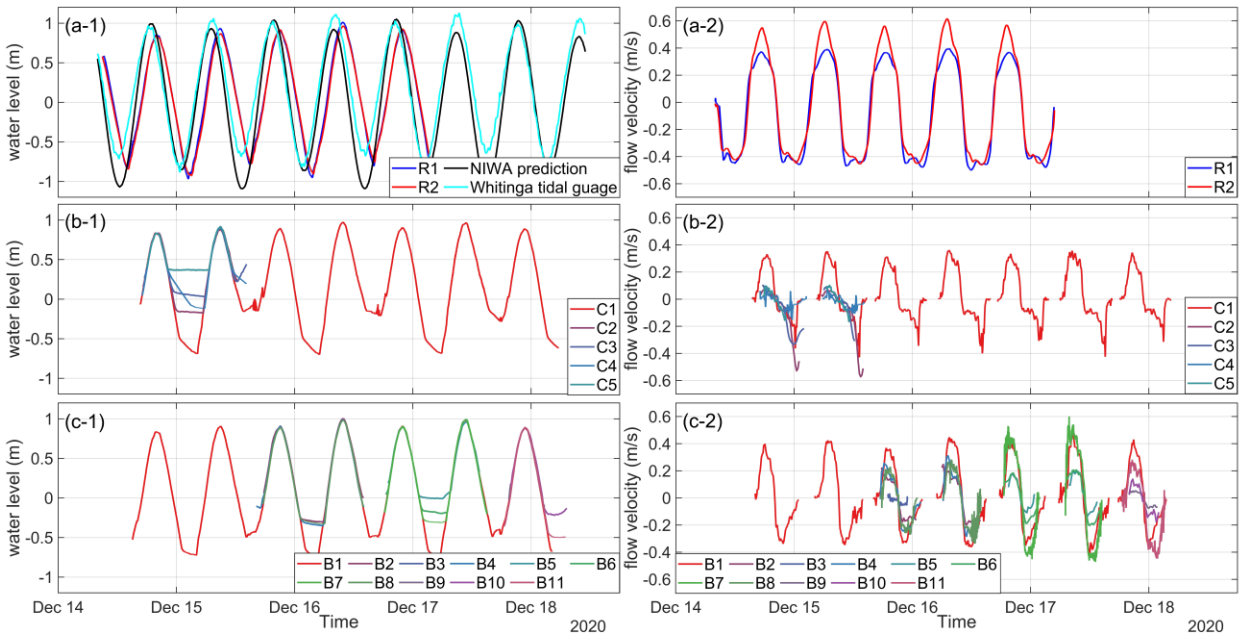

Figure 4. 5 (a-1) Water level variations at stations R1-R2, from the Whitianga tidal gauge and tides predicted by the NIWA tidal model. (a-2) flow velocity at stations R1-R2. (b-1) Water level variations at stations C1-C5. (b-2) flow velocity at stations C1-C5. (c-1) Water level variations at stations B1-B11. (c-2) flow velocity at stations B1-B11.

4.3.2. Environmental conditions

Environmental conditions during the week of observations were consistent between days, justifying the sampling regime where spatial coverage was achieved by moving a proportion of the instruments between days. Figure 6a shows which stations (locations shown in Figure 3) were occupied at which times. Salinity measured by the RBRconcerto at R1 station ranged from 13 PSU at low tide to more than 30 PSU at high tide and the patterns varied with the tide (Figure 6b). Water temperature varied throughout the tide and with air temperature, ranging from 16 to 23 °C (Figure 6c). Daily low and high air temperature were relatively similar over the 5-day field work campaign ranging from 10 °C at the end of the night to 27 °C towards the end of the day (Figure 6d). No substantial wind or precipitation events occurred. The wind speed reached 6 m/s in late afternoon, dropping at night (Figure 6e), and the Waiwawa river level stayed relatively constant within a 2 cm range (Figure 6f).

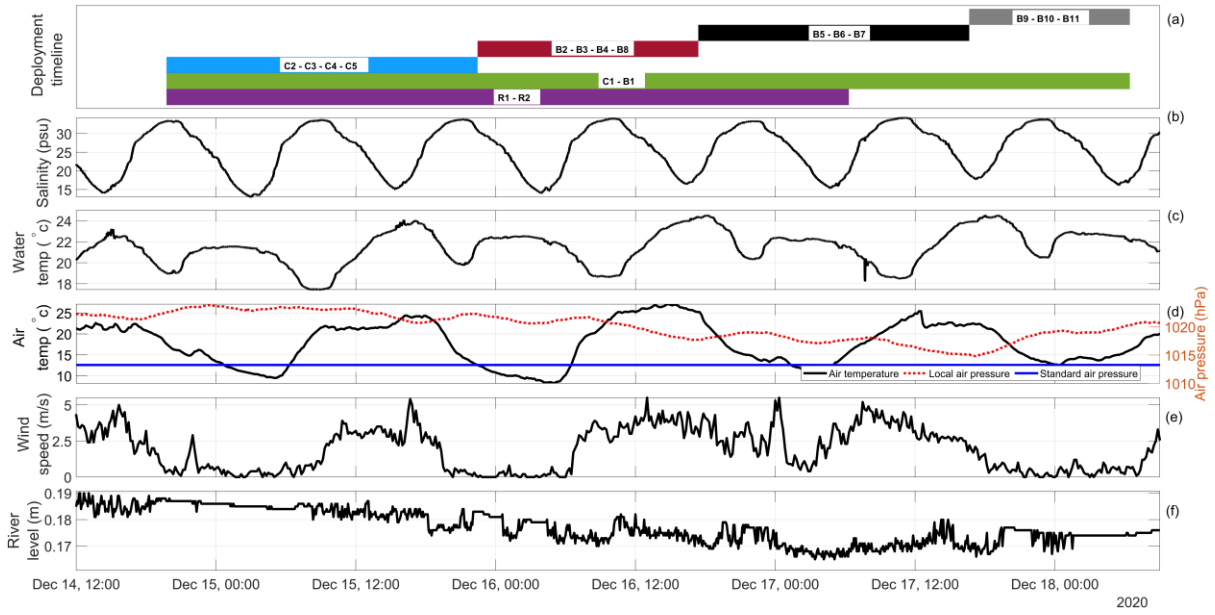

Figure 4. 6 (a) The deployment duration for each instrument. (b) Water salinity measured by RBRconcerto in the river station R1. (c) Water temperature measured by river RBRconcerto at station R1. (d) Air temperature, local air pressure and (e) wind speed sourced from NIWA climate station (https://cliflo.niwa.co.nz/) that is located in the Whitianga Estuary. (f) The Waiwawa river water level measured at 36°56'12.63"S, 175°40'28.19"E every 5 minutes above assumed local datum provided by Waikato Regional Council (https://www.waikatoregion.govt.nz/).

4.3.3. Tidal variability in river water characteristics

The temperature and salinity characteristics of river water provided insight into the sources of water at each stage of the tide, whether from the main channel, or draining from the adjacent vegetated tidal flats. During high tide (Figure 7, a1 and a2), oceanic water is more dominant and salinity reaches 32 PSU. The water is relatively well mixed with very slightly lower temperature and higher salinity (denser water) observed at deeper points. On the ebbing tide, the salinity declines (Figure 7b) as the salty water is advected seaward to be replaced by river-sourced water. At station R1, water is well mixed with the temperature and salinity close to 22 °C and 26 PSU, respectively. However, at the upstream station R2, there is salinity-driven stratification, which ranges from 20 PSU at the surface to 25 PSU at the bottom (b1 and b2), as fresh river water flows out at the surface. At low tide (Figure 7, c1 and c2), salinity drops to a brackish 19 PSU compared to high tide. Water at the downstream station R1 is more saline than R2. Water at R2 is well mixed but at station R1, the water column is slightly stratified in temperature. After low tide (Figure 7, d1 and d2), on the late afternoon flooding tide, strong stratification occurred both in temperature and salinity at the lower station R1 since the incoming seawater water intrudes at greater depth and is not well mixed with freshwater. At the upper station R2, stratification existed only in salinity. Note that the low tide and incoming tide profiles are taken at the end of the day, when water advected from shallow regions of the estuary would have heated up over the day.

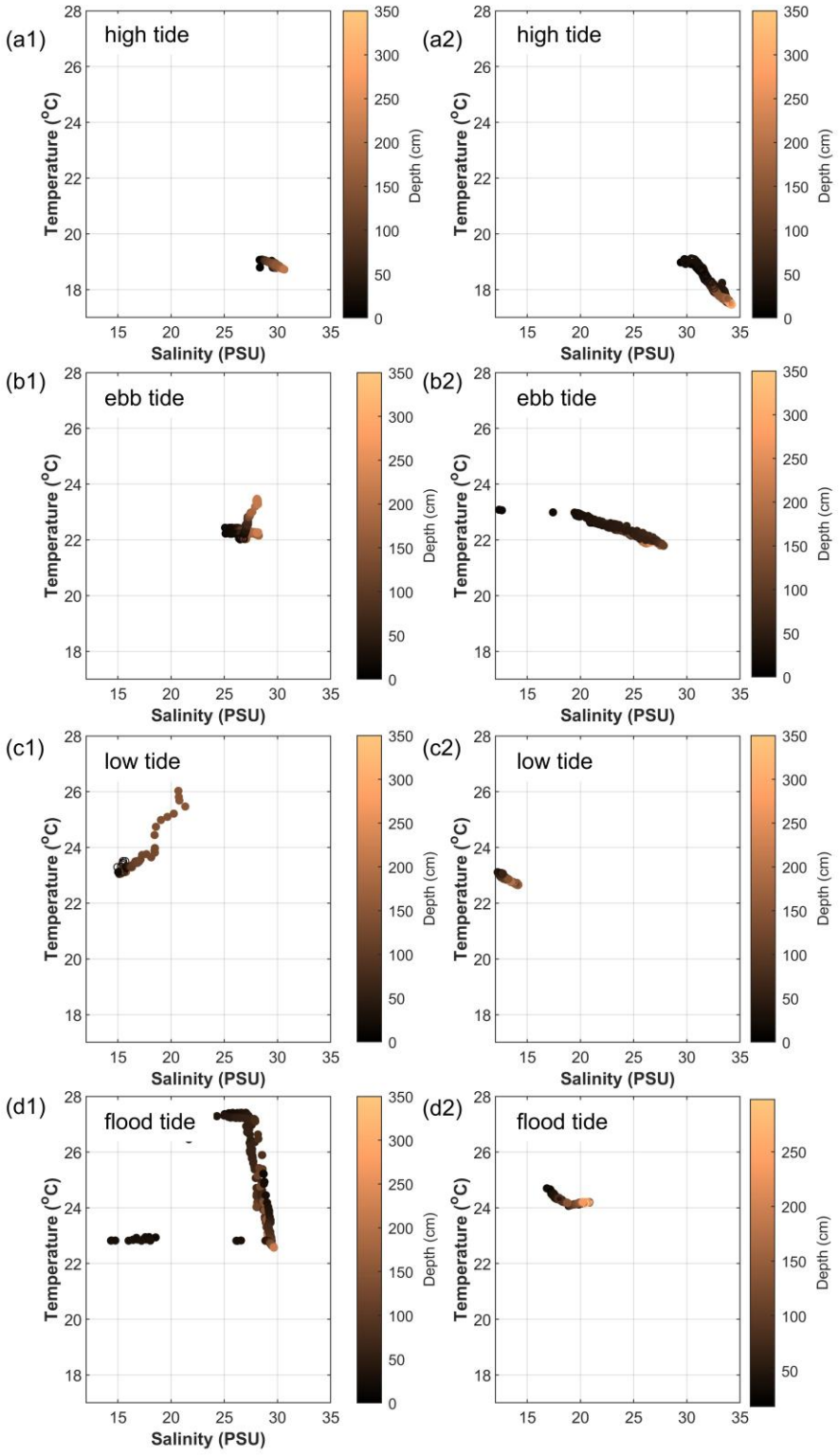

Figure 4. 7 Temperature-salinity variations over the water column (colorscale, blue=surface, red=deeper) showing all the profiles collected at each river station lower R1 (left column) and upper R2 (right column) during (a) high tide at 8:30 am (b) outgoing tide before low tide at 8:30 am (c) low tide at 2:50 pm (d) incoming tide after low tide at 5:40 pm (profiles were taken on different days, adjusted for the change in the timing of the tide).

4.3.4. Vegetation

Mature trees with heights of more than one meter were found mostly at station V3, which represents the oldest part of the forest. However, in general, the height, width and diameter of trees taller than one meter was greater at station V2 compared to the other stations, indicating that trees grew more upward in the mature forest and more outward nearer the fringe. There were no trees shorter than one meter at stations V2 and V3, and the forest at site V1 was the densest, covered by short trees with the average height of 90 cm. However, the width, the diameter and the number of stems for short trees was greater at stations V4 and V5 compared to the “mangrove island”. Highest average pneumatophore widths were found in stations V2 and V1, respectively. However, the density of pneumatophores was higher at stations V4 and V5. Pneumatophores at stations V2 and V1 were the tallest and shortest with a height of 66.5 mm and 29.8 mm, respectively. The height, density and width of the mangrove trees and pneumatophores were not the same across the forest (Table 2) confirming that development rate was not the same all over the study site.

Table 4. 2 Shows the result of vegetation survey. Note that pneumatophore height and width were calculated based on 5 randomly-chosen.

		Station				
		V1	**V2**	**V3**	**V4**	**V5**
Trees >1 meter	Density ($1/m^2$)	0.20	0.16	0.48	0.40	0.20
	Height (m)	1.80	3.60	3.10	2.70	1.60
	Width (m)	2.10	3.30	1.60	1.90	1.30
	D30 (mm)	57.20	114.75	68.30	108.40	33.50
	N_{stem}	2.40	1.750	2.60	1.40	2.60
Trees < 1 meter	Density ($1/m^2$)	0.16	NONE	NONE	0.04	0.12
	Height (m)	0.90			0.70	0.90
	Width (m)	0.50			0.70	0.53
	D30 (mm)	12.25			21	14.50
	N_{stem}	1.50			2	2.67
Pneumatophores	Density ($1/m^2$)	232.80	424.80	365.33	477.60	447.20
	Height (mm)	29.78	66.50	48.52	64.37	59.16
	$Width_{bottom}$	6.51	6.83	5.50	6.35	5.82
	$Width_{mid}$	6.00	6.46	5.65	5.92	4.78
	$Width_{top}$	4.78	5.20	4.39	4.81	3.92

4.3.5. Sediment texture and mud layer thickness

Observed mean grain size on the edge of the shoal was larger than close to the fringe and inside the mangrove forest. Sediments in the top layer of the mangrove creek and inside the forest were similar, mainly silt with a similar mean grain size. However, lower organic content was observed in the creek which increased landward. In general, sediments fined landward with the exception of the shoal channel, which consisted of medium and coarse sand sediments. There was a positive relationship between the organic carbon percentage and mud layer thickness, and vegetation cover. Loss-on-ignition measurements showed 2.6 % organic content in sediments with close proximity to the main river channel and up to 13.2% in sediment samples collected inside the forest. Between the fringe and the mangrove island, organic carbon ranged from 3% to 13%. Mud

layer thickness on the shoal was zero except for the points that were close to the mangrove island (Figure 8a). On the edge of the mangrove forest and inside the mangrove island, the thickness of the mud layer ranged from 30-50 cm. At the innermost site inside the forest, where vegetation was dense, a 58 cm mud layer was measured (Figure 8b). Note that the mud layer thickness and the texture near the mangrove island and near the fringe of the main forest was more similar to the characteristics of the mangrove areas than the shoal areas, showing how the influence of mangroves extends beyond their immediate vegetative footprint.

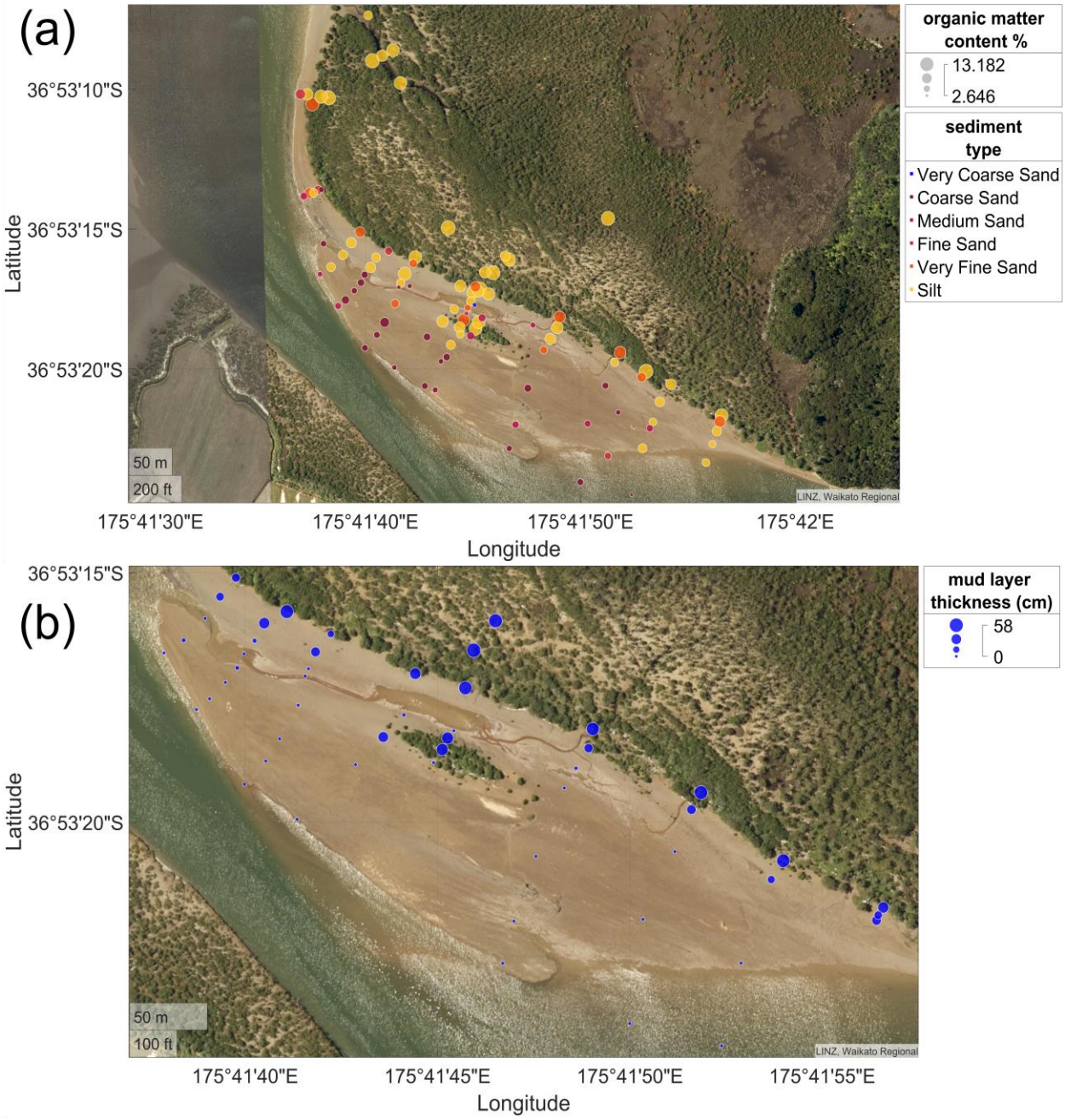

Figure 4. 8 (a) Map of the spatial variation of sediment texture and organic content percentage of the top layer of the sediment. (b) Spatial distribution of the mud layer thickness. Background photos are from Land Information New Zealand.

4.3.6. Stage-velocity curves and SSC

The shoal, forest and channels shaped the flows and sediment transport pathways that occurred in the region, causing substantial spatial variability. To illustrate this, Figure 8 shows the stage-velocity curves coloured with SSCs (where available). In addition, the direction and magnitude of the peak flow at each station is shown with cyan and red lines symbolising flood tide and ebb tide, respectively. At the river stations, the direction of the flow during ebb and flood was along the channel. At both river stations, flow speed was generally lower than 0.6 m/s with slight asymmetries. Peak currents were observed before low tide during ebb at both stations, however at flood tide, velocity was highest before high tide and at mid tide for stations R1 and R2, respectively. Although higher velocities were observed in station R2 compared to R1 at flood tide, higher SSC was observed at station R2. Apart from these peaks, concentrations were generally similar. For the stations that were located inside the mangrove creek, the direction of the flow during ebb and flood was along the fairly sinuous mangrove creek. Currents are weaker compared to the main river, except for station C2 ebb flow. At station C5 inside the forest, the direction of the flow was almost perpendicular to the creek as water drains from the forest to the stream. Along the mangrove-dominated creek, the suspended sediment concentrations increased toward the edge of the forest, and were larger on the ebbing tide. Direction of the flow at flood and ebb tide changed dramatically over the scale of ~20 m for the points located on the shoal. In general, for the points that were located on the fringe close to the forest and inside the shoal channel (stations B4 and B8), water flowed in and drained out by the shoal channel and the direction at flood tide and ebb tide was landward and towards the river channel, respectively. For the points that were located on the edge of the shoal, the direction at flood tide and ebb tide was along the river channel with southeastern and northwestern directions, respectively. Between shoal stations, highest SSCs were observed at B1 in the shoal channel.

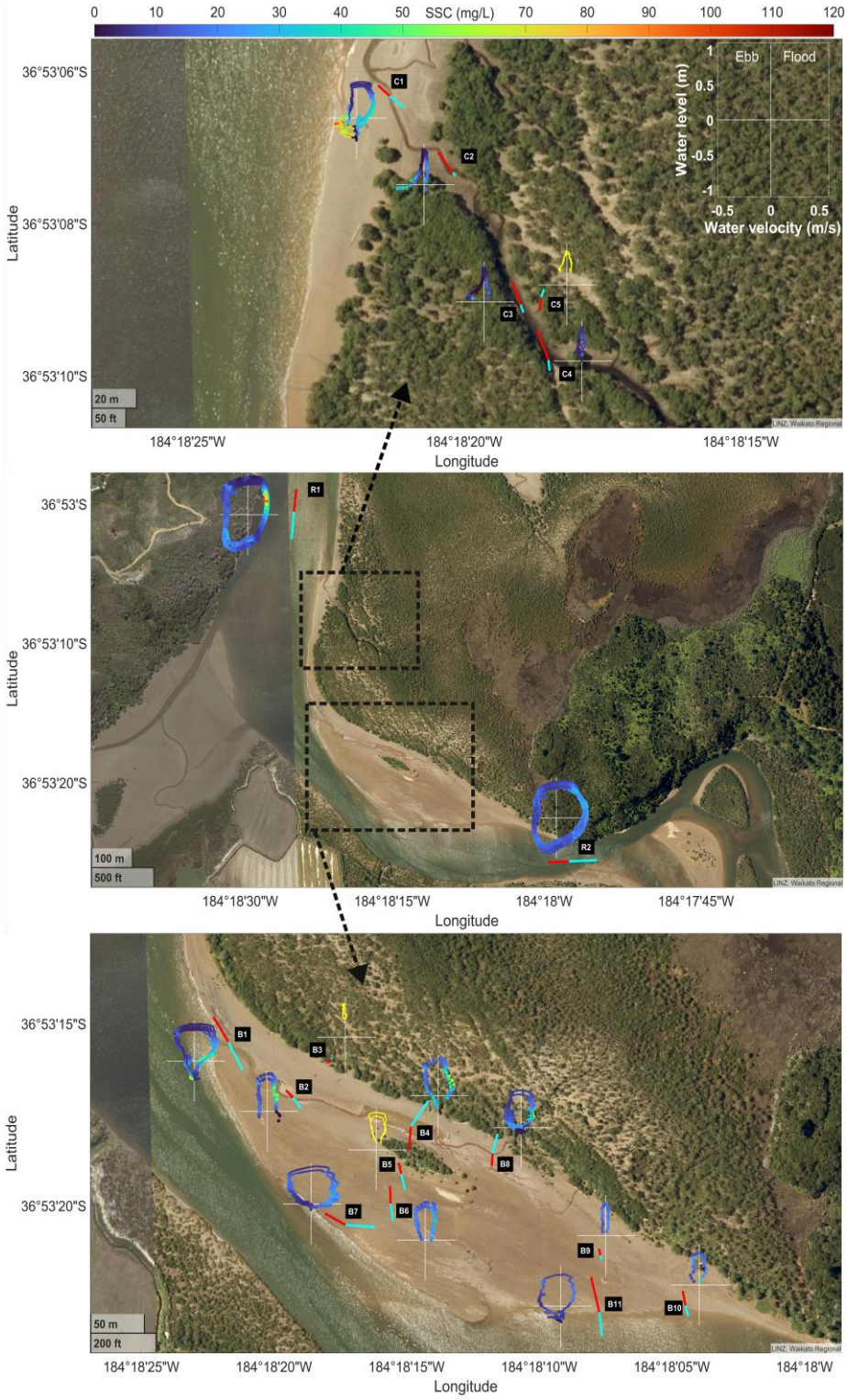

Figure 4. 9 The stage-velocity curves coloured by SSCs at channel stations (top panel), river stations (middle panel) and for the shoal stations (bottom panel). The curves that are plotted in plain yellow did not have collocated turbidity sensors. The cyan and red lines at each site represent magnitude and orientation of peak ebb (red) and flood (cyan) currents. Curves (to be read anti-clockwise over time) are offset from the station locations which are located at the centre point of the cyan and red lines.

4.4. Discussion

4.4.1. Evolution of the forest

Recent observational studies have presented different hypotheses for mangrove establishment and their role in eco-geomorphological evolution of estuarine systems. Studies on colonization of mangroves of Westernport Bay, Australia suggest that establishment of mangroves starts when the morphological (bed elevation) and ecological conditions are suitable and the presence of mangroves promotes sediment trapping and further accretion (Bird, 1986). Swales et al. (2015a) used sediment cores and historical images to reconstruct the multi-decadal evolution of the mangroves in the Firth of Thames (New Zealand). Their results confirmed that the expansion of mangroves seaward is dependent on environmental conditions being established seaward (mainly favourable inundation characteristics by sediment deposition) and that the mangroves do not noticeably improve sedimentation only by their presence. Conversely, other authors e.g., Willemsen et al. (2016) and Friess et al. (2012) showed evidence that mangroves trap and accumulate fine sediment, and so create the environment that is conducive to their establishment. Are mangroves opportunistic colonisers or as engineers creating their own environment?

Analysis of the photographic records of the large-scale decadal evolution of the shoal allows us to observe the conditions under which colonisation first occurred. Lateral expansion of the shoal occurred before the colonization of mangroves (Figure 2- 1944). In both shoal-colonisation events, mangroves first colonised the centre region of the shoal (Figure 2- 1966 & 2001), perhaps to avoid the higher energy conditions, lower bed level and longer inundation periods that occur in the shoal channel, expanding laterally through time. Although, fine sand and silt were found on the upper layer of the bed in both vegetated and unvegetated parts of the shoal (Figure 8a), the mud layer thickness was higher in the parts where mangroves established (Figure 8b), and increased as the forest became denser in the established areas (pneumatophore density at the fringe is nearly double that of the recently colonised patch, V1 in Table 1). This suggests that, under conditions of mud supply, mangroves begin by creating their own micro-environment, enhancing entrapment and accumulation of mud on their substrate, and the regions immediately surrounding them. Although mangroves seem opportunistic colonisers in first instance, our observations show that once established they quickly take on an eco-engineering role, creating their own environment.

4.4.2. Suspended sediment transport and pathways

The existence of the shoal imprints a pattern on the processes which ultimately triggers the creation of mangrove-friendly environment. The stage plots and the cumulative sediment fluxes paint a consistent picture of the processes around the shoal. The initial conduit of sediment is the flood-dominant river currents bringing sediment rich flow through the main river channel from the wider estuary seaward of the field site (Figure 10, the flooding cumulative sediment fluxes are greater than the ebbing tide). Even though the currents are ebb-dominated at the lower station R1 (Figure 11b) and the duration of falling tide is longer than rising tide (Figure 11d), the net sediment flux after one tidal cycle is positive, showing that net movement is in an upper river direction. At the edge of the shoal, the flooding currents move sediment across the fringe (Figure 10a, sediment fluxes at B7 and C1), while the ebbing currents are more aligned along the creeks and channel. The lack of stratification of the ebbing tidal water at station R1 just river-ward of the mangrove creek compared to station R2 (Figure 7-b1&b2) confirms the role of the creek as a conduit of ebbing flow.

The stage plot can be used to infer different types of asymmetries, some more relevant for sand movement, and some more for the fine fractions (Hunt et al., 2015). The combination of sediment fluxes directed into the forest, and the drop in currents at high tide, particularly along the mangrove creek (Figure 9, C1-C5) means that there is sufficient time for fine sediments to fall from suspension while they are transported landward (Hunt et al., 2015); therefore fines are likely deposited in low energy zones inside the mangrove forest or on the shallow parts of the shoal, which provides an explanation of why this location might be first to be colonised by mangroves (Figure 2). At the edge of the dense vegetation, incised by the mangrove creek, the long low energy time at high tide shows that there is plenty of time for the finer fraction to settle out. In addition, the attenuation of currents over a short distance, means that once settles, the ebbing currents at the more landward location would be insufficiently strong to resuspend and move the sediment seaward. Settling of fines in a landward direction is associated with a reduction in currents landward (described in Postma, 1961) combined with a long slack water duration at high tide (described in Dronkers, 1986), both effects occur along the mangrove creek (C1-C5). In contrast, coarser sediments are found inside the main river channel, the shoal channel and on the edge of the shoal (Figure 8a) due to strong currents, which stay strong even at high tide, allowing

little opportunity for fines to settle here. This can be observed in stage-velocity curves at stations R1, R2, B1 and B7 (Figure 9) where the curve is flat at high tide, indicating a short slack duration and a little available time for settlement of fine sediment (Hunt et al., 2015). Settlement of coarser fraction at the shoal edges (Figure 8) may also be due to levee formation when coarser particles settle faster than finer material when the shoal is initially flooded (note the drop in energy between station B7 and B6, at the location of the levee). Again, the currents are less energetic toward the centre of the shoal, which is an indicator of on-bank transport (e.g., Hunt et al., 2015).

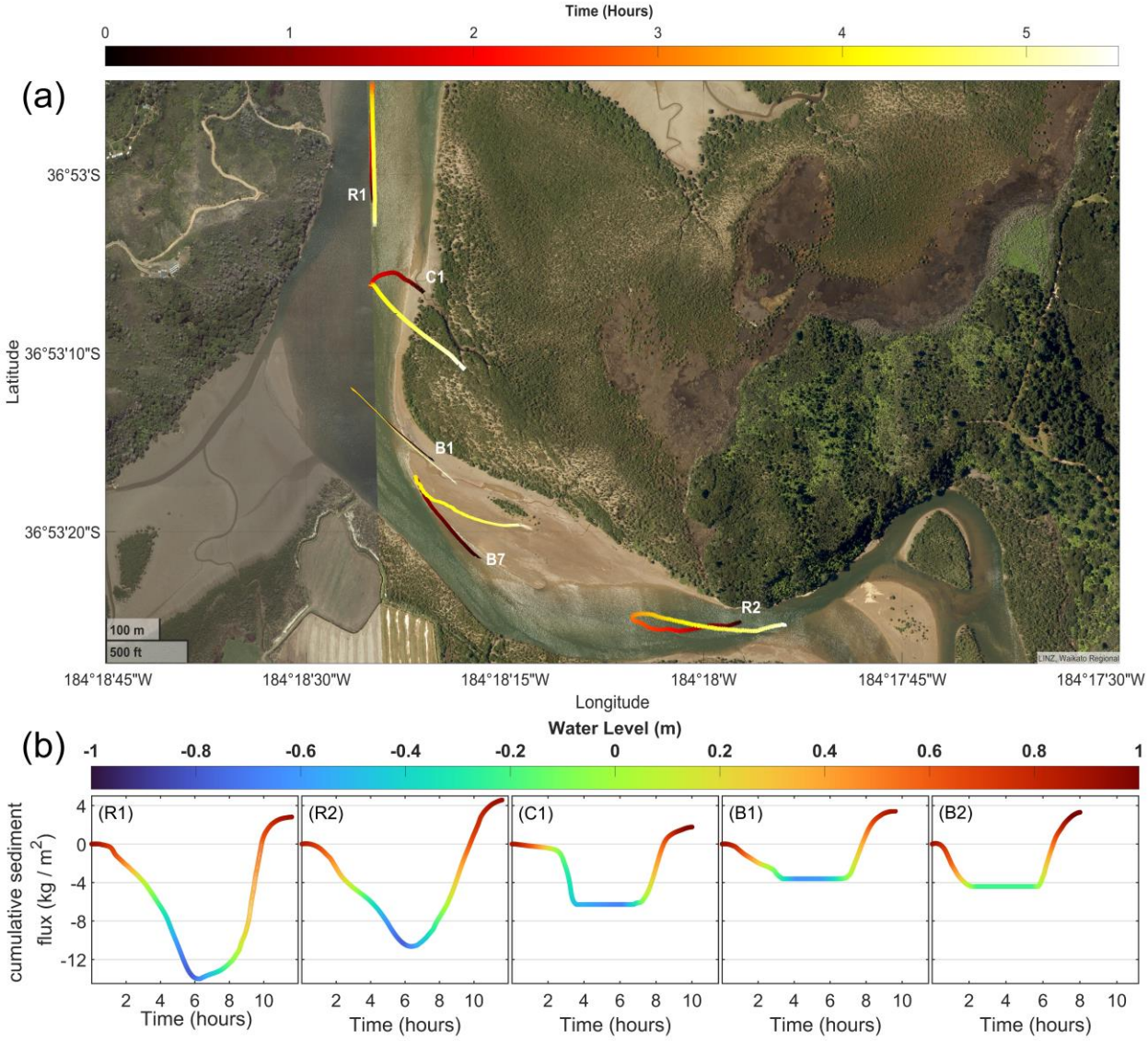

Figure 4. 10 (a) Shows the cumulative suspended sediment flux at each station to infer sediment transport pathways (for one tidal cycle starting from high tide to high tide, coloured with time series, black at the start and white at the end of the tidal cycle) and (b) cumulative sediment fluxes during one tidal cycle at stations R1, R2, C1, B1 and B7, negative is seaward. In panel b, the points are coloured by the elevation of the tide.

4.4.3. Tidal and flow asymmetry

A critical process shaping the net sediment fluxes is the occurrence and spatial variations in tidal and flow asymmetries. Asymmetries can be studied using a number of approaches such as calculating the ratio of peak velocities during ebb and flood tides (Hunt et al., 2015, de Ruiter et al., 2019), the water level skewness (Nidzieko, 2010), and the relative amplitude and phases of the M4 overtide (Friedrichs and Aubrey, 1988). The latter asymmetry is caused by distortion of the tidal wave, which can also be quantified by duration of the ebb and flood currents which we use here because our timeseries are insufficiently long for tidal harmonic analysis. In the absence of residual flows, these methods should generally provide consistent results because flood dominance caused by a higher peak velocity at flood tide results in shorter duration of flood tide and the ebb dominated flow with higher peak ebb current is an indicator of shorter duration of falling tide (Dronkers, 1986; Kumbier et al., 2022). However, in a complex inter-tidal vegetated shoal system where topographic steering is strong and in the presence of river flow these indicators may not be consistent. Interactions between diurnal and semi-diurnal tide can also cause flow asymmetries, but these are not evident during the one-week observation period (Figures 4 and 7). For the river stations, at the upper station R2, there is a slight flood dominance with flow asymmetry ~ 1.3 as there is a higher peak flood velocity and the duration of flood is shorter than ebb with the ratio ~ 0.8 (Figure 11b & 11d). Contrastingly, the duration of ebb is larger than flood at station R1 (11d), but currents are ebb-dominated (Figure 11b). In estuarine systems, this outcome has sometimes been connected with the effects of the river discharge (Friedrichs and Aubrey, 1988), although, in that case, both R stations should show the same behaviour. Following Kumbier et al. (2022), this may also be due the drainage of vegetated zones surrounding R1 influencing flow asymmetry in the main channel. Indeed, the strong temperature differences of the deep and shallow water at R1 of low tide (Figure 7-c1) supports the conclusion that the water here is advected off the shallow vegetated tidal flats where it heats up during the day (which cannot be observed at R2).

The direction of the flow during flood and ebb tide and flow asymmetry at shoal stations suggest that a uniform understanding of flow asymmetry cannot be assigned in such complex environments and hydrodynamic conditions observed at a single point, or few points (e.g., Fricke et al. (2017) and Bryan et al. (2017)), will give a poor representation of the whole system (Kumbier et al., 2022). Our results show that flow and tidal asymmetries may vary substantially over a scale

of about 20 m on the shoal. In all shoal stations except station B3 (which is located inside the mangroves close to the edge of the forest), asymmetries with ratios between 0.5 and 1.5 are observed (Figure 11b). Some points remain quite symmetric (stations B4 and B6), some are ebb-dominated (stations B3, B8, B9, B10 and B11) while flood-dominance can also be observed (at station B1, B2, B5, B7). The shape of stage-velocity curves varies over the study site, which indicates that each station functions according to its local conditions including morphology, vegetation and hydrodynamics (Figure 9).

Because station C1 is located outside the forest with sparse vegetation, currents are mainly governed by the same processes as station R1 inside the main channel (Figure 11b). Similar observation was reported by Horstman et al. (2013) that stated at sparsely vegetated zones, hydrodynamics are susceptible to the flow outside the vegetation. However, during ebb tide, the first velocity peak does not occur at C1 and also the duration of flood and ebb is lower due to limited river flow impacts and bed level differences (Figure 9 & 11d).

Similar to the findings of Horstman et al. (2021), we observe that flow asymmetry at stations inside the creek were mostly dominated by the large-scale hypsometry and the vegetation rather than the creek geometry. All the channel stations inside the creek and the mangrove forest are ebb-dominated by the ebb/flood velocity ratio, although the duration of the ebb is longer than flood (Figure 11b & 11d). Lowest asymmetry was observed at station C1, which is located at the entrance of the creek outside the forest and the highest asymmetry was observed at station C2 located inside the creek close to the edge of the forest (Figure 11b). Among the stations that were located in the creek within the forest (stations C2, C3 and C4), we observe that ebb duration asymmetry increases landward (Figure 11c) whereas tidal flow asymmetry decreases landward (Figure 11b) which is associated with decreasing of the peak velocity at ebb (Figure 11a). This behaviour is consistent with the observations of similar studies in mangroves and salt marshes (Horstman et al., 2021; Stark et al., 2015; Willemsen et al., 2016). Inside the shoal channel, flood-dominance decreases from the entrance (station B1) to the middle part (station B4), and the flow converts to ebb-dominance at the head of the channel at station B8 (Figure 11d).

4.4.4. Channel functional shift

As with many locations in New Zealand over recent decades, the study area has been subjected to excessive sediment supply due to deforestation in the river catchment (Horstman et al., 2018).

As a result, the estuary has been filling in and the river stretch between R1 and R2 has narrowed due to the shoal expansion. Historical images (Figure 2) show that before lateral expansion of mangroves, the modern-date mangrove creek was a once a shoal channel (here we define a shoal channel as a small sandy channel that separates the shoal from land, which drains the shoal of ebbing tidal water). The shoal channel has similar morphological characteristics to a chute cut-off channel (defined as a channel that forms on the inner bend of a floodplain which leads to closure of the old abandoned channel by sediment deposition (Eekhout and Hoitink, 2015)). In our case, historical images revealed that it the shoal channel is not a remnant of a former river channel, but formation likely initiated during reworking of the bed by draining water from the evolving shoal. After establishment of mangroves, the shoal channel evolved quickly into a mangrove creek, while a new shoal channel initiated in the 1980s, with the creek eventually evolving to a meandering fully-incised channel. As the shoal evolved to a creek, flows would have evolved from flood-dominated to ebb-dominated, since the modern date shoal channel and the mangrove creek were entirely flood-dominated and ebb-dominated, respectively (Figure 9 & 11b). This shift in channel function is associated with mangrove expansion increasing friction in the forest and impacting water and sediment circulation and geo-morphodynamic development (D'Alpaos et al., 2007; Temmerman et al., 2005). Vegetation growth probably caused not only the shrinkage of the present time mangrove creek, but also promoted a regime shift from a flood dominant channel to an ebb dominant creek.

Presumably, the dynamics of the present-day shoal channel will gradually transition to reflect the mangrove creek through time, as the colonising vegetation on the shoal expands and exerts a greater frictional effect on the ebbing tide. The shoal would reach a friction-mediated ‘tipping point’, which would start a gradual shift to ebb dominance in the shoal channel, ultimately starting a process of scour and channel incision. As mangrove roots extend into the channel and the mangrove platform flattens (as is commonly observed, Bryan et al. (2017)), the draining flows slow, contributing to an increase in sinuosity. Glover et al. (2022) show that changes to channel sinuosity can accompany changes to the extent of mangrove dominance (in their case caused by anthropogenic removal). In summary, the emergence of new vegetation on inter-tidal flats can impose a control on the morphology and hydrodynamics of channels, which ultimate causes a regime shift in the way in which the channels function.

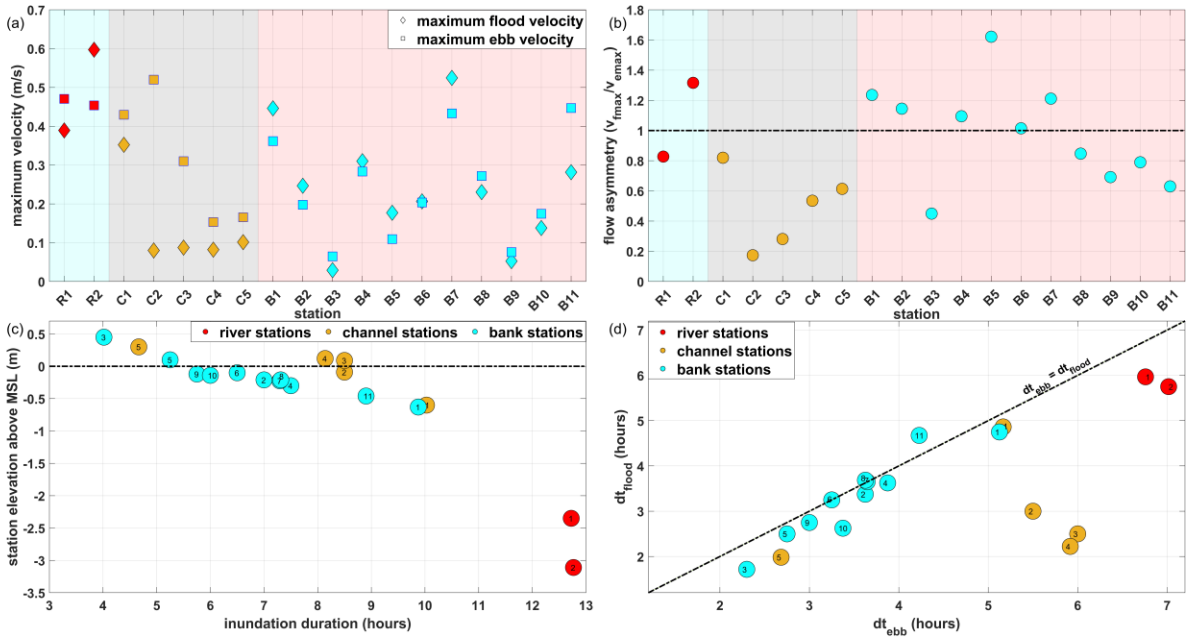

Figure 4. 11 (a) Magnitude of velocity at ebb and flood (b) Tidal velocity asymmetry (V_{fmax} and V_{emax} are maximum speed at flood and ebb tide, respectively) (c) duration of inundation during each tidal cycle and station elevation above mean sea level (d) duration of ebb and flood for each station.

4.5. Conclusions

Here we presented field observations around a mangrove shoal that characterise flow, suspended sediment concentration (SSC), sediment flux, and bed sediment characteristics at high spatial and temporal resolution. We observed that the direction of the flow during flood and ebb tide changes dramatically over the scale of ~20 m which suggests that understanding such complex environments, requires a detailed measurement of hydrodynamics since observations of a few points cannot be representative of the whole system. Moreover, we showed how vegetation can affect the hydrodynamics of the channels by presenting flow patterns of the main river channel and two other drainage channels (the mangrove creek and the shoal channel) that, although located only ~200 meters away in the same estuarine system, exhibited entirely different functions. Observations within these channels suggest a regime transition may occur in channel function as the forest expands, mediated by colonising vegetation on the shoal. Furthermore, the historical aerial and satellite images show that although lateral expansion of the shoals can occur prior to colonization of mangroves, our in-situ measurements show that even small areas of colonising mangroves can enhance trapping and deposition of mud if sediments are available.

Chapter 5: The impact of mangroves on tidal circulation and asymmetry in an estuarine channel-shoal system

Amin Rahdarian[1,2], Karin R. Bryan[1], Mick van der Wegen[3,4]

[1] School of Science, Faculty of Science and Engineering, University of Waikato, Hamilton, New Zealand.

[2] Institute of Geosciences, Christian-Albrechts-Universität Zu Kiel, CAU, Kiel, Germany

[3] IHE-Delft Institute for Water Education, Delft, Netherlands.

[4] Deltares, Delft Netherlands.

Contribution of Authors:

Chapter 5 presents "The impact of mangroves on tidal circulation and asymmetry in an estuarine channel-shoal system", to be submitted to *Geomorphology*. The Whitianga Estuary field data was collected in December 2020 by Amin Rahdarian with the assistance of Karin R. Bryan, Ben Stewart, Chris Morcom, Ted Conroy and Wagner Costa assisted in the field for measurements and sampling. Whitianga Estuary model was created by Amin Rahdarian with the direction and advice from Karin R. Bryan and Mick van der Wegen. I wrote the initial draft and it was subsequently edited based on my co-author's comments.

Abstract

This study explores the controls on landscape-scale tidal hydrodynamics around an estuarine shoal covered with mangroves. We developed and validated a hydrodynamic model based on a site where mangroves have recently expanded onto a shoal in Whitianga Estuary (Aotearoa New Zealand). Model results clearly reveal areas of ebb and flood dominance in the model domain, where mangrove surrounded creeks are ebb dominant and shoal incising channels are flood dominant. Within the forest, the seaward part of mangroves is ebb-dominated in contrast flood-dominance toward the back of the forest where mangroves at higher elevations are mostly observed. Removing vegetation led to a large-scale change in flow routing and tidal asymmetry with flood dominant creeks whereas when creeks were infilled, local changes were observed only around the location of the creeks. In order to investigate the multi-decadal role of mangrove expansion on local channel hydrodynamics historical images of the site were used to re-create the forest structure and bathymetry in 1944. Model results on the 1944 reproduced bathymetry show that the expansion of mangroves caused a regime shift of the channels. The ebb-dominated modern-date mangrove creek was once a fully flood-dominated shoal channel in 1944 prior to colonization of mangroves in the inner bend of the shoal.

5.1. Introduction

Channel-shoal systems are a fundamental component of morphology in estuarine environments. Their formation is associated with morphodynamic instability where positive feedback between tidal hydrodynamics and morphology leads to development of stable estuarine shoal-channel patterns (D'Alpaos et al., 2005; Fagherazzi and Overeem, 2007; Hughes, 2012; van der Wegen and Roelvink, 2012; Elmilady et al., 2020; Hanssen et al., 2022). Tidally driven water containing sediments, nutrients and contaminants is exchanged between estuarine channels and flats, salt marshes and mangrove forests (Temmerman et al., 2007). Channel-shoal patterns are an essential component to ecosystems and estuarine morphology is inherently mediated by the growth of vegetation such as seagrass, mangroves and saltmarsh.

Mangroves are a type of salt-tolerant vegetation that often evolves on inter-tidal shoals in sub-tropical region estuaries. Mangroves develop under complex hydrodynamic and salinity conditions (Bryan et al., 2017; Woodroffe et al., 2016). Riverine mangroves are characterised by a wide and flat forest expanding on floodplains alongside banks of rivers while the currents in these systems are mostly tidal (Kobashi and Mazda, 2005). During flood, tidal flow first inundates the channels (creek flow) and then overtops the creek bank, flowing into the forest (sheet flow). During ebb, water in the forest is conveyed to the creeks and then flushes out of the system (Kobashi and Mazda, 2005; Mazda and Ikeda, 2006; Horstman et al., 2013).

Tidal channels (also referred to as courses or creeks) are widespread and abundant in intertidal environments, in particular, those characterised by mangrove forests. Channels are a major flow pathway for water, sediments, pollution and other material between the inner and outer part of tidal flats (Kearney and Fagherazzi, 2016). They affect short-term, tidal timescale hydrodynamic circulation and sediment exchange as well as long-term morphodynamic evolution (Stefanon et al., 2010). In general, the formation of tidal channels is initiated when movement of water over the tidal flat during flood and ebb is not efficient. Mangrove creeks are usually initiated when water begins to converge in lower friction areas at ebb, and with time, channels are scoured by erosional processes (Wolanski et al., 1980; Wolanski, 1992; Furukawa et al., 1997). Contrastingly, other types of channels in estuarine systems can be triggered by flooding events intersecting the sinuosity of the river channels and taking the most efficient route (Zinger et al., 2013; van Dijk et al., 2014). The physical “services” provided by these channels can be quite different depending

on their geomorphic context. For example, mangrove creeks are consistently identified to be ebb-dominated, where stronger ebb currents erode coarser sediments and keep the channels scoured, whereas in many cases channels in unvegetated environments are observed to be flood-dominated with larger flood velocities (Wolanski et al., 1980; Friedrichs, 2011; Horstman et al., 2021). Hence, it is unlikely that a channel intersecting an intertidal flat conveys similar ebb and flood flows (Friedrichs et al., 1992; Kumbier et al., 2022a).

Numerical models of estuarine shoals covered with mangroves are rare because of the spatial coverage of water levels and flow velocity data required to calibrate and validate such models. The modelling work by Wolanski et al. (1980) was one of the first to describe the hydrodynamics in mangroves forests. Following on, the interaction between tidal creeks and vegetation was studied by using a simplified, schematic or analytical models (Mazda et al., 1995; Furukawa et al., 1997; Aucan and Ridd, 2000; Mazda et al., 2005). Although these studies isolated the fundamental flow dynamics of vegetation-creek interaction, detailed simulations of vegetated inter-tidal enviroments, calibrated and validated with field observations, have not been possible until recent developement of advanced numerical models and measuring equipment. Now, with use of numerical tools, there are studies spanning, for example, the interplay between tidal currents and river discharge (van der Wal et al., 2002; Guo et al., 2014), the formation of channel-shoal systems in general (Elmilady et al., 2020; Elmilady et al., 2022), the mangrove-creek interaction (Wolanski et al., 1980; Mazda et al., 2005), flow routing in vegetation (Temmerman et al., 2005; Horstman et al., 2013; Horstman et al., 2015), sediment exchange and sedimentation in mangroves (Willemsen et al., 2016; Bryan et al., 2017) and water level attenuation in mangroves (Montgomery et al., 2022). However, these studies generally focus on simpler areas, for example with no direct river source or with spatial domains consisting of only the vegetated part of the shoal. In reality, complex flow patterns will exist at many scales, where small scales processes may not correctly be reflected in low-resolution landscape-scale studies and models (Elmilady et al., 2022).

In this work, we use a Delft3D model to explores the role of vegetation and channel presence on the hydrodynamic circulation end morphodynamic evolution of a mangrove covered estuarine shoal. The system reflects a natural setting (Whitianga Estuary, Aotearoa New Zealand) which includes a river channel, shoal channel, mangrove creeks, and vegetated and un-vegetated shoal areas. The model is calibrated and validated using water level and velocity data measured during

a one-week instrument deployment. First, the model is used to explore large-scale short-term tidal flooding patterns and flow routing over the estuarine shoal. Second, two scenarios are designed to assess the relative impact of vegetation presence (mangroves) and tidal creeks on landscape-scale hydrodynamics and tidal asymmetry. Finally, field data and historical images are combined in a scenario recreating estimated conditions in the 1940s (associated with the earliest image data) to infer the effects of mangroves on shaping estuarine morphology. The third scenario is specifically focused the transition of channel dynamics accompanying the expansion of mangroves post 1940. Our hypothesis is that vegetation cover plays a crucial role in the large-scale hydrodynamic circulation and resulting morphodynamic evolution of the estuarine shoal.

5.2. Material and Methods

5.2.1. Study Site

The complex shoal system used for this study lies in the Whitianga Estuary, located on the northeast coast of Aotearoa New Zealand. It is the biggest estuary in the Coromandel Peninsula (Figure 5.1a) with a total area of 12.9 km^2 (Woods, 2012) and it contains mangroves, salt marshes and tidal flats. Despite a global reduction trend of mangroves (Duke et al., 2007), they are expanding in Aotearoa New Zealand because of land use change in the recent decades has increased the sediment supply and consequently led to rapid tidal flat expansion (Horstman et al., 2018; Swales et al., 2021). Currently, the coverage of halophytic vegetation is approximately 5.2 km^2 (Reeve, 2008). The study site is located 6.5 km from the mouth of the estuary (36°53'13.08"S, 175°41'40.80"E) (Figure 5.1b) and consists of a part of a channel, a shoal, and a mangrove forest with multiple creeks (Figure 5.1c).

Figure 5. 1 Shows (a) the location of the Coromandel Peninsula and Whitianga Estuary. (b) The location of the study site in the estuary. (c) A satellite image provided by Maxar Satellite Imagery of the mangrove forest, the river channel, and the shoal.

The mangrove forest consists of three parts: the inner area of the forest that developed pre-1940, the edge of the forest that started growing in the 1940s, and a newly grown mangrove island that emerged around 2002 (marked in Figure 5.1c and Figure 5.2c). A shoal intersecting channel has been surrounded by mangrove expansion between 1940 and 2002 so that it evolved into a mangrove creek. A new shoal intersecting channel developed at the southern mangrove forest edge. Multiple creeks of different dimensions and directions within the forest make a complex morphology.

Figure 5. 2 (a) Aerial image from 1944 provided by RetroLens (https://retrolens.co.nz/) that shows the old part of the forest (marked by red dashed line). (b) Aerial image from 2001 provided by Google Earth that shows the part of the forest that started growing since the 1940s (red dashed-new growth, blue dashed-old part). (c) A new mangrove "island" marked with red dashed line can be observed on the aerial image from 2020 provided by Google Earth.

5.2.2. Field measurements, data processing and important features of the landform

In December 2020, measurements were collected focusing around three spots which were believed to play important role in dynamics of the shoal: (a) the shoal channel that floods and drains the water on the shoal and the mangrove island located on the shoal (Figure 5.3a), (b) the mangrove creek that plays a role in water circulation in the forest (Figure 5.3b) and (c) the edge (younger part) of the mangrove forest (Figure 5.3c). Hydrodynamic data were collected over a week fieldwork during spring tides using a set of nine instruments consisting of five Nortek Aquadopps (2 MHz), two Nortek Vectors and two Sontek Tritons between 14th to 18th of December 2020. Four of the Aquadopps were deployed in the river (2-at the upper and lower model boundaries of the river channel), entrance of the tidal creek (1) and the entrance of the shoal channel (1) for the whole period of field work. For the other stations, the approach was to deploy the instruments at stations for two tidal cycles (one day and one night), then move these to other locations in the morning for the following two tidal cycles. The timing of the deployment was chosen so that the tide was very similar for the whole duration of the experiment and was during a spring tide (with amplitude of approximately 1.9 m) so that the mangrove areas were inundated. Table 1 shows the details of instrument deployments.

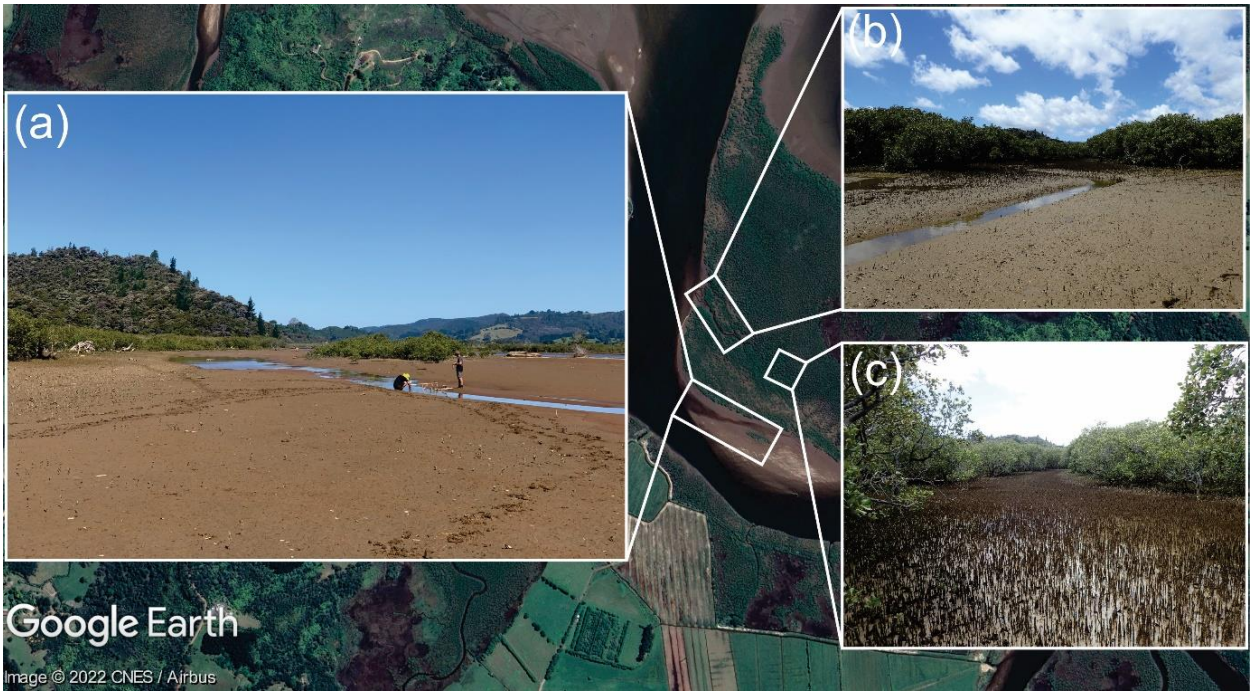

Figure 5. 3 The location of (a) the shoal channel and the mangrove island (on the right side) located on the shoal and (b) the main mangrove creek at the entrance of the forest, and (c) is a photo taken close to the edge of the mangrove forest.

Velocity data were recorded in relative x-y-z direction and filtered in the way that data with signal strength below a threshold were removed (50 counts for Aquadopps and Vectors, and below 70 counts for Sontek (generally indicating above the surface recordings and the period that instruments were out of water)). Aquadopp and Sontek data were low-pass filtered, and Vector data were burst-averaged since waves were not present and dynamics were tidal. Atmospheric pressure was removed from water level by using local atmospheric observations from the NIWA database (https://cliflo.niwa.co.nz/) (Horstman et al., 2021). The pressure sensors were affected by variations to temperature within the instrument housings, and the response to temperature could be assessed when the instruments were exposed at low tide. To correct timeseries of water level, the relationship between temperature inside the housing and recorded water pressure by the instrument was derived using a polynomial fit and the effect of temperature was removed from water level observations (Rahdarian et al., in preparation).

Table 5. 1 Table 1: Details of instrument deployments, locations of sites shown in Figure 5.4a.

Name	Latitude	Longitude	Start time	End time	Instrument height above bed	Sampling interval
R1	36°52'57.14"S	175°41'33.38"E	14th 09:00:00	17th 05:00:00	0.15 (m)	30 (s)
R2	36°53'26.29"S	175°41'58.02"E	14th 09:00:00	17th 05:00:00	0.15 (m)	30 (s)
C1	36°53'6.39"S	175°41'38.67"E	14th 09:00:00	18th 09:00:00	0.15 (m)	5 (s)
C2	36°53'7.36"S	175°41'40.14"E	14th 09:00:00	15th 16:00:00	0.20 (m)	450 burst sampling every 900 (s)
C3	36°53'8.80"S	175°41'40.79"E	14th 09:00:00	15th 16:00:00	0.20 (m)	450 burst sampling every 900 (s)
C4	36°53'9.78"S	175°41'41.63"E	14th 09:00:00	15th 16:00:00	0.15 (m)	5 (s)
C5	36°53'8.61"S	175°41'41.28"E	14th 09:00:00	15th 16:00:00	0.18 (m)	60 (s)
B1	36°53'15.52"S	175°41'38.06"E	14th 09:00:00	18th 09:00:00	0.15 (m)	5 (s)
B2	36°53'17.03"S	175°41'42.06"E	15th 16:00:00	16th 14:00:00	0.18 (m)	450 burst sampling every 900 (s)
B3	36°53'16.00"S	175°41'42.32"E	15th 16:00:00	16th 14:00:00	0.18 (m)	60 (s)
B4	36°53'17.70"S	175°41'45.09"E	15th 16:00:00	16th 14:00:00	0.20 (m)	450 burst sampling every 900 (s)
B5	36°53'18.75"S	175°41'44.42"E	16th 14:00:00	17th 17:00:00	0.18 (m)	450 burst sampling every 900 (s)
B6	36°53'19.72"S	175°41'43.52"E	16th 14:00:00	17th 17:00:00	0.17 (m)	450 burst sampling every 900 (s)
B7	36°53'20.60"S	175°41'42.77"E	16th 14:00:00	17th 17:00:00	0.10 (m)	5 (s)
B8	36°53'18.43"S	175°41'47.80"E	15th 16:00:00	16th 14:00:00	0.13 (m)	5 (s)
B9	36°53'21.54"S	175°41'51.76"E	17th 17:00:00	18th 09:00:00	0.16 (m)	450 burst sampling every 900 (s)
B10	36°53'21.88"S	175°41'53.38"E	17th 17:00:00	18th 09:00:00	0.17 (m)	450 burst sampling every 900 (s)
B11	36°53'23.10"S	175°41'51.28"E	17th 17:00:00	18th 09:00:00	0.09 (m)	5 (s)

5.2.3. Model Description

5.2.3.1 Delft3d

The Delft3D process-based model is used to simulate tidal dynamics of the estuarine shoal in Whitianga Estuary. Delft3D is a modelling suite developed by Deltares (Netherlands) that allows for a multi-disciplinary modelling approach applied to coastal and estuarine environments (Lesser et al., 2004). The software is composed of a set of modules that can simulate flow, sediment

transport and morphodynamics. Since the focus of this work concerns the patterns of the flow and tidal asymmetry around an estuarine mangrove-covered shoal, only the hydrodynamic module including the effects of vegetation in 2D depth-averaged mode is used. The model simulates flow by solving the momentum and mass continuity shallow water equations for unsteady and incompressible flow (Deltares, 2017).

5.2.3.2. Grid and Bathymetry

The domain covers an area of an approximately 1 km × 1 km and consists of a rectilinear structured grid with 2 m × 2 m resolution. The grid has two open boundaries at the upper and lower end of the river channel. In order to velocity-up the model runtime, grid cells that were constantly dry in the whole period of the simulation, were removed from the domain (Figure 5.4b). Except for the points located in the main river channel, the bathymetry is derived from LiDAR, surveyed in 2008 by the Waikato Regional Council and Land Information New Zealand (LINZ, 2008) and converted to the WGS1984 UTM zone 60S coordinate system. Following Montgomery et al. (2022), within the forest, the lowest value of the lidar point cloud within every 10 m × 10 m area is considered as the topography in order to prevent incorrect bed level measurements associated with trees. For the river channel points, LiDAR is not used because the channel depths cannot be captured accurately in subtidal areas due to turbidity effects. The depth of the river channel is calculated by interpolating the depths at the R1 and R2 points (measured by Nortek Aquadopps pressure sensors) located at the boundaries of the model grid. The bathymetry in the main river channel is smoothed, but in order to maintain the complex in-situ conditions of the points located on the shoal and inside the forest, depth values in these areas were not modified (Figure 5.4a).

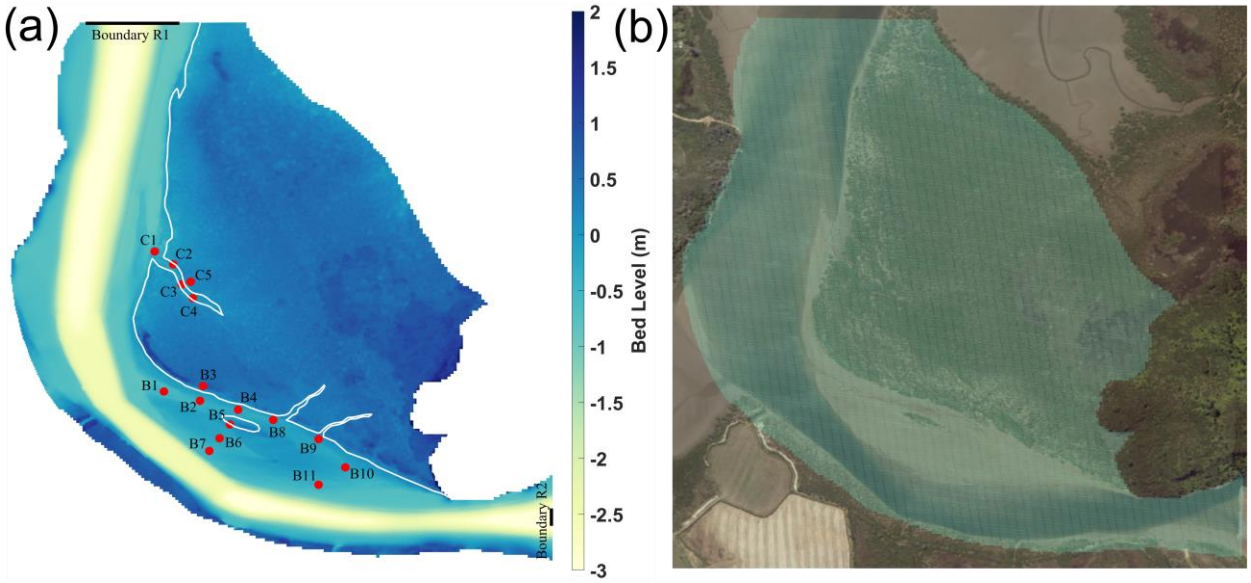

Figure 5. 4 Shows (a) the bathymetry of the domain, the location of the boundaries (black lines), the location observation points (red dots) in the domain and the coverage of mangroves (white polygons) (b) the computational grid.

5.2.3.3. Modelling Vegetation Effects

The effect of vegetation can be incorporated into the Delft3D model. In one approach, which is widely used for studies in mangrove forests and salt marshes, vegetation is represented as a number of rigid cylinders. In the so called '3D vegetation model' (Uittenbogaard, 1998; Uittenbogaard and Vossen, 2003; Deltares, 2017), vegetation coverage is defined by polygons. In our model, mangroves coverage is defined using two polygons created in Google Earth Pro based on the most recent satellite image, one polygon for the mangrove forest and one for the mangrove island (Figure 5.4a). The influence of vegetation is implemented in the model by adding a friction force given below to the momentum equation (Deltares, 2017):

$$F\ (z) = \frac{1}{2}\ \rho_0\ C_D\ \phi(z)\ n(z)\ |u(z)|\ u(z) \qquad [N/m^3]$$

where $F\ (z)$ is the friction force, ρ_0 is the density of water $[kg/m^3]$, $C_D$cylindrical drag coefficient [unitless], $\phi(z)$ is the stem width as a function of height $[m]$, $n(z)$ is the number of stems per unit area as a function of height $[1/m^2]$ and $u(z)$ the horizontal flow velocity $[m/s]$.

5.2.3.4. Boundary Conditions and Model Parameters

The largest tidal constituent at the entrance to Whitianga Harbour is the semi-diurnal M_2 and the two other dominant constituents are S_2 and N_2 (constituents were extracted from the NIWA tidal model https://tides.niwa.co.nz/). The tide during the experiments was nearing spring tides. The model is forced at two open boundaries: (1) the open boundary R1 located at downstream using measured water level data from 14th to 18th of December 2020 (Figure 5.4a), and (2) the open boundary R2 located at upstream forced by current boundary condition using measured velocity at station R2 (Figure 5.4b). The currents in the river channel were mostly tidal and the amplitude of spring tides is approximately 1.9 m. At the river station R2, the tidal current reaches 0.6 m/s during flood and 0.45 m/s at ebb. The boundary at R1 covers the river channel and excludes the parts with vegetation in order to prevent flow disturbance at the boundary caused by mangroves (Figure 5.3c). The boundary at R2 only includes grid cells around the thalweg of the river (where data at station R2 were measured) in order to prevent unrealistic discharges caused by across-river variations. The simulation time step is 0.02 minutes.

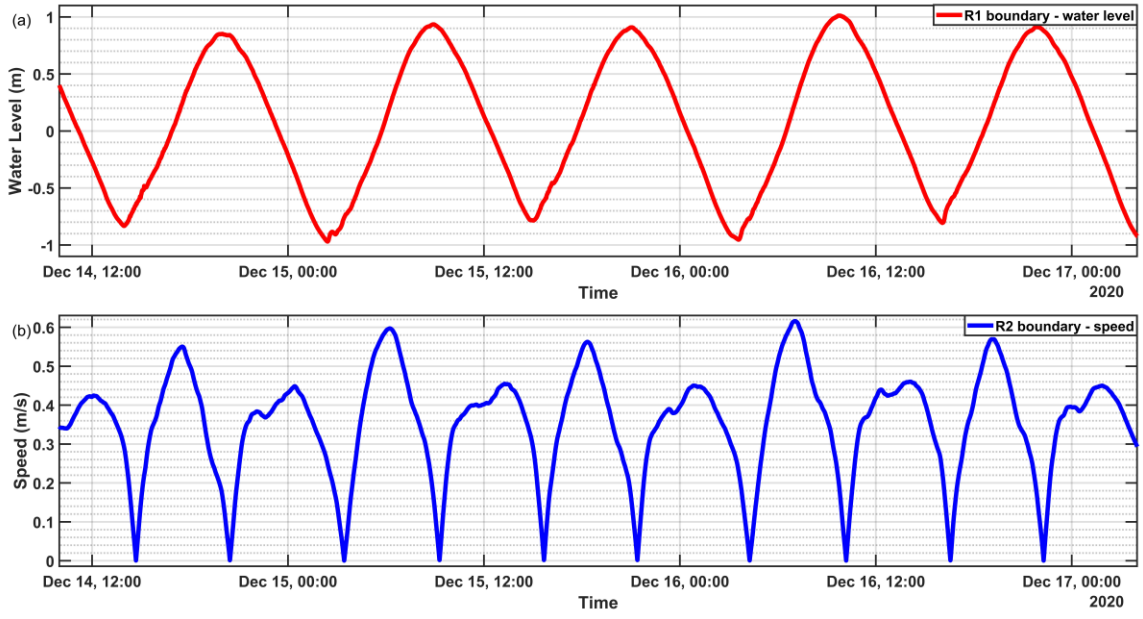

Figure 5. 5 Shows (a) water level boundary condition at boundary R1. (b) Current boundary condition at boundary R2.

Environmental conditions during the week of observations were consistent between days. Table 1 shows which stations (locations shown in Figure 5.3c) were occupied at which times. Winds and precipitation were not included in the model since no events occurred; wind velocity reached 6 m/s in late afternoon, dropping at night (Figure 5.4a), and the Waiwawa river level 5-minute observations provided by Waikato Regional Council (https://waikatoregion.govt.nz/) shows relatively constant (within a 2 cm range) levels (Figure 5.4b).

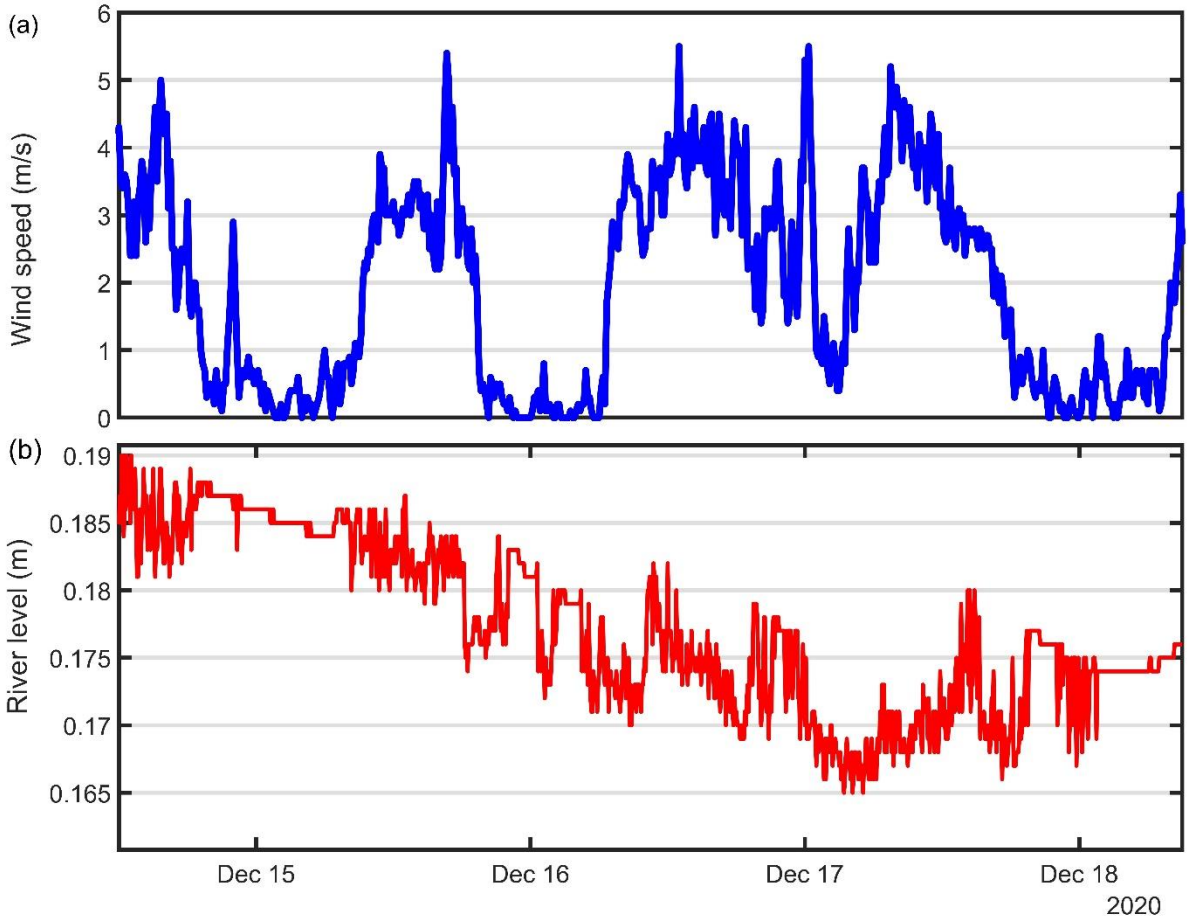

Figure 5. 6 The (a) wind velocity and (b) Waiwawa river level above mean sea level measured every 5 minutes above assumed local datum provided by Waikato Regional Council for the duration of simulation.

5.2.3.5. Scenarios

The calibrated model is modified to create three scenarios: 1- a scenario with no vegetation: mangroves were removed everywhere from the grid. 2- a scenario with channels infilled: the channels were removed and mangroves added to the old channel locations (the bathymetry

around the creeks is smoothed based on the elevation of the right and left side of mangrove creeks), and 3- the historic 1940s scenario: in this scenario, the vegetation expansion is based on the conditions of the forest based on historical aerial images collected in 1944 (the earliest available). In scenario 3, the modern date shoal channel is removed and the elevation of the edge of the forest (the part that emerged in 1940s) is lowered by ~50 cm on average by removing the top layer mud, with the amount removed based on mud layer thickness measurements collected during the field campaign (Rahdarian et al., in preparation).

5.3. Results

5.3.1. Model calibration

We used the Brier Skill Score (BSS) (Sutherland et al., 2004) in order to quantify the model performance of water level and velocity based on the following equation:

$$\mathrm{BSS} = 1 - \frac{\mathrm{MSE}\,(\mathrm{Y},\mathrm{X})}{\mathrm{MSE}\,(\mathrm{B},\mathrm{X})} = 1 - \frac{\langle(\mathrm{Y}-\mathrm{X})^2\rangle}{(\mathrm{X}-\langle\mathrm{X}\rangle)^2} \qquad (1)$$

where Y represents the model result, X represents the in-situ measured data and $\langle \mathrm{X} \rangle$ is the average of the measured data. With this method, scores between 0.5 and 1 are classified as excellent, 0.2< BSS <0.5 as good, 0.1< BSS <0.2 as fair, 0.0 < BSS <0.1 as poor while negative scores are considered to be bad. After each simulation, the BSS scores were calculated for water level and velocity at all stations and an average BSS is examined to select the best model configuration.

The best model performance is observed when horizontal eddy viscosity is 1 $\frac{m^2}{s}$, density is 1025 $\frac{kg}{m^3}$, and bottom roughness is defined with spatially varying Chézy values of 65 $\frac{m^{1/2}}{s}$ in the river channel and 45 $\frac{m^{1/2}}{s}$ for the remaining points in the domain. For the points that are located inside the vegetation polygons, the assigned roughness is updated by the vegetation model. Table 2 shows the summary of calibration statistics at each station for the optimal model run. The BSS score of the final model run demonstrates a category of 'excellent' for water level results and 'good' for velocity (Table 2). The lowest BSS is observed at the station B7 (Figure 5.7-b7) on the edge of the shoal and station B8 (Figure 5.7-b7) located in the middle of the shoal channel, at the confluence of two mangrove drainage creeks.

Table 5. 2 BSS score for each station.

Station	Water Level	Speed
C1	0.86	0.38
C2	0.99	0.25
C3	0.96	0.31
C4	0.95	0.32
C5	0.95	0.14
B1	0.99	0.54
B2	0.97	0.21
B3	0.96	0.11
B4	0.87	0.18
B5	0.98	0.24
B6	0.99	0.22
B7	0.99	0.07
B8	0.99	0.02
B9	0.97	0.21
B10	0.99	0.23
B11	0.87	0.14
mean	0.95 (excellent)	0.209 (good)

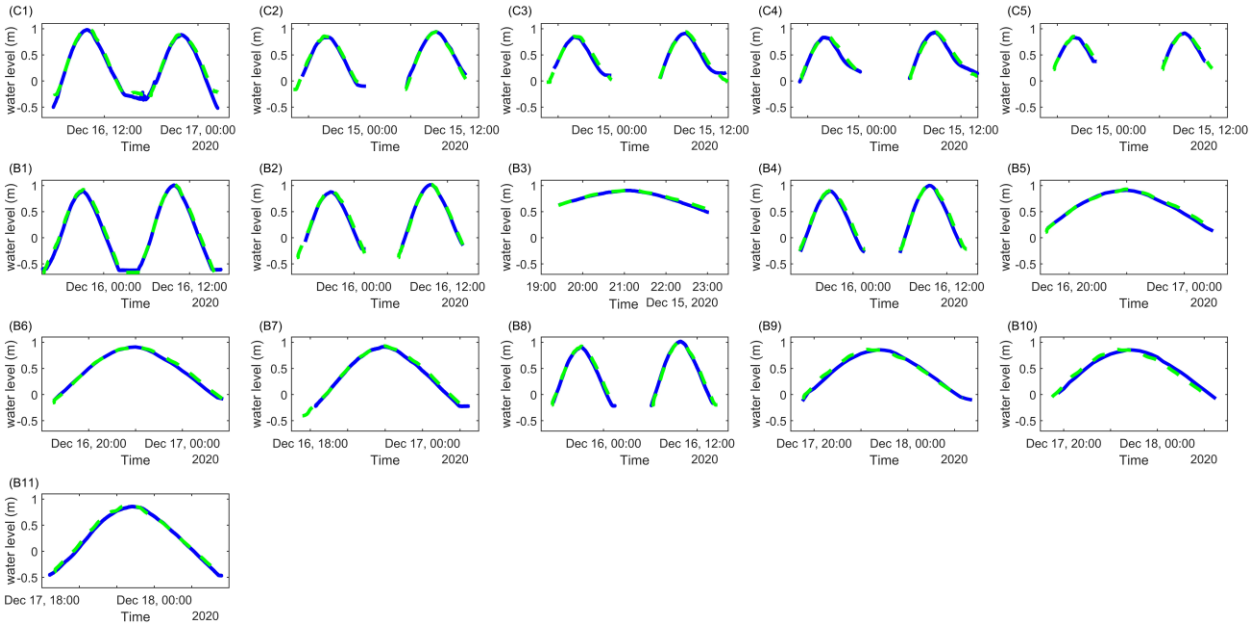

Figure 5. 7 Measured water level (blue solid line) versus modelled water level (dashed green line) at each station, with locations shown in Figure 5.4a.

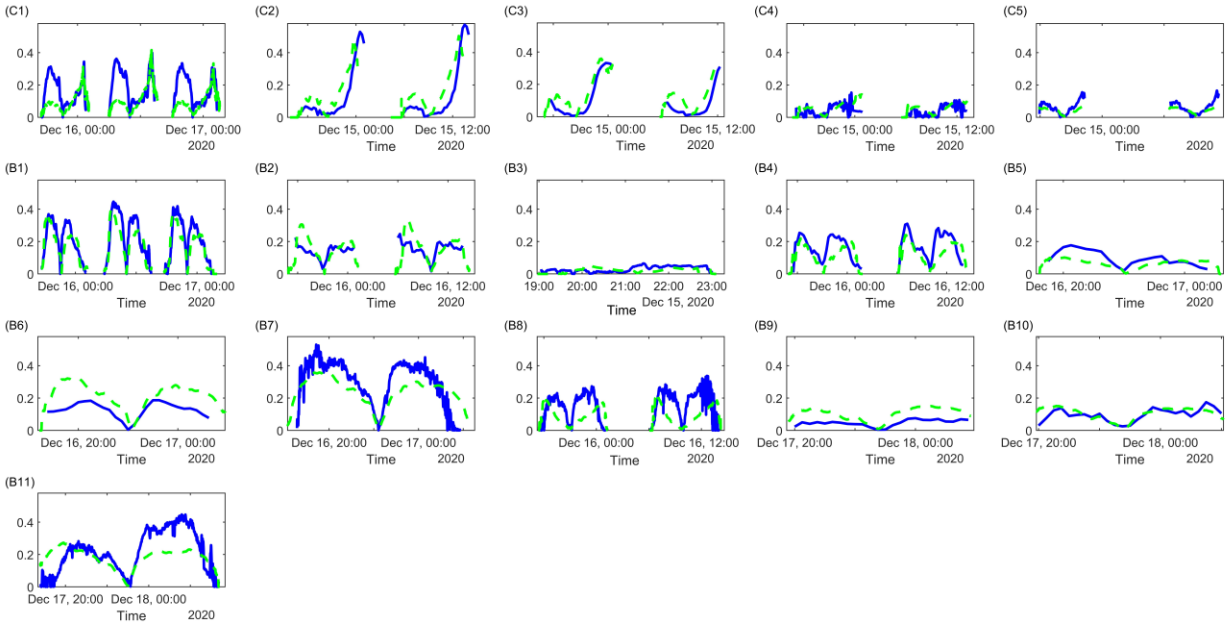

Figure 5. 8 Measured velocity (blue solid line) versus modelled velocity (dashed green line) at each station, with locations shown in Figure 5.4a.

5.3.2. Maximum velocity

Maximum velocity during both ebb and flood changes from the river channel to the shoal and mangrove forest. For the points located inside the main river channel, the flow is consistently stronger than the points inside the mangrove forest. During both ebb and flood, currents at the river downstream reach 0.5 m/s whereas currents in the upstream part of the study site reach up to ~0.7 m/s (Figure 5.8a & 5.8b). For sites that are close to the shoal, in general, higher velocities were observed in the shoal channel and close to the edge of the shoal. Currents reached 0.4 m/s and 0.6 m/s at the entrance of the shoal channel (close to station B1) and on the edge of the shoal (close to station B7), respectively. Around the mangrove island, currents become weaker near mangrove trees and roots and velocity does not exceed 0.2 m/s at any time (Figure 5.8a-5.8b). Similar to the river channel, inflow and outflow velocities on the shoal are not substantially different. Maximum ebb flows are concentrated in drainage channels, whereas flood flow is larger at the shoal than during ebb, but smaller in the channels. Conversely, Station C1 is located at the entrance of the mangrove creek draining through the forest and currents are concentrated over a short duration at ebb, with similar peak velocities to the ones observed in the river channel, up to 0.4 m/s during ebb. Simulated currents close to C2 and C3 (inside the mangrove creek), show a peak current of ~0.12 m/s during flood, and ~0.5 m/s at ebb. For the points around stations C4

and C5 that are inside the forest, located in close proximity to the creek (~15 meters away), currents never exceed 0.1 m/s and 0.15 m/s during flood and ebb, respectively. Within the forest, flow velocity does not exceed ~ 0.1 m/s at any time (Figure 5.8a–5.8b). During inundation, currents become weaker on the unvegetated shoal comparatively. At both ebb and flood, velocity is higher inside the mangrove creeks compared to the forest, although the difference is more pronounced at ebb due to drainage of outflow water.

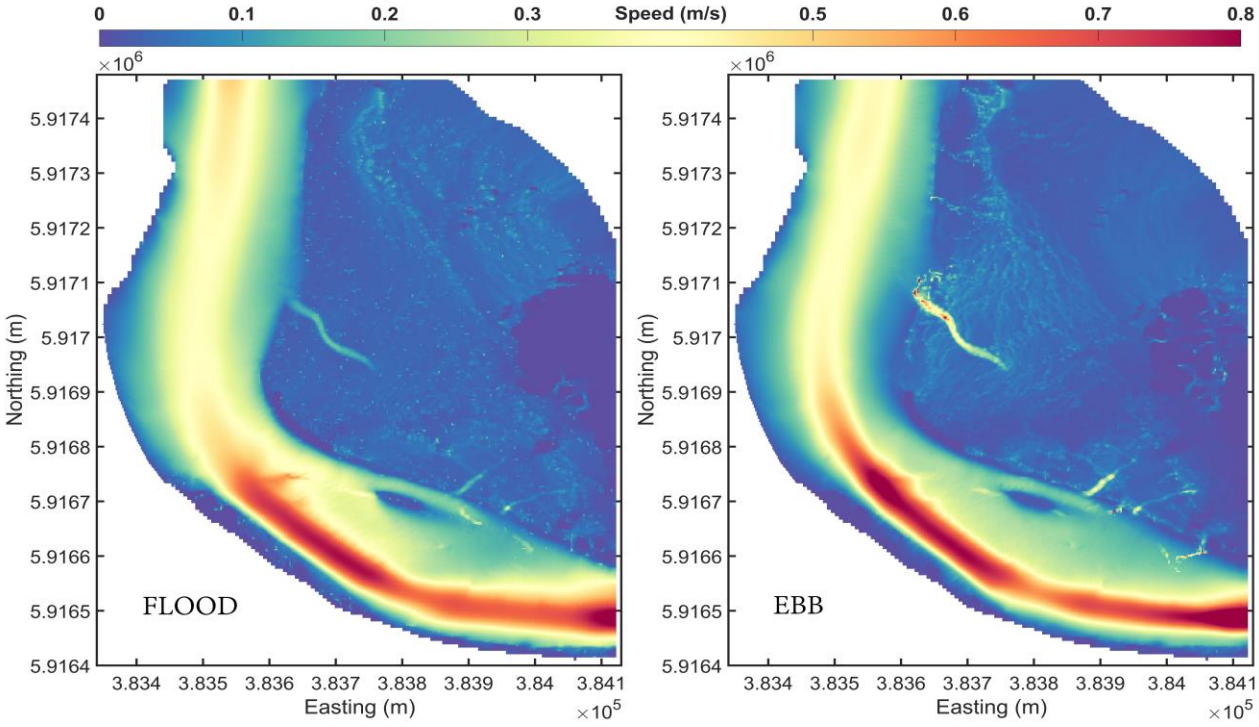

Figure 5. 9 (a) Maximum velocity during flood at each grid cell. (b) Maximum velocity during ebb at each grid cell.

The scenarios without vegetation show that vegetation influences currents in both the forest and on the shoal (Figure 5.9-a & b). On the flood, after removing vegetation from the domain, flow velocity increases all over the forest except the most elevated parts in the eastern region where the velocity is slightly reduced. Inside the main mangrove creek, velocity decreases similarly. The little mangrove island on the shoal (the red ellipse on the shoal just south of the main mangrove areas on Figures 5.2c), the edge and the backside of the forest are the places where velocity increases the most (Figure 5.9a). In addition, stronger currents are observed inside the shoal channel. On the ebbing tide, the velocity reduction in the mangrove creeks is considerable

compared to the case where vegetation is included. However, same as during flooding, in most parts of the forest, through the mangrove island and inside the shoal channel currents become stronger with no vegetation. In addition, currents become slightly weaker on the un-vegetated shoal (Figure 5.9b).

Although the hydrodynamic impact of filling in the creeks is smaller than the effect of removing vegetation (Figure 5.9), currents are still affected by creek infilling (Figure 5.9-c & d). By infilling creeks, on the flood, inside the forest, changes in the maximum current velocity are small (Figure 5.9-c) except for the locations around and inside the infilled creeks. Currents are observed to become smaller inside the infilled creeks, whereas the velocity increases around them. On the ebbing tide, velocity decreases considerably inside the infilled mangrove creeks and currents are slightly weaker around them. Since the water does not converge towards and drain through the creeks in this scenario, velocity increases considerably on the edge of the forest when water drains out of the forest with a sheet flow at ebb. In general, the main effect of removing creeks is around the creeks and on the edge of the forest.

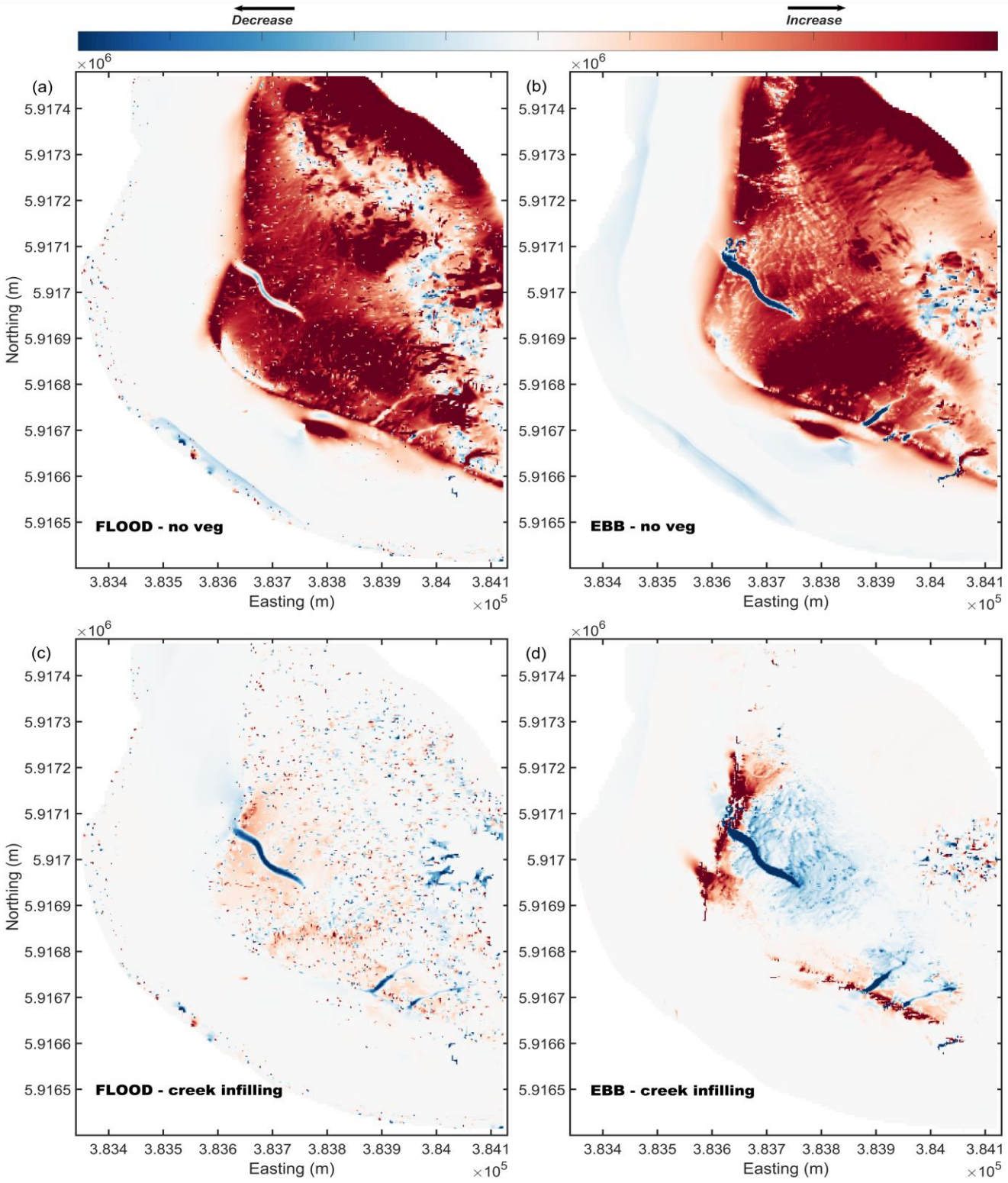

Figure 5. 10 The difference between results of the scenario in which vegetation is removed and unmodified (modern date) conditions for (a) maximum velocity during flood at each point and (b) Maximum velocity during ebb at each point. Bottom panels show the difference between results of the scenario in which channels were infilled and unmodified conditions for (c) maximum velocity during flood at each point and (d) maximum velocity during ebb at each point.

5.3.3. Tidal asymmetry

Tidal asymmetries can be studied using two approaches: by calculating the ratio of (1) peak velocities during ebb and flood or (2) by the relative duration of ebb and flood. Here, tidal asymmetry is computed by dividing peak velocities. Tidal asymmetry can be used as an indicator of the net direction of sediment transport (Friedrichs and Aubrey, 1988; Hunt et al., 2016). At each grid cell, tidal asymmetry is assessed by computing the ratio between peak flood and ebb velocities during a tidal cycle. Therefore, this ratio reflects flood dominance if larger than one (shown with blue colour on Figure 5.8), and ebb dominance if smaller (shown with orange colour on Figure 5.8). Note that due to tidal phase lag differences across the domain, peak velocities may not occur at the same time everywhere on the grid (which has been accounted for in asymmetry calculations).

The shoal channel is mainly flood-dominated, except the small part at the end where the mangrove creek drains water into the shoal channel. Within the shoal part, tidal asymmetry is observed to be flood-dominated at the entrance of the shoal channel at stations B1, flood-dominated on the edge of the shoal close to station B7, and ebb-dominated at the end of the shoal channel at station B11. Although the area around the mangrove island is flood-dominated, ebb-dominance is observed inside the vegetation. Although the river channel is mainly flood-dominated, some parts are observed to be ebb-dominated. Due to across-river variations, different tidal asymmetry can be observed in some cross sections (Figure 5.8a). However, the difference in peak velocities at flood and ebb are low, resulting in only slight asymmetries. In contrast to the shoal channel, the mangrove creeks are consistently ebb-dominated. The area inside the forest, around the seaward part that is covered with low-lying mangroves, close to the edge of the forest, is ebb-dominated, whereas in the back of the forest with higher elevated mangroves away from the creeks, flood-dominance is mostly observed. However, largest asymmetries are observed inside the creeks. The bigger mangrove creeks have higher capacity to drain the outflowing water, resulting in the bigger the area around the head of the creek with ebb-dominance characteristics (Figure 5.8a).

In the scenarios without mangroves, tidal velocity asymmetry type changes substantially all over the forest, although this ratio remains quite similar inside the river channel and on the shoal, except for the former mangrove island that becomes flood-dominated (Figure 5.8b). The ebb-

dominance inside the mangrove creeks is not observed anymore. In addition, ebb-dominance can be observed in the central and higher elevated part of the former forest, while the southwestern part of the shoal becomes flood-dominated (Figure 5.8b).

In the scenario where creeks are filled in, the tidal asymmetry remains similar for most parts of the domain except for the creek areas themselves. By channel infilling, the mouth of the creek remains ebb-dominated whereas a flood-dominance is observed around and inside the head of the creeks (Figure 5.8c).

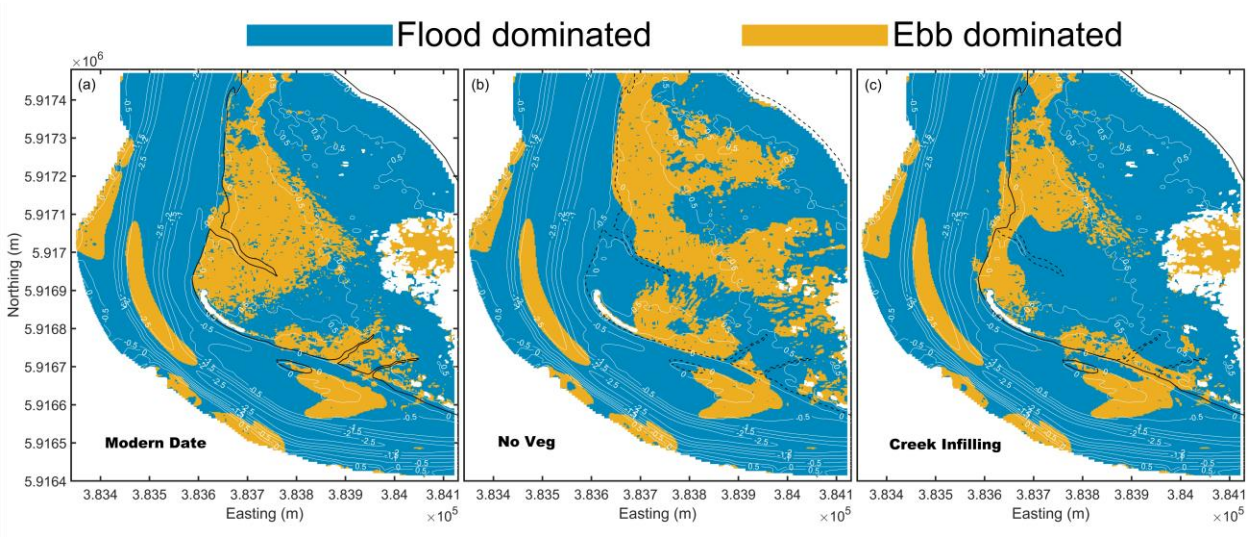

Figure 5. 11 Computed tidal asymmetry for each grid cell for (a) modern date model. Solid black line shows the expanse of vegetation. (b) scenario that vegetation is removed. Dashed black lines show the vegetation polygon that is removed) and (c) channel infilling scenario. Solid black like shows the expanse of vegetation and dashed black line shows the location of the creeks that are infilled in the scenario. White contours show the depth lines, grid cells shaded with blue are flood-dominated and cells shaded with orange are ebb-dominated.

5.3.4. Tidal flooding and flow patterns

Water circulation in mangrove forests is divided into two major stages: (1) creek flow stage and (2) sheet flow stage (Horstman et al., 2013; Horstman et al., 2021). During every tidal cycle, starting from low tide, at initial stages of flooding, water first flows into the creeks (since channels are deeper than the forest) known as creek flow stage. In our case study, mangrove creeks are not very wide or deeply incised. Therefore, the shift to sheet flow occurs early in the flooding tide, in the lower lying mangrove areas near the creek (also in the western and southern parts of the forested domain) (Figure 5.11a). At this stage, the flow direction inside the creek and the forest is

parallel to the creek (Figure 5.11a). Compared to the base-case scenario, the water level on the shoal is higher in the scenario that vegetation is removed and lower in the one in which creeks are infilled (Figure 5.11a-c). Subsequently, when the flow overtops the creek bank and the edge of the forest, water flows into the forest from both the creek and directly from the river channel known as the sheet flow stage with a parallel-to-the-creeks direction (Figure 5.11a). During the sheet flow stage, the role of the channels becomes less pronounced as very small differences in velocity vector size and direction can be observed between the base case and the channel infilling scenario (Figure 5.11-a & c). In the scenario that vegetation is removed, a completely different tidal flooding pattern from the two other cases can be observed, when water overtops the flat on the northwestern part during the sheet flow stage, it is directed to the southeastern part and flows back to the main river channel again, whereas in the presence of vegetation, the water remains on the flat during flooding tide (Figure 5.11d-f). In general, in the no-vegetation scenario, higher velocities are observed compared to in other scenarios (Figure 5.11).

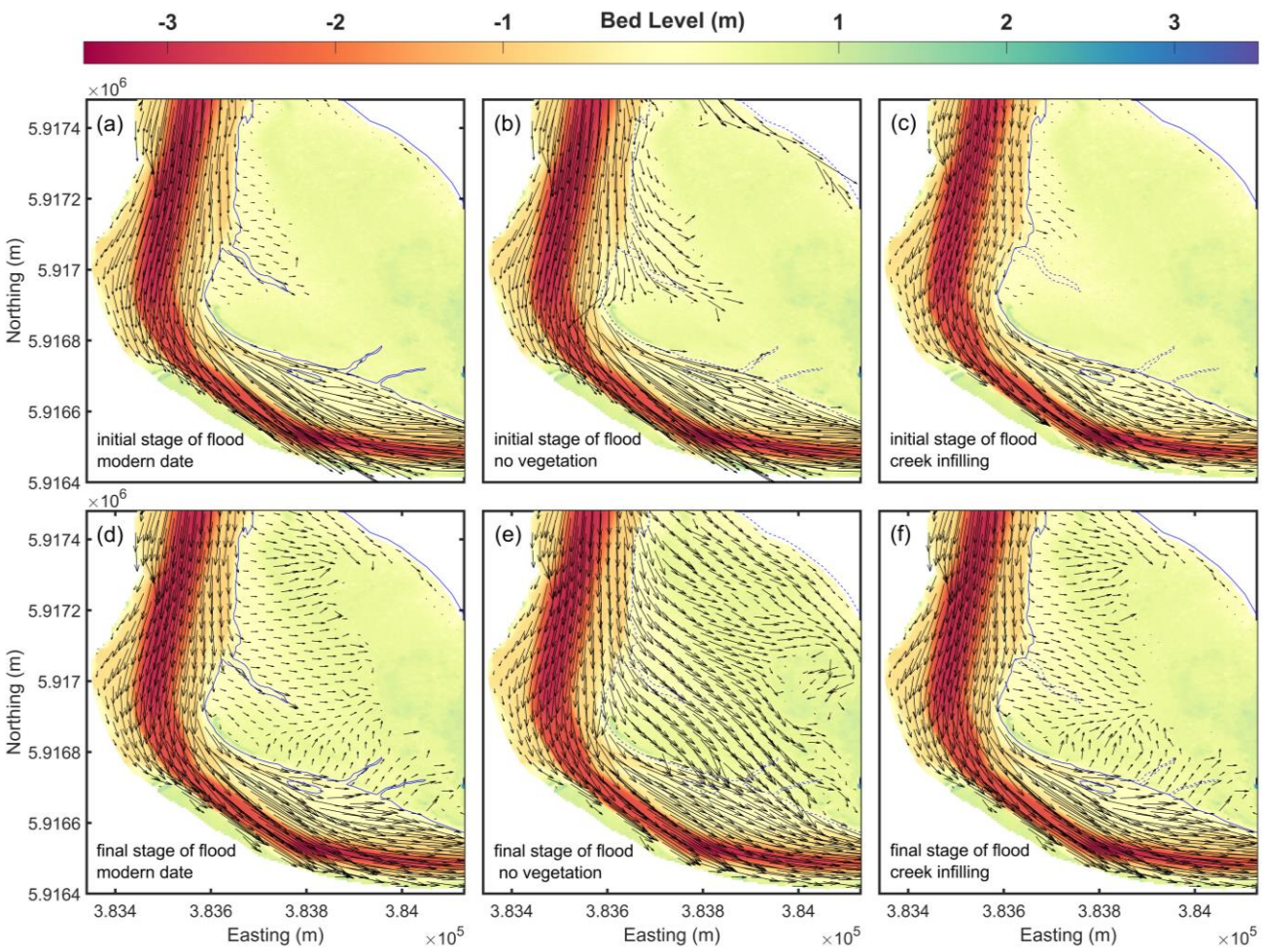

Figure 5. 12 The flow patterns occuring during the initial stages of flooding for (a) modern date model (b) no vegetation scenario (c) channel infilling scenario and final stages of flooding for (d) modern date model (e) no vegetation scenario and (f) channel infilling scenario during a tidal cycle.

During the initial stages of ebb, the forest is inundated and water drainage starts with sheet flow which is parallel to the creeks (Figure 5.12a). The tidal ebbing pattern in the no-vegetation scenario is different from the two other cases: water overtops the flat on the southeastern part and flows back to the main river channel from the northwestern part, whereas in the presence of vegetation, the water drains back to the river from both sides of the forest (Figure 5.12a-c). In the final stages of the sheet flow during the ebbing tide, when water level decreases to below the forest elevation, another creek flow initiates (Figure 5.12d-f). At this stage, water drains back into the creek with an angle depending on the topography and local gradients (Figure 5.12d). This shows that the creek impacts flow fields only in relatively shallow water on the mangrove plain during the tidal cycle. During final stages of ebb, higher velocities are observed at the location

where creeks were in the base case scenario (where they were infilled for this scenario) (Figure 5.12a & c). Furthermore, when creeks are infilled, velocity increases considerably around the edge of the forest on the northwestern part (Figure 5.12f). In the absence of mangroves, water drains out more quickly (Figure 5.12e).

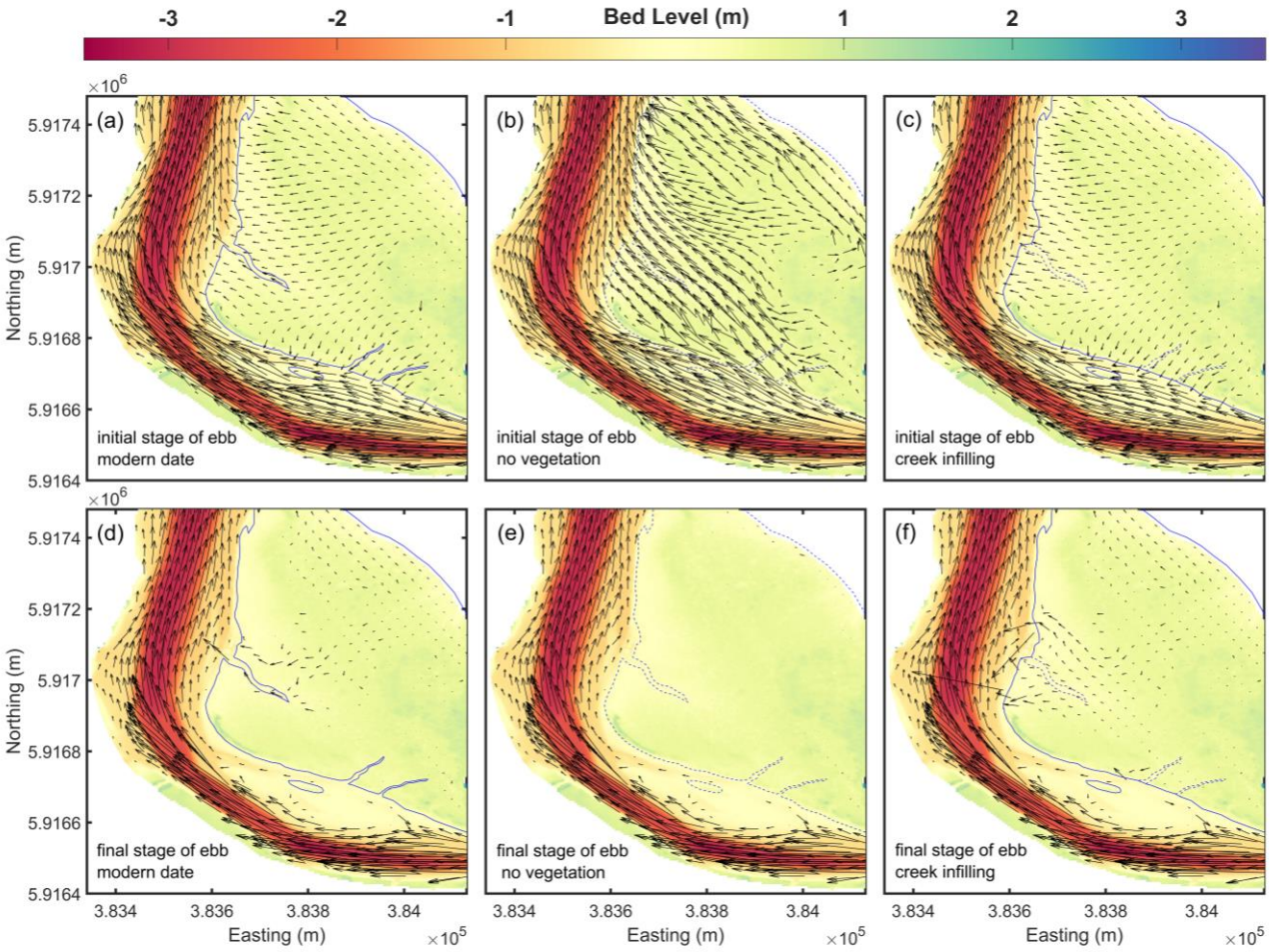

Figure 5. 13 The flow patterns occuring during the initial stages of ebbing for (a) modern date model (b) no vegetation scenario (c) channel infilling scenario and final stages of ebbing for (d) modern date model (e) no vegetation scenario and (f) channel infilling scenario during a tidal cycle.

5.3.5. 1944 scenario

Historical images of the Whitianga Estuary mangrove forest suggest that the creeks have emerged as a response to different processes (Figure 5.13). In 1944, mangroves were only present in north-eastern part of the study site, and the present-time main mangrove creek in the western part of the forest is a pre-existing shoal channel in the inner bend of the shoal

(Figure 5.13-a). Later, after establishment of mangroves, the shoal channel eventually converted into a mangrove creek. During this transition, the shoal channel evolved from a wide and braided channel to a more sinuous, narrow creek (Figure 5.13-b). Augur cores collected inside this area (reported Rahdarian et al., in prep.) show sand covered in a thick deposit of silt, so the transition of channel type is likely associated with a transition in sediment texture. The other two mangrove creeks that are located in the southern part of the forest formed after mangrove colonization, and with time, the channels perhaps were scoured by erosional processes (when water began to converge in lower friction areas where flow is slightly more efficient) as a consequence of vegetation growth (Figure 5.13-c).

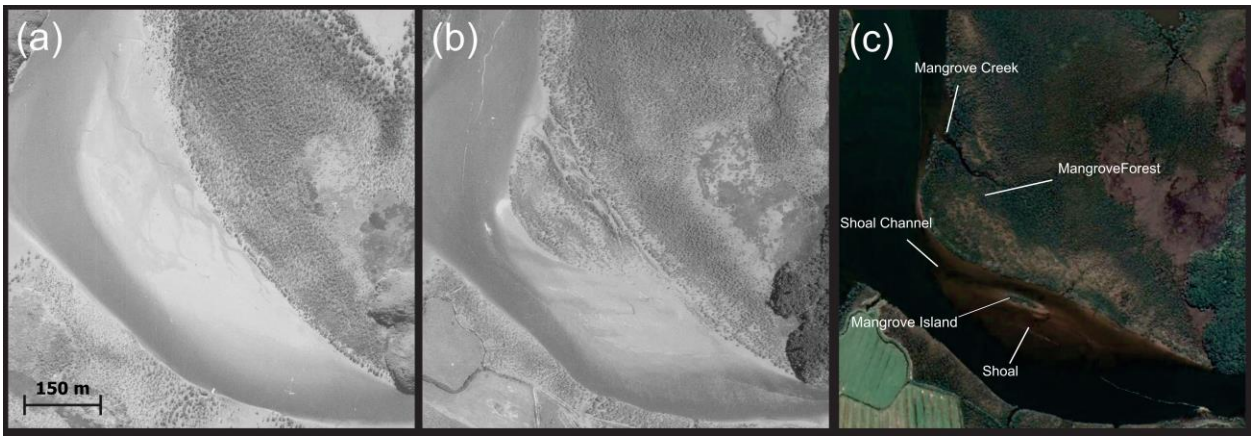

Figure 5. 14 Historical images of the study site (a) in 1944, (b) in 1984 provided by RetroLens (https://retrolens.co.nz/) and (c) in 2020 provided by Google Earth.

The final scenario is set up to elucidate the processes that were important in 1944. By removing mangroves that started growing after 1940s from south-western part of forest, this area becomes mostly flood-dominated. Before existence of mangrove around the edge of the forest, the pre-existing shoal channel (modern date mangrove creek) is fully flood-dominated. In addition, ebb-dominated tidal asymmetry is observed in a major part of the river channel near the bend. (Figure 5.14).

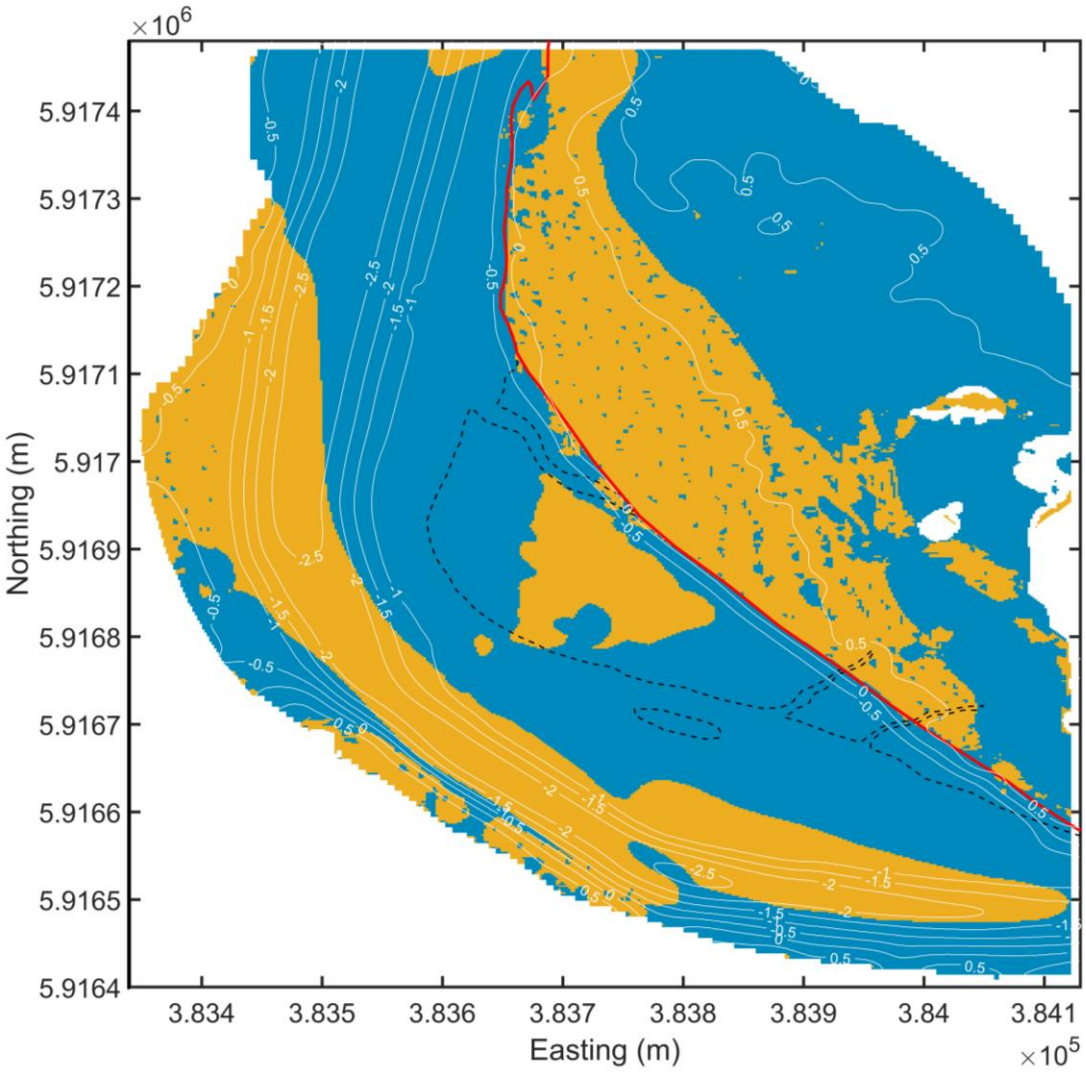

Figure 5. 15 Computed tidal asymmetry for each grid cell for 1944 scenario. White contours show the depth lines, dashed black lines show the expanse of vegetation in modern date condition and red line shows the expanse of vegetation in 1944.

5.4. Discussion

Mapping peak velocities and tidal asymmetry helps to unveil the relative importance of channels and vegetation in shaping tidal flow around a complex estuarine-riverine shoal. Similar to conclusions by Kumbier et al. (2022a), tidal asymmetry may vary dramatically over a scale of ~20 m suggesting that a uniform tidal asymmetry type cannot be assigned to an entire shoal. In the river channel outside the forest, the flow is slightly asymmetric ~ 0.8 to 1.2 with patches of both ebb-dominated and flood-dominated flow, even changing over the cross-section (Figure 5.8). In contrast, the shoal channel and the mangrove creeks were entirely flood-dominated and ebb-

dominated, respectively. Supporting the results of previous work (Temmerman et al., 2005; Horstman et al., 2013), flow direction inside the creek and the forest is observed to be parallel to the creek, except for the final stages of the sheet flow at ebbing tide, when water drains back into the creek with almost at perpendicular angle depending on the topography and local depressions.

Recent numerical studies in mangroves show that presence of a vegetation cover is identified as the key factor controlling the flow dynamics and sedimentation patterns (Temmerman et al., 2005; D'Alpaos et al., 2007), and our scenarios support this. When vegetation is removed, the flow patterns during flood and ebb were completely different from the other cases (Figure 5.11 & 5.12). In addition, removing vegetation not only affects tidal asymmetry on major part of the flat, but also converted the ebb-dominated creeks to fully flood-dominated channels (Figure 5.10 a & b).

The role of tidal creeks on large-scale dynamics and tidal asymmetry depends on the scale (size of the creek compared to the area of the forest) and the topography of the vegetated flat. For example, Sullivan et al. (2019) used a Delft3D model to investigate the effect of channels on drainage density and hydrodynamics of a channel-marsh system in Grove creek, USA. Their results show that by removing the first and second order creeks (smaller and minor channels), the drainage density decreases but the over-marsh circulation is not significantly affected. However, when third and fourth order creeks are removed, not only drainage density is reduced, but tidal asymmetry is also affected and the system converts from ebb to flood dominated. Contrastingly, in another study site, where the ratio of the forest area to creek is ~7.5, the results of the model revealed that channelization has more influence on large-scale flow routing and hydrodynamics than vegetation density (Montgomery et al., 2022). Here, the ratio of the forest area to the area of the creeks is ~50 and the role of mangrove creeks on the overall flow around and within the forest is far smaller than the effect of the vegetation. Although the effect of mangrove creek infilling on the large-scale hydrodynamics is small, by creek infilling, the ratio of peak velocities at ebb and flood changed inside the domain. Without the creeks, tidal asymmetry changes are mostly local and occurred around the landward end of the creeks where flood-dominance developed towards the head of the creeks (Figure 5.10c). Creeks are observed to play a more important role at initial stages of flood as they enhance progression of water on the flat (Figure 5.11 a & c) and at final stages of ebb when they facilitate water drainage (Figure 5.12d & f). Creeks also may promote the stability of edge of mangrove forests, since velocities on the edge of the

forest at ebb increase considerably in the creek infilling scenario which may lead to higher bed shear stresses and subsequent decay of vegetation (Figure 5.9d & 5.12f). Our results show that the velocity change on the flat is considerably higher when mangroves are removed compared to the creek infilling scenario (Figure 5.9).

Although creek flow and sheet flow stages are two main flow stages that occur typically in mangrove forests, a distinct creek flow stage may not be seen depending on the topography (Horstman et al., 2013). studied flow routing in different mangrove forests in Thailand, where they did not observe a creek flow in low-lying mangroves. However, in a more highly-elevated forest, at water levels below the vegetation, a creek flow stage is observed. In our study site, we did not observe a dominant creek flow stage and soon after flooding tide started, the creek flow converted to a sheet flow because the elevation of the mangroves are low and mangrove creeks are not deep and wide. Similar to Temmerman et al. (2005) and Fagherazzi et al. (2008), velocity vectors showed that water flows from the edge of the forest at water levels above the creek bank.

Many previous works have observed tidal creeks and the forest to be ebb dominant and flood dominated, respectively. This pattern usually applies to fairly homogenous systems where flood dominance at high tide and ebb dominance at ebbing tide is inevitable in a high friction flat vegetated landform which delays the water draining off the tidal flat (Fagherazzi et al., 2008). However, contrasting cases have been observed in different sites. Idealized modelling results of Mazda et al. (1995) showed an ebb-dominance inside the forest close to the creeks, while at the points located far from the creek were flood-dominated. In contrast, field measurements of velocity at another site show that the creeks are consistently ebb-dominated and the forest is always flood-dominated (Horstman et al., 2021). Even in some cases the flats were observed to be ebb dominated and the mangrove creek is flood dominated (Schettini et al., 2020). Our tidal velocity asymmetry mapping (Figure 5.10a) revealed that not only mangrove creeks are consistently ebb-dominated, but also the area surrounding the mangrove creeks. The size of this ebb-dominated area is directly related to the size of the mangrove creeks. We also associate this behaviour to the control that is imposed the larger scale topography and the sub-catchment of the creeks. In general, tidal asymmetry inside the creeks and around the head of the creeks changed to flood-dominated after channel infilling (Figure 5.10c). In contrast, the parts located close to the edge of the forest were mostly ebb-dominated due to the general drainage of outflow

water (as sheet flow) as these parts remained ebb-dominated in the creek infilling scenario (Figure 5.10a).

Some theories state that tidal creeks are inherited from un-vegetated tidal flats prior to emergence of vegetation, whereas other studies consider colonization of vegetation the key factor for development of channel networks (Perillo et al., 1996). Observation of channel initiation in vegetated landforms showed that tidal channels can develop either due to erosional or depositional processes (Perillo and Iribarne, 2003). The historical image of 1944 shows that the shoal channel existed before mangroves colonised the area and perhaps depositional processes caused sediment accretion along the inner bend of the river which then initiated the shoal channel. On the other hand, in the scenario with infilled tidal creeks, velocity increased considerably on the ebbing tide at the location of local topographic undulations in the forest; these caused concentration of flow due to absence of the main drainage creek (Figure 5.9d). This suggests that here, after emergence of mangroves on flat, the development of channels on eastern part of the forest is caused by erosional processes. However, successful formation of channels after the moment of initiation depends on increasing velocity within the nascent channel to cause further deepening and widening. Otherwise, the newly formed minor creeks will be infilled and plants will regrow (Perillo and Iribarne, 2003).

Our results suggest that when mangroves expand in a coastal environment, they take control of the system and gradually imprint on the dynamics surrounding them (not just changing conditions within the forest itself). Recently work suggests that mangroves are opportunistic and play no role in shaping the geomorphology of the regions into which they expand, whereas in other works they have given the label ecosystem engineers because they can affect the sedimentation and bed stabilization through biophysical feedbacks (Bird, 1986; Woodroffe, 1992; Furukawa et al., 1997; Swales et al., 2015b). Our results give strong evidence of the latter, and show that mangroves can affect short-term and long-term dynamics of the landform. First, field measurements showed that on the unvegetated shoal, mud layer thickness is higher inside and around the mangrove island, confirming that mangroves can promote mud trapping (Rahdarian et al., in prep). Second, here we observed that in the scenario where mangroves were removed, velocity (short-term dynamics) not only changed within the main forest, but is also affected around the edge of the forest, inside the shoal channel and on the un-vegetated shoal, suggesting that the ecosystem engineering effect of mangroves extends to the surrounding environment. In

addition, the 1940s scenario shows that the ebb dominated mangrove creek is likely a fully flood-dominated channel before mangroves expanded on inner bend of the shoal, showing a dynamical shift of the pre-existing shoal channel to an ebb-dominant mangrove channel, driven by the presence of mangroves in the surrounding area.

5.5. Conclusion

A high-resolution hydrodynamic model of an estuarine shoal covered with mangroves in Whitianga Estuary is created and the model is validated with field observations in order to simulate short-term hydrodynamics, the effect of vegetation and channels on large-scale tidal asymmetry. Vegetation had a large-scale influence on the current velocity, flow routing and tidal asymmetry within the forest and inside the channels (mangrove creeks and the shoal channel), whereas the effect of the mangrove creeks were mostly local and around the creeks only. The ratio of the channel area to size of the forest is small, and so channels had little impact on larger scale processes. Comparison of the modern-date model with the removing vegetation scenario and the 1940s scenario highlighted the effect of mangrove colonization on their surrounding environment. Expansion of mangroves not only affected the short-term dynamics, but also shifted the regime of the channel from being a fully flood-dominated shoal drainage channel to an ebb-dominated mangrove creek. Therefore, these mangroves are likely to be eco-engineers of the estuarine ecosystem.

Chapter 6: General Conclusion

This thesis used numerical models and field measurements to generate new understanding on the initiation, short-term and long-term dynamics of tidal environments. The overarching aim of the thesis was to explore how physical services in tidal environments are controlled by their antecedent conditions, sediment supply and vegetation (mangroves). Different methods were applied in each Chapter aimed to answer the research questions presented in the general introduction.

Chapter 3 focused on numerical modelling of idealized cases. The results revealed how initial configuration of the models can affect equilibrium conditions and the response of tidal basins to sea level rise. Moreover, the effect of channels on averaged asymmetries and residence times for the sandy cases, and the effect of mud concentration at the open boundaries in shaping the channels in the case of mixed sand and muddy environments were shown.

Due to difficulties and complexities of doing field measurements in and around estuarine shoals and mangroves, detailed observations of hydrodynamics and sediment dynamics in estuarine mangroves are limited. Moreover, rapid expansion of mangroves during the last decades in Aotearoa New Zealand has enabled observations of the expansion of mangroves, subsequent changes in channels and initiation of new mangrove creeks to be captured by satellite and aerial images. However, field studies that show short-term dynamics and the bio-geomorphic feedback of vegetation are still lacking. Therefore, was still little known about how vegetation can shift the function of channels and influence the upper bed sediment characteristics. Chapter 4 was designed to address this gap.

Finally, in Chapter 5, field data of the estuarine shoal in Whitianga Estuary, Aotearoa New Zealand was used to calibrate and validate a numerical model, and fill in understanding gaps in the field study of Chapter 4. The results of the modelling study demonstrated the landscape-scale role of vegetation and channels on flow routing and asymmetry. In addition, a regime shift of a channel caused by the expansion of mangroves was investigated.

There are some clear themes in my thesis that span the three research papers, firstly on the role of channels, then on vegetation, then on the development of equilibrium and finally the influence of sea level rise. These are summarised in the Sections following.

6.1.1. What is the role of channels in shaping processes?

Removing channels from the morphology increased residence time. Moreover, water circulation was observed to be improved in the presence of channels. In Chapter 3, where evolution of idealized sandy tidal basins was simulated, the equilibrium morphology became channelized in all three cases that were explored (concave, convex and mixed initial profiles). Although in basin-wide averaged assessments, the influence of channels was not pronounced, studying the tidal velocity in cross-sections and removing the channels from the equilibrium morphology revealed the role of channels in shaping tidal currents. In deeper parts of the channels, peak water velocity was higher and more ebb-dominant compared to the points located outside the channels. In addition, channels reduced the residence time and improved water circulation although basin-wide tidal asymmetry remained relatively the same. Perhaps this is because as long as the size of the channels compared to the basin is not large and their removal does not lead to a shift in width-averaged tidal asymmetry (in magnitude, from being highly ebb/flood dominated to flood/ebb dominated), the basin-wide tidal asymmetry is mainly controlled by large-scale mean dynamics whereas even small channels create flow pathways with where water velocity locally increases (higher peak velocity in the thalweg) that can enhance the flushing time.

Although the role of channels in general is to promote tidal water exchange between the estuary or sub-tidal area and the flat, their physical services can be different. In Chapter 4, field measurement inside two channels that were located close to each other showed that the mangrove creek is consistently ebb-dominated, improving water drainage out of the forest during ebb, whereas the role of the shoal channel was more pronounced during flood tides where the higher peak velocity at flood can lead to an increase in sediment delivery onto the shoal and further shoal accretion.

Although the large-scale impact of channels on tidal flooding and tidal asymmetry was relatively small, channels had a strong local influence inside and around the head of tidal creeks. This was shown in Chapter 5, where a series of scenarios were developed around the calibrated Whitianga Harbour model. By infilling mangrove creeks in one of the scenarios in Chapter 5, short-term impact of channels on landscape-scale hydrodynamics and tidal asymmetry was studied. When creeks were infilled, a decrease in velocity was observed in the location of the creeks (in base scenario) whereas the velocity increased around them. Removal of the creeks led to a

considerable velocity increase at the location of local topographic undulations in the forest. With no creeks, these undulations captured and channelized the tide ebbing out of the mangrove forest. The effect of creeks on tidal asymmetry were local, mostly limited to the area around the creeks and the impact on large-scale tidal asymmetry was small. The influence of the channels was observed around and inside the head of the creeks since the tidal asymmetry shifted to flood-dominated, and the area around the mouth of the creek remained ebb-dominated after channel infilling. To some extent this can be due to the size of the channels compared to the area of forest. In our study site, the ratio of the channel area to size of the forest is small, and the role of channels on landscape-scale processes was not pronounced as in other studies (Wolanski et al., 1980; Mazda et al., 1995; Montgomery et al., 2022).

6.1.2. What is the role of mangrove vegetation in short-term landscape-scale dynamics and tidal asymmetry?

In this theme, I focused on mangrove vegetation because it is the dominant ecosystem engineer in our local estuaries. Mangroves had a strong impact on large-scale tidal circulation and asymmetry type inside the channels on the shoal. Chapter 5 presented a scenario in which mangroves were removed from the study site. The results of this scenario revealed the impact of vegetation on short-term landscape-scale dynamics and tidal asymmetry. Removing vegetation resulted in large-scale change in current velocity, flow routing and tidal asymmetry within the forest, inside the mangrove creeks and the shoal channel. In the absence of vegetation, in most parts of the forest, flow velocity increased during both ebbing and flooding tide, except around the most elevated parts of the forest where the velocity reduced slightly. With no vegetation, currents were weaker inside the mangrove creeks; however, the decrease was more pronounced during the ebbing tide. Contrastingly, higher velocities were observed inside the shoal channel. In addition, a completely different tidal flooding pattern occurred compared to the base case scenario; without vegetation, water overtopped the flat on the northwestern part during the sheet flow stage and it was directed to the southeastern part and eventually flowed back to the river channel again during flooding. Finally, tidal velocity asymmetry changed substantially all over the forest. Mangrove creeks were converted to flood-dominant and ebb-dominance could be observed in the central and higher elevated part of the former forest. The modelling was supported by field observations. Chapter 4 presented detailed observations of flow, suspended sediment concentration, sediment flux, and bed sediment characteristics around a mangrove

shoal. The currents in the river channel were mostly tidal. The direction of the flow at flood and ebb tide changed dramatically over the scale of ~20 m, suggesting that a uniform tidal asymmetry cannot be representative of such complex environments. The mangrove creek and the point inside mangroves close to the creek were consistently ebb-dominated, although the duration of the ebb was longer than flood. Among the stations located inside the creek within the forest, ebb duration asymmetry increased landward whereas tidal flow asymmetry decreased landward which is associated with decreasing of the peak velocity at ebb. Inside the shoal channel, flood-dominance decreased from the entrance to the middle part, and the flow converted to ebb-dominant at the head of the channel.

Field observations also showed the impact of changes to hydrodynamic processes shown in the modelling, and the vegetation and sediment accumulation patterns (which were not modelled but inferred). The height, density and width of the mangrove trees and pneumatophores were unequal. Mean grain sizes were finer close to the fringe and inside the mangrove forest compared to the edge of the shoal. Sediments in the top layer of the mangrove creek were mainly silt and the mean grain size was similar to the sediments observed inside the forest. In the mangrove creek, samples contained lower organic content compared to the forest. Inside the creek organic matter content increased inland. In general, sediments fined landward except for the points that were located inside the shoal channel, which consist of medium and coarse sand sediments. There was a positive relationship between the organic carbon percentage and mud layer thickness, and vegetation cover. Mangroves had a clear influence extended beyond their vegetative footprint; the mud layer thickness and the texture near the mangrove island and near the fringe of the main forest was more similar to the characteristics of the mangrove areas than the shoal areas. Sediment flux was aligned in the channel, while the flux around the edges followed a more diverse pattern while net sediment transports were landward.

6.1.3. Equilibrium conditions in tidal environments

This thesis also addressed the development of equilibrium geomorphology in tidal settings. Chapter 3 showed that equilibrium is not an absolute state, where a whole system reaches that state at once. Some areas change very quickly to reach equilibrium, and some much more slowly. Chapter 3 showed the pathway to equilibrium over long time periods, and Chapters 4 and 5 focused on the detailed processes controlling equilibrium over very short time scales (a week),

and medium scales (1940-2021). The focused study highlights the role of vegetation in reaching a new state (which was not included in the initial model).

The results of three idealized cases in Chapter 3 showed that a morphodynamic equilibrium state is dependent on the initial bathymetry. Different initial profiles functioned similarly through reaching equilibrium condition and forming final bed. In sandy environments, the morphology tends to develop towards reaching tidal asymmetry index of one as the system approached an equilibrium. Simulations started from different initial bathymetries and were continued until equilibrium condition was reached in the domain. After reaching the equilibrium condition, similar patterns in the three cases were observed (especially at equal depths). In all three cases of sandy bed tidal embayments without a sediment supply from the offshore boundary, morphology developed after ~500 morphological years and the inter-tidal area was the first zone that reached the equilibrium condition. However, the detail of the patterns and the shape of profiles were not the same. Although a similar profile was observed, especially in the points close to mean sea level, some key aspects that determine how the equilibrium tidal flat functions in shaping a coastal ecosystem like channel formation, residence time and energy dissipation were dependent on antecedent morphology and did not develop in the same way.

In addition, channels and formed patterns on each of the three profiles developed differently. These channels can change the flushing time and tidal prism characteristics, which ultimately impacts sediment redistribution and accumulation although their effect on overall ebb-flood asymmetry of the system is relatively small. In idealized cases with sandy beds and mud input at the boundaries, bed development occurred in ~100 years and equilibrium reached five times faster compared to the sand only cases without sediment input. Bathymetry and channel formation were dominated by the mud coming from the offshore boundary and were not inherited from initial bathymetry. Mud influx resulted in sediment accretion in the domain and morphological changes started with several narrow and shallow channels and during the evolution process, the number of shallow channels decreased, they joined together and formed a deeper ebb-dominated channel to circulate the tidal water in the domain.

The impact of mangrove colonization on inter-tidal in multi-decadal time-scale was explored by combining measured data from the field, numerical models and historical images from Whitianga Estuary in Chapter 4 and Chapter 5. The results suggested that the expansion of vegetation on

intertidal flats can impose a control on the morphology and hydrodynamics. Historical aerial and satellite images of the study site showed the large-scale decadal evolution of the shoal since 1940s. The shoal started to expand before mangroves colonized in the area. In both events of vegetation expansion on the inner bend of the shoal and the mangrove island, mangroves first colonized the centre region of shoal and expanded laterally afterwards. Although expansion of the shoal occurred before existence of mangrove, mud layer thickness was higher in the parts where mangroves established indicating they can enhance sediment trapping and mud accumulation in the availability of mud supply.

Observations and results of the numerical model within a shoal channel and a mangrove creek suggested that expansion of the forest may result in a regime transition of the channel function, from a flood-dominated shoal channel to an ebb-dominated mangrove drainage channel. Tidal asymmetry type changed in channels from flood to ebb dominant. Before establishment of mangroves around the edge of the forest, the pre-existing shoal channel (at the location of the modern mangrove creek) was fully flood-dominated. Therefore, these mangroves are likely to be eco-engineers of the estuarine ecosystem. Although mangroves seem to be opportunistic colonizers in first instance, they may quickly become eco-engineers creating their own environment and impacting sediment textural environment, even outside the immediate area of vegetation.

6.1.4. The response of tidal basins to sea level rise

The role of initial bed condition became more pronounced when the response of tidal flats to sea level rise (SLR) effects were studied using the bathymetries in equilibrium state (which had evolved from different initial conditions). In Chapter 3, first sandy environments reached a dynamic equilibrium state, then simulations were extended for additional 200 morphological years with an exponential SLR reaching 2 m, 1.5 m and 1.2 m by the end of the simulation period imposed at the offshore boundary. When the effects of SLR were explored, the difference in the way the sandy profiles reached equilibrium became significant. In all bathymetries, the final slope of the profile decreased by increasing SLR simulated with different RCP scenarios. In irregular and concave-up bathymetry, as sea-level rises, sediments accreted in sub-tidal area but the supra-tidal area degraded whereas in the convex-up bathymetry case, in supra-tidal and upper inter-tidal areas sediments accretion was observed. For all RCP scenarios, irregular and concave-up

bathymetries are not able to keep pace with sea-level increases, so the inter-tidal area disappears as the tidal flat drowns. This effect is related to the lag between forcing and morphological response of the bed, limited sediment supply and accelerated SLR.

Although beyond the scope of this thesis, the fate of mangrove forests under SLR conditions and role of vegetation on the resilience of tidal flats can be discussed based on some of the results that we observed in this thesis. We highlighted that, in the absence of sediment supply, the response of the flats was dependent of their antecedent morphology, and later in historical images observed that the shoal expanded laterally before colonization of mangroves. Therefore, even without vegetation, tidal flats can accrete as sea-level rises. However, we observed that in places that mangroves colonize, mud layer thickness is larger. This confirms that mangroves can build their own environment and promote the ability of tidal flats to trap fine sediments. Therefore, when more sediments are carried on the shoal by elevated sea levels, mangroves will enhance their ability to retain their elevation. On the other side, it was observed that colonization always started from the centre of the shoal where bed level was higher and inundation period was shorter, which confirms that occurrence of mangroves is triggered by the establishment of a relatively low energy environment. Therefore, in the case of accelerated sea-level-rise, the vegetation might not expand due to high bed shear stresses and longer inundation period, and in that case sea-level rise may lead to subsequent vegetation loss and export of sediments.

6.2. Limitations and recommendations for future research

The work presented in Chapter 3 provided insights into the effects of initial bathymetry on the equilibrium conditions. While the simulations can capture the governing processes, there are limitations imposed by using a simple model configuration (i.e., using an idealized domain, uniform sediment parametrization and constant forcing and sediment concentration at open boundaries). In addition, our study is designed to simulate tide-dominated flats, and so does not include waves and wind, which would affect sediment resuspension (Mariotti and Fagherazzi, 2010) and change the morphology also. Moreover, we do not consider sediment compaction in our model. However, for long temporal scale simulations, consolidation may play a role on tidal flat morphodynamics and the results may be modified by sediment compaction (Roskoden et al., 2020; Zhou et al., 2016). Furthermore, vegetation is not included in the model, but results of previous studies confirm that vegetation plays a key role in maintaining the original profile configuration by preventing sediment resuspension and stabilizing the bed (Woodroffe, 1992; Young and Harvey, 1996; Swales et al., 2019), which can be important for the morphodynamic activities in the higher inter-tidal zone. Future research will assess the effect of initial configuration on equilibrium conditions in the presence of winds, vegetation and sediment compaction effects.

In Chapter 4, we qualitatively described the evolution of the forest based on the historical images of the site and linked them to present-time channels dynamics, sediment characteristics and mud layer thickness. I suggest further field measurements at the study site specifically focused on core sampling and measurements of sediment trapping by mangroves. By analysing and comparing the cores from vegetated and un-vegetated parts of the shoal, the long-term capacity of sediment retention by mangroves can be studied and measurements of sediment trapping can reveal short-term deposition of sediments around mangroves.

Additional field measurements should be carried out covering longer time-scales. As discussed in Friedrichs and Aubrey (1988) and Friedrichs et al. (1992), asymmetric tidal cycles can have an impact on net sediment transport. The work presented in Chapter 4 was based on a one-week field measurement that covered spring tidal cycles only. I suggest the similar study covering spring/neap tidal cycle dynamics since it might affect the tidal asymmetry, suspended sediment

concentration and sediment dynamics (although the mangrove area was likely not inundated during neap tides).

Regarding the modelling work presented in Chapter 5, I suggest coupling of the hydrodynamic model with vegetation dynamic model and including morphology in the model. This model will enable studying the 2-way interaction of morphodynamics and vegetation. One on hand the effect of mangrove colonization on eco-geomorphological evolution of the shoal, and one the other hand, by forcing the model with SLR conditions, the effect of hydrodynamics (SLR and subsequent changes in currents) and the resilience of the forest under SLR can be studied.

6.3. Outcome

In summary, my thesis provided new knowledge on the way in which tidal environments evolve, and the role of channels, mangroves and the potential impact of sea-level rise. Managers still use simplistic models of the evolution of these environments to predict the future of our vulnerable intertidal areas (such as the WARMER model), which neglect asymmetries and can neglect channelisation. I have shown that these details can make a substantial difference to how these systems evolve, differences that should be taken into account by coastal managers.

References

Amos, C.L., 1995. Chapter 10 Siliciclastic Tidal Flats. In: Perillo, G.M.E. (Ed.), Geomorphology and Sedimentology of Estuaries. Developments in Sedimentology. Elsevier, pp. 273-306. DOI:10.1016/s0070-4571(05)80030-5

Aucan, J., Ridd, P.V., 2000. Tidal asymmetry in creeks surrounded by saltflats and mangroves with small swamp slopes. Wetlands Ecology and Management, 8(4): 223-232. DOI:10.1023/A:1008459814925

Bamber, J.L., Oppenheimer, M., Kopp, R.E., Aspinall, W.P., Cooke, R.M., 2019. Ice sheet contributions to future sea-level rise from structured expert judgment. Proceedings of the National Academy of Sciences, 116(23): 11195-11200. DOI:doi:10.1073/pnas.1817205116

Bearman, J.A., Friedrichs, C.T., Jaffe, B.E., Foxgrover, A.C., 2010. Spatial Trends in Tidal Flat Shape and Associated Environmental Parameters in South San Francisco Bay. Journal of Coastal Research, 26(2): 342-349.

Belliard, J.P., Toffolon, M., Carniello, L., D'Alpaos, A., 2015. An ecogeomorphic model of tidal channel initiation and elaboration in progressive marsh accretional contexts. Journal of Geophysical Research: Earth Surface, 120(6): 1040-1064. DOI:https://doi.org/10.1002/2015JF003445

Bird, E.C.F., 1986. Mangroves and intertidal morphology in Westernport Bay, Victoria, Australia. Marine Geology, 69(3): 251-271. DOI:https://doi.org/10.1016/0025-3227(86)90042-3

Blankespoor, B., Dasgupta, S., Lange, G.-M., 2017. Mangroves as a protection from storm surges in a changing climate. Ambio, 46(4): 478-491. DOI:10.1007/s13280-016-0838-x

Bouma, T.J. et al., 2016. Short-term mudflat dynamics drive long-term cyclic salt marsh dynamics. Limnology and Oceanography, 61(6): 2261-2275. DOI:https://doi.org/10.1002/lno.10374

Boyd, R., Dalrymple, R., Zaitlin, B.A., 1992. Classification of clastic coastal depositional environments. Sedimentary Geology, 80(3): 139-150. DOI:https://doi.org/10.1016/0037-0738(92)90037-R

Braat, L., Leuven, J.R.F.W., Lokhorst, I.R., Kleinhans, M.G., 2019. Effects of estuarine mudflat formation on tidal prism and large-scale morphology in experiments. Earth Surface Processes and Landforms, 44(2): 417-432. DOI:https://doi.org/10.1002/esp.4504

Bryan, K.R., Nardin, W., Mullarney, J.C., Fagherazzi, S., 2017. The role of cross-shore tidal dynamics in controlling intertidal sediment exchange in mangroves in Cù Lao Dung, Vietnam. Continental Shelf Research, 147: 128-143. DOI:https://doi.org/10.1016/j.csr.2017.06.014

Bryce, S., Larcombe, P., Ridd, P.V., 2003. Hydrodynamic and geomorphological controls on suspended sediment transport in mangrove creek systems, a case study: Cocoa Creek, Townsville, Australia. Estuarine, Coastal and Shelf Science, 56(3): 415-431. DOI:https://doi.org/10.1016/S0272-7714(02)00192-0

Coco, G. et al., 2014. Beach response to a sequence of extreme storms. Geomorphology, 204: 493-501. DOI:https://doi.org/10.1016/j.geomorph.2013.08.028

Coco, G. et al., 2013. Morphodynamics of tidal networks: Advances and challenges. Marine Geology, 346: 1-16. DOI:10.1016/j.margeo.2013.08.005

Cowell, P.J., Thom, B.G., 1995. Morphodynamics of coastal evolution. In: Carter, R.W.G., Woodroffe, C.D. (Eds.), Coastal Evolution: Late Quaternary Shoreline Morphodynamics. Cambridge University Press, Cambridge, pp. 33-86. DOI:DOI: 10.1017/CBO9780511564420.004

D'Alpaos, A. et al., 2007. Spontaneous tidal network formation within a constructed salt marsh: Observations and morphodynamic modelling. Geomorphology, 91(3): 186-197. DOI:https://doi.org/10.1016/j.geomorph.2007.04.013

D'Alpaos, A., Lanzoni, S., Marani, M., Fagherazzi, S., Rinaldo, A., 2005. Tidal network ontogeny: Channel initiation and early development. Journal of Geophysical Research: Earth Surface, 110(F2). DOI:https://doi.org/10.1029/2004JF000182

Dai, Z.-J., Du, J.-z., Li, C.-C., Chen, Z.-S., 2007. The configuration of equilibrium beach profile in South China. Geomorphology, 86(3): 441-454. DOI:https://doi.org/10.1016/j.geomorph.2006.09.016

Dai, Z. et al., 2018. Scaling properties of estuarine beaches. Marine Geology, 404: 130-136. DOI:https://doi.org/10.1016/j.margeo.2018.07.011

Dam, G., van der Wegen, M., Labeur, R.J., Roelvink, D., 2016. Modeling centuries of estuarine morphodynamics in the Western Scheldt estuary. 43(8): 3839-3847. DOI:https://doi.org/10.1002/2015GL066725

Dastgheib, A., Roelvink, J.A., Wang, Z.B., 2008. Long-term process-based morphological modeling of the Marsdiep Tidal Basin. Marine Geology, 256(1): 90-100. DOI:https://doi.org/10.1016/j.margeo.2008.10.003

de Haas, T. et al., 2018. Holocene evolution of tidal systems in The Netherlands: Effects of rivers, coastal boundary conditions, eco-engineering species, inherited relief and human interference. Earth-Science Reviews, 177: 139-163. DOI:https://doi.org/10.1016/j.earscirev.2017.10.006

Dean, W.E., 1974. Determination of carbonate and organic matter in calcareous sediments and sedimentary rocks by loss on ignition; comparison with other methods. Journal of Sedimentary Research, 44(1): 242-248. DOI:10.1306/74D729D2-2B21-11D7-8648000102C1865D %J Journal of Sedimentary Research

Deltares, 2017. Delft3D-FLOW: Simulation of multi-dimensional hydrodynamic flows and transports phenomena, including sediments. User Manual, Version 3.15, Revision 45038, Delft, The Netherlands: Deltares.

Dieckmann, R., Osterthun, M., Partenscky, H.W., 1987. Influence of water-level elevation and tidal range on the sedimentation in a German tidal flat area. Progress in Oceanography, 18(1): 151-166. DOI:https://doi.org/10.1016/0079-6611(87)90031-0

Dissanayake, D.M.P.K., Ranasinghe, R., Roelvink, J.A., 2012. The morphological response of large tidal inlet/basin systems to relative sea level rise. Climatic Change, 113(2): 253-276. DOI:10.1007/s10584-012-0402-z

Dronkers, J., 1986. Tidal asymmetry and estuarine morphology. Netherlands Journal of Sea Research, 20(2): 117-131. DOI:https://doi.org/10.1016/0077-7579(86)90036-0

Dronkers, J., 2005. Dynamics of Coastal Systems, pp. 197–324. World Scientific.

Duke, N.C. et al., 2007. A World Without Mangroves? , 317(5834): 41-42. DOI:doi:10.1126/science.317.5834.41b

Duke, N.C., 1991. A systematic revision of the mangrove genus <I>Avicennia</I> (Avicenniaceae) in Australasia*. Australian Systematic Botany, 4(2): 299-324.

Eekhout, J.P.C., Hoitink, A.J.F., 2015. Chute cutoff as a morphological response to stream reconstruction: The possible role of backwater. Water Resources Research, 51(5): 3339-3352. DOI:https://doi.org/10.1002/2014WR016539

Elmilady, H., van der Wegen, M., Roelvink, D., Jaffe, B.E., 2019. Intertidal Area Disappears Under Sea Level Rise: 250 Years of Morphodynamic Modeling in San Pablo Bay, California. Journal of Geophysical Research: Earth Surface, 124(1): 38-59. DOI:https://doi.org/10.1029/2018JF004857

Elmilady, H., van der Wegen, M., Roelvink, D., van der Spek, A., 2020. Morphodynamic Evolution of a Fringing Sandy Shoal: From Tidal Levees to Sea Level Rise. 125(6): e2019JF005397. DOI:https://doi.org/10.1029/2019JF005397

Elmilady, H., van der Wegen, M., Roelvink, D., van der Spek, A., 2022. Modeling the Morphodynamic Response of Estuarine Intertidal Shoals to Sea-Level Rise. 127(1): e2021JF006152. DOI:https://doi.org/10.1029/2021JF006152

Fagherazzi, S., Hannion, M., D'Odorico, P., 2008. Geomorphic structure of tidal hydrodynamics in salt marsh creeks. Water Resources Research, 44(2). DOI:https://doi.org/10.1029/2007WR006289

Fagherazzi, S., Overeem, I., 2007. Models of Deltaic and Inner Continental Shelf Landform Evolution. Annual Review of Earth and Planetary Sciences, 35(1): 685-715. DOI:10.1146/annurev.earth.35.031306.140128

Fan, D., 2012. Open-Coast Tidal Flats. In: Davis Jr, R.A., Dalrymple, R.W. (Eds.), Principles of Tidal Sedimentology. Springer Netherlands, Dordrecht, pp. 187-229. DOI:10.1007/978-94-007-0123-6_9

Fricke, A.T., Nittrouer, C.A., Ogston, A.S., Vo-Luong, H.P., 2017. Asymmetric progradation of a coastal mangrove forest controlled by combined fluvial and marine influence, Cù Lao Dung, Vietnam. Continental Shelf Research, 147: 78-90. DOI:https://doi.org/10.1016/j.csr.2017.07.012

Friedrichs, C.T., 2011. 3.06 - Tidal Flat Morphodynamics: A Synthesis. In: Wolanski, E., McLusky, D. (Eds.), Treatise on Estuarine and Coastal Science. Academic Press, Waltham, pp. 137-170. DOI:https://doi.org/10.1016/B978-0-12-374711-2.00307-7

Friedrichs, C.T., Aubrey, D.G., 1988. Non-linear tidal distortion in shallow well-mixed estuaries: a synthesis. Estuarine, Coastal and Shelf Science, 27(5): 521-545. DOI:https://doi.org/10.1016/0272-7714(88)90082-0

Friedrichs, C.T., Aubrey, D.G., Speer, P.E., 1990. Impacts of Relative Sea-level Rise on Evolution of Shallow Estuaries, Residual Currents and Long-Term Transport, pp. 105-122. DOI:https://doi.org/10.1029/CE038p0105

Friedrichs, C.T., Lynch, D.R., Aubrey, D.G., 1992. Velocity Asymmetries in Frictionally-Dominated Tidal Embayments, Dynamics and Exchanges in Estuaries and the Coastal Zone, pp. 277-312. DOI:https://doi.org/10.1029/CE040p0277

Friess, D.A. et al., 2012. Are all intertidal wetlands naturally created equal? Bottlenecks, thresholds and knowledge gaps to mangrove and saltmarsh ecosystems. Biological Reviews, 87(2): 346-366. DOI:https://doi.org/10.1111/j.1469-185X.2011.00198.x

Furukawa, K., Wolanski, E., Mueller, H., 1997. Currents and Sediment Transport in Mangrove Forests. Estuarine, Coastal and Shelf Science, 44(3): 301-310. DOI:https://doi.org/10.1006/ecss.1996.0120

Ganju, N.K., Schoellhamer, D.H., 2010. Decadal-Timescale Estuarine Geomorphic Change Under Future Scenarios of Climate and Sediment Supply. Estuaries and Coasts, 33(1): 15-29. DOI:10.1007/s12237-009-9244-y

Gao, S., Collins, M., 1994. Tidal Inlet Equilibrium, in Relation to Cross-sectional Area and Sediment Transport Patterns. Estuarine, Coastal and Shelf Science, 38(2): 157-172. DOI:https://doi.org/10.1006/ecss.1994.1010

Glover, H.E., Stokes, D.J., Ogston, A.S., Bryan, K.R., Pilditch, C.A., 2022. Decadal-scale impacts of changing mangrove extent on hydrodynamics and sediment transport in a quiescent, mesotidal estuary. Earth Surface Processes and Landforms, 47(5): 1287-1303. DOI:https://doi.org/10.1002/esp.5317

Guo, L., van der Wegen, M., Roelvink, J.A., He, Q., 2014. The role of river flow and tidal asymmetry on 1-D estuarine morphodynamics. Journal of Geophysical Research: Earth Surface, 119(11): 2315-2334. DOI:10.1002/2014jf003110

Hanssen, J.L.J., van Prooijen, B.C., Volp, N.D., de Vet, P.L.M., Herman, P.M.J., 2022. Where and why do creeks evolve on fringing and bare tidal flats? Geomorphology, 403: 108182. DOI:https://doi.org/10.1016/j.geomorph.2022.108182

Hibma, A., Schuttelaars, H.M., de Vriend, H.J., 2004. Initial formation and long-term evolution of channel–shoal patterns. Continental Shelf Research, 24(15): 1637-1650. DOI:https://doi.org/10.1016/j.csr.2004.05.003

Hibma, A., Schuttelaars, H.M., Wang, Z.B., 2003. Comparison of longitudinal equilibrium profiles of estuaries in idealized and process-based models. Ocean Dynamics, 53(3): 252-269. DOI:10.1007/s10236-003-0046-7

Hood, W.G., 2006. A conceptual model of depositional, rather than erosional, tidal channel development in the rapidly prograding Skagit River Delta (Washington, USA). Earth Surface Processes and Landforms, 31(14): 1824-1838. DOI:https://doi.org/10.1002/esp.1381

Hood, W.G., 2010. Tidal channel meander formation by depositional rather than erosional processes: examples from the prograding Skagit River Delta (Washington, USA). Earth Surface Processes and Landforms, 35(3): 319-330. DOI:10.1002/esp.1920

Horstman, E.M., Bryan, K.R., Mullarney, J.C., 2021. Drag variations, tidal asymmetry and tidal range changes in a mangrove creek system. Earth Surface Processes and Landforms, n/a(n/a). DOI:https://doi.org/10.1002/esp.5124

Horstman, E.M., Dohmen-Janssen, C.M., Bouma, T.J., Hulscher, S.J.M.H., 2015. Tidal-scale flow routing and sedimentation in mangrove forests: Combining field data and numerical modelling. Geomorphology, 228: 244-262. DOI:https://doi.org/10.1016/j.geomorph.2014.08.011

Horstman, E.M., Dohmen-Janssen, C.M., Hulscher, S.J.M.H., 2013. Flow routing in mangrove forests: A field study in Trang province, Thailand. Continental Shelf Research, 71: 52-67. DOI:https://doi.org/10.1016/j.csr.2013.10.002

Horstman, E.M. et al., 2018. The Dynamics of Expanding Mangroves in New Zealand. In: Makowski, C., Finkl, C.W. (Eds.), Threats to Mangrove Forests: Hazards, Vulnerability, and Management. Springer International Publishing, Cham, pp. 23-51. DOI:10.1007/978-3-319-73016-5_2

Hu, Z., Wang, Z.B., Zitman, T.J., Stive, M.J.F., Bouma, T.J., 2015. Predicting long-term and short-term tidal flat morphodynamics using a dynamic equilibrium theory. Journal of Geophysical Research: Earth Surface, 120(9): 1803-1823. DOI:https://doi.org/10.1002/2015JF003486

Hughes, Z.J., 2012. Tidal Channels on Tidal Flats and Marshes. In: Davis Jr, R.A., Dalrymple, R.W. (Eds.), Principles of Tidal Sedimentology. Springer Netherlands, Dordrecht, pp. 269-300. DOI:10.1007/978-94-007-0123-6_11

Hume, T.M., Swales, A., 2003. How Estuaries Grow Old. . NIWA. Water and Atmosphere. 11 (1) 2003.

Hunt, S., Bryan, K.R., Mullarney, J.C., Pritchard, M., 2016. Observations of asymmetry in contrasting wave- and tidally-dominated environments within a mesotidal basin: implications for estuarine morphological evolution. Earth Surface Processes and Landforms, 41(15): 2207-2222. DOI:https://doi.org/10.1002/esp.3985

Jones, H., 2008. Coastal Sedimentation: What We Know and the Information Gaps. Environment Waikato Technical Report 2008/12.

Kearney, W.S., Fagherazzi, S., 2016. Salt marsh vegetation promotes efficient tidal channel networks. Nat Commun, 7: 12287. DOI:10.1038/ncomms12287

Khojasteh, D., Felder, S., Heimhuber, V., Glamore, W., 2023. A global assessment of estuarine tidal response to sea level rise. Science of The Total Environment, 894: 165011. DOI:https://doi.org/10.1016/j.scitotenv.2023.165011

Khojasteh, D. et al., 2022. Sea level rise will change estuarine tidal energy: A review. Renewable and Sustainable Energy Reviews, 156: 111855. DOI:https://doi.org/10.1016/j.rser.2021.111855

Kirby, R., 2000. Practical implications of tidal flat shape. Continental Shelf Research, 20(10): 1061-1077. DOI:https://doi.org/10.1016/S0278-4343(00)00012-1

Klein, G.d., 1985. Intertidal Flats and Intertidal Sand Bodies. In: Davis, R.A. (Ed.), Coastal Sedimentary Environments. Springer New York, New York, NY, pp. 187-224. DOI:10.1007/978-1-4612-5078-4_3

Knight, J.M., Dale, P.E.R., Dunn, R.J.K., Broadbent, G.J., Lemckert, C.J., 2008. Patterns of tidal flooding within a mangrove forest: Coombabah Lake, Southeast Queensland, Australia.

Estuarine, Coastal and Shelf Science, 76(3): 580-593. DOI:https://doi.org/10.1016/j.ecss.2007.07.044

Kobashi, D., Mazda, Y., 2005. Tidal Flow in Riverine-Type Mangroves. Wetlands Ecology and Management, 13(6): 615-619. DOI:10.1007/s11273-004-3481-4

Krauss, K.W., Allen, J.A., Cahoon, D.R., 2003. Differential rates of vertical accretion and elevation change among aerial root types in Micronesian mangrove forests. Estuarine, Coastal and Shelf Science, 56(2): 251-259. DOI:https://doi.org/10.1016/S0272-7714(02)00184-1

Kumbier, K., Hughes, M.G., Carvalho, R.C., Woodroffe, C.D., 2022a. Intertidal wetland geomorphology influences main channel hydrodynamics in a mature barrier estuary. Estuarine, Coastal and Shelf Science, 267: 107783. DOI:https://doi.org/10.1016/j.ecss.2022.107783

Kumbier, K. et al., 2022b. An Eco-Morphodynamic Modelling Approach to Estuarine Hydrodynamics & Wetlands in Response to Sea-Level Rise. Frontiers in Marine Science, 9. DOI:10.3389/fmars.2022.860910

Lauzon, R. et al., 2018. Effects of Marsh Edge Erosion in Coupled Barrier Island-Marsh Systems and Geometric Constraints on Marsh Evolution. Journal of Geophysical Research: Earth Surface, 123(6): 1218-1234. DOI:https://doi.org/10.1029/2017JF004530

Lesser, G.R., Roelvink, J.A., van Kester, J.A.T.M., Stelling, G.S., 2004. Development and validation of a three-dimensional morphological model. Coastal Engineering, 51(8): 883-915. DOI:https://doi.org/10.1016/j.coastaleng.2004.07.014

Maan, D.C., van Prooijen, B.C., Wang, Z.B., De Vriend, H.J., 2015. Do intertidal flats ever reach equilibrium? Journal of Geophysical Research: Earth Surface, 120(11): 2406-2436. DOI:https://doi.org/10.1002/2014JF003311

MacDonald, I.T., 2009. Flocculation of fine sediment in turbulent flows, ResearchSpace@ Auckland.

Marciano, R., Wang, Z.B., Hibma, A., de Vriend, H.J., Defina, A., 2005. Modeling of channel patterns in short tidal basins. Journal of Geophysical Research: Earth Surface, 110(F1). DOI:https://doi.org/10.1029/2003JF000092

Mariotti, G., Canestrelli, A., 2017. Long-term morphodynamics of muddy backbarrier basins: Fill in or empty out? Water Resources Research, 53(8): 7029-7054. DOI:https://doi.org/10.1002/2017WR020461

Mariotti, G., Fagherazzi, S., 2010. A numerical model for the coupled long-term evolution of salt marshes and tidal flats. 115(F1). DOI:https://doi.org/10.1029/2009JF001326

Mazda , Hiroyuki Yokochi , Sato, Y., 1990. Groundwater Flow in the Bashita-Minato Mangrove Area, and its Influence on Water and Bottom Mud Properties.

Mazda, Y., Ikeda, Y., 2006. Behavior of the groundwater in a riverine-type mangrove forest. Wetlands Ecology and Management, 14(6): 477-488. DOI:10.1007/s11273-006-9000-z

Mazda, Y., Kanazawa, N., Wolanski, E., 1995. Tidal asymmetry in mangrove creeks. Hydrobiologia, 295(1): 51-58. DOI:10.1007/BF00029110

Mazda, Y., Kobashi, D., Okada, S., 2005. Tidal-Scale Hydrodynamics within Mangrove Swamps. Wetlands Ecology and Management, 13(6): 647-655. DOI:10.1007/s11273-005-0613-4

Mazda, Y., Wolanski, E., 2009. Hydrodynamics and modelling of water flow in mangrove areas.

McGranahan, G., Balk, D., Anderson, B., 2007. The rising tide: assessing the risks of climate change and human settlements in low elevation coastal zones. Environment and Urbanization, 19(1): 17-37. DOI:10.1177/0956247807076960

McLachlan, R.L. et al., 2020. Impacts of tidal-channel connectivity on transport asymmetry and sediment exchange with mangrove forests. Estuarine, Coastal and Shelf Science, 233: 106524. DOI:https://doi.org/10.1016/j.ecss.2019.106524

Montgomery, J.M., Bryan, K.R., Coco, G., 2022. The role of mangroves in coastal flood protection: The importance of channelization. Continental Shelf Research, 243: 104762. DOI:https://doi.org/10.1016/j.csr.2022.104762

Montgomery, J.M., Bryan, K.R., Horstman, E.M., Mullarney, J.C., 2018. Attenuation of Tides and Surges by Mangroves: Contrasting Case Studies from New Zealand. 10(9): 1119.

Montgomery, J.M., Bryan, K.R., Mullarney, J.C., Horstman, E.M., 2019. Attenuation of Storm Surges by Coastal Mangroves. 46(5): 2680-2689. DOI:https://doi.org/10.1029/2018GL081636

Morales, J.A., 2022. Fluvial-Influenced Systems I: Estuaries. In: Morales, J.A. (Ed.), Coastal Geology. Springer Nature Switzerland, Cham, pp. 309-327. DOI:10.1007/978-3-030-96121-3_21

Morrisey, D.J. et al., 2010. THE ECOLOGY AND MANAGEMENT OF TEMPERATE MANGROVES. Oceanography and Marine Biology, 48: 43-160.

Morrisey, D. et al (2007). The New Zealand Mangrove: Review of the Current State of Knowledge. Auckland Regional Council Technical Publication Number 325

Mullarney, J.C., Henderson, S.M., Reyns, J.A.H., Norris, B.K., Bryan, K.R., 2017. Spatially varying drag within a wave-exposed mangrove forest and on the adjacent tidal flat. Continental Shelf Research, 147: 102-113. DOI:https://doi.org/10.1016/j.csr.2017.06.019

Nidzieko, N.J., 2010. Tidal asymmetry in estuaries with mixed semidiurnal/diurnal tides. Journal of Geophysical Research: Oceans, 115(C8). DOI:https://doi.org/10.1029/2009JC005864

Palmer, K., Watson, C., Fischer, A., 2019. Non-linear interactions between sea-level rise, tides, and geomorphic change in the Tamar Estuary, Australia. Estuarine, Coastal and Shelf Science, 225: 106247. DOI:https://doi.org/10.1016/j.ecss.2019.106247

Perillo, G.M.E., Iribarne, O.O., 2003. Processes of tidal channel development in salt and freshwater marshes. Earth Surface Processes and Landforms, 28(13): 1473-1482. DOI:10.1002/esp.1018

Perillo, G.M.E., Ripley, M.D., Piccolo, M.C., Dyer, K.R., 1996. The Formation of Tidal Creeks in a Salt Marsh: New Evidence from the Loyola Bay Salt Marsh, Rio Gallegos Estuary, Argentina. Mangroves and Salt Marshes, 1(1): 37-46. DOI:10.1023/A:1025942111382

Pritchard, D., Hogg, A.J., 2003. Cross-shore sediment transport and the equilibrium morphology of mudflats under tidal currents. 108(C10). DOI:https://doi.org/10.1029/2002JC001570

Pritchard, D., Hogg, A.J., Roberts, W., 2002. Morphological modelling of intertidal mudflats: the role of cross-shore tidal currents. Continental Shelf Research, 22(11): 1887-1895. DOI:https://doi.org/10.1016/S0278-4343(02)00044-4

Rahdarian, A., Bryan, K.R., Van Der Wegen, M., 2022. On the influence of antecedent morphology on development of equilibrium bathymetry in estuaries past and future. Journal of Geophysical Research: Earth Surface, n/a(n/a): e2022JF006621. DOI:https://doi.org/10.1029/2022JF006621

Reeve, G.M.D., 2008. Sedimentation And Hydrodynamics of Whitianga Estuary. Masters Thesis, The University of Waikato, Hamilton, New Zealand.

Rinaldo, A., Fagherazzi, S., Lanzoni, S., Marani, M., Dietrich, W.E., 1999a. Tidal networks: 2. Watershed delineation and comparative network morphology. Water Resources Research, 35(12): 3905-3917. DOI:10.1029/1999wr900237

Rinaldo, A., Fagherazzi, S., Lanzoni, S., Marani, M., Dietrich, W.E., 1999b. Tidal networks: 3. Landscape-forming discharges and studies in empirical geomorphic relationships. Water Resources Research, 35(12): 3919-3929. DOI:https://doi.org/10.1029/1999WR900238

Roberts, W., Le Hir, P., Whitehouse, R.J.S., 2000. Investigation using simple mathematical models of the effect of tidal currents and waves on the profile shape of intertidal mudflats. Continental Shelf Research, 20(10): 1079-1097. DOI:https://doi.org/10.1016/S0278-4343(00)00013-3

Rodríguez-Iturbe, I. et al., 1992. Energy dissipation, runoff production, and the three-dimensional structure of river basins. 28(4): 1095-1103.

Roelvink, J.A., 2006. Coastal morphodynamic evolution techniques. Coastal Engineering, 53(2): 277-287. DOI:https://doi.org/10.1016/j.coastaleng.2005.10.015

Roskoden, R.R., Bryan, K.R., Schreiber, I., Kopf, A., 2020. Rapid transition of sediment consolidation across an expanding mangrove fringe in the Firth of Thames New Zealand. Geo-Marine Letters, 40(2): 295-308. DOI:10.1007/s00367-019-00589-9

Ruiter, P.J., Mullarney, J.C., Bryan, K.R., Winter, C., 2019. The links between entrance geometry, hypsometry and hydrodynamics in shallow tidally dominated basins. Earth Surface Processes and Landforms, 44(10): 1957-1972. DOI:10.1002/esp.4622

Schettini, C.A.F. et al., 2020. Circulation and fine-sediment dynamics in the Amazon Macrotidal Mangrove Coast. 45(3): 574-589. DOI:https://doi.org/10.1002/esp.4756

Schuttelaars, H., De Swart, H.J.J.o.G.R.O., 2000. Multiple morphodynamic equilibria in tidal embayments. 105(C10): 24105-24118.

Schwarz, C. et al., 2014. Impacts of salt marsh plants on tidal channel initiation and inheritance. Journal of Geophysical Research: Earth Surface, 119(2): 385-400. DOI:https://doi.org/10.1002/2013JF002900

Seminara, G., Lanzoni, S., Tambroni, N., Toffolon, M., 2010. How long are tidal channels? Journal of Fluid Mechanics, 643: 479-494. DOI:10.1017/S0022112009992308

Seminara, G., Tubino, M., 2001. Sand bars in tidal channels. Part 1. Free bars. Journal of Fluid Mechanics, 440: 49-74. DOI:10.1017/S0022112001004748

Soares, M.L.G., 2009. A Conceptual Model for the Responses of Mangrove Forests to Sea Level Rise. Journal of Coastal Research: 267-271.

Spalding, M., 2010. World Atlas of Mangroves (1st ed.). Routledge. . DOI:https://doi.org/10.4324/9781849776608

Stark, J., Van Oyen, T., Meire, P., Temmerman, S., 2015. Observations of tidal and storm surge attenuation in a large tidal marsh. 60(4): 1371-1381. DOI:https://doi.org/10.1002/lno.10104

Stefanon, L., Carniello, L., D'Alpaos, A., Lanzoni, S., 2010. Experimental analysis of tidal network growth and development. Continental Shelf Research, 30(8): 950-962. DOI:10.1016/j.csr.2009.08.018

Sullivan, J.C., Torres, R., Garrett, A., 2019. Intertidal Creeks and Overmarsh Circulation in a Small Salt Marsh Basin. Journal of Geophysical Research: Earth Surface, 124(2): 447-463. DOI:https://doi.org/10.1029/2018JF004861

Sutherland, J., Peet, A.H., Soulsby, R.L., 2004. Evaluating the performance of morphological models. Coastal Engineering, 51(8): 917-939. DOI:https://doi.org/10.1016/j.coastaleng.2004.07.015

Swales, A., Bentley, S.J., Lovelock, C., Bell, R.G., 2007. Sediment Processes and Mangrove-Habitat Expansion on a Rapidly-Prograding Muddy Coast, New Zealand, Coastal Sediments '07, pp. 1441-1454. DOI:doi:10.1061/40926(239)111

Swales, A., Bentley Sr, S.J., Lovelock, C.E., 2015a. Mangrove-forest evolution in a sediment-rich estuarine system: opportunists or agents of geomorphic change? Earth Surface Processes and Landforms, 40(12): 1672-1687. DOI:https://doi.org/10.1002/esp.3759

Swales, A., Bentley Sr, S.J., Lovelock, C.E., 2015b. Mangrove-forest evolution in a sediment-rich estuarine system: opportunists or agents of geomorphic change? , 40(12): 1672-1687. DOI:https://doi.org/10.1002/esp.3759

Swales, A., Denys, P., Pickett, V.I., Lovelock, C.E., 2016. Evaluating deep subsidence in a rapidly-accreting mangrove forest using GPS monitoring of surface-elevation benchmarks and sedimentary records. Marine Geology, 380: 205-218. DOI:https://doi.org/10.1016/j.margeo.2016.04.015

Swales, A., Pritchard, M., McBride, G.B., 2021. Chapter 1 - Biogeomorphic evolution and expansion of mangrove forests in New Zealand's sediment-rich estuarine systems. In: Sidik, F., Friess, D.A. (Eds.), Dynamic Sedimentary Environments of Mangrove Coasts. Elsevier, pp. 3-45. DOI:https://doi.org/10.1016/B978-0-12-816437-2.00013-6

Swales, A., Reeve, G., Cahoon, D.R., Lovelock, C.E., 2019. Landscape Evolution of a Fluvial Sediment-Rich Avicennia marina Mangrove Forest: Insights from Seasonal and Inter-annual Surface-Elevation Dynamics. Ecosystems, 22(6): 1232-1255. DOI:10.1007/s10021-018-0330-5

Taylor Perron, J., Fagherazzi, S., 2012. The legacy of initial conditions in landscape evolution. 37(1): 52-63. DOI:https://doi.org/10.1002/esp.2205

Temmerman, S. et al., 2005. Impact of vegetation on flow routing and sedimentation patterns: Three-dimensional modeling for a tidal marsh. Journal of Geophysical Research: Earth Surface, 110(F4). DOI:https://doi.org/10.1029/2005JF000301

Temmerman, S. et al., 2007. Vegetation causes channel erosion in a tidal landscape. Geology, 35(7): 631-634. DOI:10.1130/g23502a.1

Terry, M.H., Herdendorf, C.E., 1992. Factors Controlling Tidal Inlet Characteristics on Low Drift Coasts. Journal of Coastal Research, 8(2): 355-375.

Thatcher, M.L., Harleman, D.R.F., 1972. Prediction of unsteady salinity intrusion in estuaries : mathematical model and user's manual.

Thrush, S.F. et al., 2004. Muddy Waters: Elevating Sediment Input to Coastal and Estuarine Habitats. Frontiers in Ecology and the Environment, 2(6): 299-306. DOI:10.2307/3868405

Uittenbogaard, R.E., 1998. Model for eddy diffusivity and viscosity related to sub-grid velocity and bed topography. Tech. rep., WL | Delft Hydraulics, Delft, The Netherlands.

Uittenbogaard, R.E., Vossen, B.V., 2003. Subgrid-scale model for Quasi-2D turbulence in shallow water.” In In: Shallow flows: proceedings of the international symposium, pages 575–582.

van der Vegt, M., Schuttelaars, H.M., de Swart, H.E., 2007. Modeling the formation of undulations of the coastline: The role of tides. Continental Shelf Research, 27(15): 2014-2031. DOI:https://doi.org/10.1016/j.csr.2007.04.006

van der Wal, D., Pye, K., Neal, A., 2002. Long-term morphological change in the Ribble Estuary, northwest England. Marine Geology, 189(3): 249-266. DOI:https://doi.org/10.1016/S0025-3227(02)00476-0

van der Wegen, M., 2013. Numerical modeling of the impact of sea level rise on tidal basin morphodynamics. Journal of Geophysical Research: Earth Surface, 118(2): 447-460. DOI:https://doi.org/10.1002/jgrf.20034

van der Wegen, M., Jaffe, B., Foxgrover, A., Roelvink, D., 2017. Mudflat Morphodynamics and the Impact of Sea Level Rise in South San Francisco Bay. Estuaries and Coasts, 40(1): 37-49. DOI:10.1007/s12237-016-0129-6

van der Wegen, M., Roelvink, J.A., 2008. Long-term morphodynamic evolution of a tidal embayment using a two-dimensional, process-based model. 113(C3). DOI:https://doi.org/10.1029/2006JC003983

van der Wegen, M., Roelvink, J.A., 2012. Reproduction of estuarine bathymetry by means of a process-based model: Western Scheldt case study, the Netherlands. Geomorphology, 179: 152-167. DOI:https://doi.org/10.1016/j.geomorph.2012.08.007

van der Wegen, M., Roelvink, J.A., Jaffe, B.E., 2019. Morphodynamic Resilience of Intertidal Mudflats on a Seasonal Time Scale. 124(11): 8290-8308. DOI:https://doi.org/10.1029/2019JC015492

van der Wegen, M., Wang, Z.B., Savenije, H.H.G., Roelvink, J.A., 2008. Long-term morphodynamic evolution and energy dissipation in a coastal plain, tidal embayment. 113(F3). DOI:https://doi.org/10.1029/2007JF000898

van Dijk, W.M., Schuurman, F., van de Lageweg, W.I., Kleinhans, M.G., 2014. Bifurcation instability and chute cutoff development in meandering gravel-bed rivers. Geomorphology, 213: 277-291. DOI:https://doi.org/10.1016/j.geomorph.2014.01.018

Van Goor, M.A., Zitman, T.J., Wang, Z.B., Stive, M.J.F., 2003. Impact of sea-level rise on the morphological equilibrium state of tidal inlets. Marine Geology, 202(3): 211-227. DOI:https://doi.org/10.1016/S0025-3227(03)00262-7

van Maanen, B., Coco, G., Bryan, K.R., 2011. A numerical model to simulate the formation and subsequent evolution of tidal channel networks. Australian Journal of Civil Engineering, 9(1): 61-72. DOI:10.1080/14488353.2011.11463969

van Maanen, B., Coco, G., Bryan, K.R., 2013a. Modelling the effects of tidal range and initial bathymetry on the morphological evolution of tidal embayments. Geomorphology, 191: 23-34. DOI:10.1016/j.geomorph.2013.02.023

van Maanen, B., Coco, G., Bryan, K.R., 2015. On the ecogeomorphological feedbacks that control tidal channel network evolution in a sandy mangrove setting. Proc Math Phys Eng Sci, 471(2180): 20150115. DOI:10.1098/rspa.2015.0115

van Maanen, B., Coco, G., Bryan, K.R., Friedrichs, C.T., 2013b. Modeling the morphodynamic response of tidal embayments to sea-level rise. Ocean Dynamics, 63(11): 1249-1262. DOI:10.1007/s10236-013-0649-6

Vandenbruwaene, W., Meire, P., Temmerman, S., 2012. Formation and evolution of a tidal channel network within a constructed tidal marsh. Geomorphology, 151-152: 114-125. DOI:https://doi.org/10.1016/j.geomorph.2012.01.022

Verschelling, E., van der Perk, M., Middelkoop, H., 2018. The impact of climate change on the morphology of a tidal freshwater wetland affected by tides, discharge, and wind. River Research and Applications, 34(6): 516-525. DOI:https://doi.org/10.1002/rra.3282

Vundavilli, H., Mullarney, J.C., MacDonald, I.T., Bryan, K.R., 2021. The interaction of buoyant coastal river plumes with mangrove vegetation and consequences for sediment deposition and erosion in a tidal environment. Continental Shelf Research, 222: 104417. DOI:https://doi.org/10.1016/j.csr.2021.104417

Wentworth, C.K., 1922. A Scale of Grade and Class Terms for Clastic Sediments. The Journal of Geology, 30(5): 377-392.

Willemsen, P.W.J.M., Horstman, E.M., Borsje, B.W., Friess, D.A., Dohmen-Janssen, C.M., 2016. Sensitivity of the sediment trapping capacity of an estuarine mangrove forest. Geomorphology, 273: 189-201. DOI:https://doi.org/10.1016/j.geomorph.2016.07.038

Wolanski, E., 1992. Hydrodynamics of mangrove swamps and their coastal waters. Hydrobiologia, 247(1): 141-161. DOI:10.1007/BF00008214

Wolanski, E., Jones, M., Bunt, J., 1980. Hydrodynamics of a tidal creek-mangrove swamp system. %J Marine and Freshwater Research. 31(4): 431-450. DOI:https://doi.org/10.1071/MF9800431

Woodroffe, C.D., 1990. The impact of sea-level rise on mangrove shorelines. Progress in Physical Geography: Earth and Environment, 14(4): 483-520. DOI:10.1177/030913339001400404

Woodroffe, C., 1992. Mangrove Sediments and Geomorphology, Tropical Mangrove Ecosystems, pp. 7-41. DOI:https://doi.org/10.1029/CE041p0007

Woodroffe, C.D. et al., 2016. Mangrove Sedimentation and Response to Relative Sea-Level Rise. Annual Review of Marine Science, 8(1): 243-266. DOI:10.1146/annurev-marine-122414-034025

Woods, J.L.D., 2012. The Evolution of a Holocene Estuarine Barrier on the Coromandel Coast, New Zealand. Geographical Research, 50(1): 89-101. DOI:https://doi.org/10.1111/j.1745-5871.2011.00711.x

Wu, F., Tong, C., Torkelson, M., Wang, Y., 2020. Evolution of shoals and vegetation of Jiuduansha in the Changjiang River Estuary of China in the last 30 years. Acta Oceanologica Sinica, 39(8): 71-78. DOI:10.1007/s13131-020-1636-7

Xie, D., Schwarz, C., Kleinhans, M.G., Zhou, Z., van Maanen, B., 2022. Implications of Coastal Conditions and Sea-Level Rise on Mangrove Vulnerability: A Bio-Morphodynamic Modeling Study. Journal of Geophysical Research: Earth Surface, 127(3): e2021JF006301. DOI:https://doi.org/10.1029/2021JF006301

Xu, F., Coco, G., Zhou, Z., Tao, J., Zhang, C., 2017. A numerical study of equilibrium states in tidal network morphodynamics. Ocean Dynamics, 67(12): 1593-1607. DOI:10.1007/s10236-017-1101-0

Young, B.M., Harvey, E.L., 1996. A Spatial Analysis of the Relationship Between Mangrove (Avicennia marinavar.australasica) Physiognomy and Sediment Accretion in the Hauraki

Plains, New Zealand. Estuarine, Coastal and Shelf Science, 42(2): 231-246. DOI:https://doi.org/10.1006/ecss.1996.0017

Zarzuelo, C. et al., 2019. Natural and Human-Induced Flow and Sediment Transport within Tidal Creek Networks Influenced by Ocean-Bay Tides, Water. DOI:10.3390/w11071493

Zhang, K. et al., 2012. The role of mangroves in attenuating storm surges. Estuarine, Coastal and Shelf Science, 102-103: 11-23. DOI:https://doi.org/10.1016/j.ecss.2012.02.021

Zhang, Y. et al., 2018. Simulating the Formation of Tidal Channels Along an Open-Coast Tidal Flat: The Effects of Initial Perturbation. Coastal Engineering Proceedings(36). DOI:10.9753/icce.v36.papers.84

Zheng, J. et al., 2021. The impact of wind-waves and sea level rise on the morphodynamics of a sandy estuarine shoal. 46(15): 3045-3062. DOI:https://doi.org/10.1002/esp.5207

Zhou, Z. et al., 2014. A comparative study of physical and numerical modeling of tidal network ontogeny. Journal of Geophysical Research: Earth Surface, 119(4): 892-912. DOI:https://doi.org/10.1002/2014JF003092

Zhou, Z., van der Wegen, M., Jagers, B., Coco, G., 2016. Modelling the role of self-weight consolidation on the morphodynamics of accretional mudflats. Environmental Modelling & Software, 76: 167-181. DOI:https://doi.org/10.1016/j.envsoft.2015.11.002

Zinger, J.A., Rhoads, B.L., Best, J.L., Johnson, K.K., 2013. Flow structure and channel morphodynamics of meander bend chute cutoffs: A case study of the Wabash River, USA. Journal of Geophysical Research: Earth Surface, 118(4): 2468-2487. DOI:https://doi.org/10.1002/jgrf.20155